Lecture #1: Stagnation Point Heating

Background

- **The kinetic energy of an entry vehicle is dissipated by transformation into thermal energy (heat) as the entry system decelerates**

- **The magnitude of this thermal energy is so large that if all of this energy were transferred to the entry system it would be severely damaged and likely vaporize**
  - Harvey Allen - the blunt body concept

- **Only a small fraction of this thermal energy is transferred to the entry system**
  - The thermal transfer fraction is dependant on vehicle shape, size, aerodynamic regime and velocity
  - Near peak heating, 1% to 5% of the total thermal energy is transferred to the entry system
  - Example: at the peak heating point the freestream energy transfer for Pathfinder was $\dot{q}_\infty = \frac{1}{2}\rho V^3 \sim 4,000$ W/cm^2 but only about 110 W/cm^2 (2.7%) was actually transferred to the surface

Example

3

Energy density: $\dfrac{E}{m} = \dfrac{V^2}{2} + g_o h$

Entry	V (km/s)	E/m (MJ/kg)
MER	5.6	16
Apollo	11.4	66
Mars Return	14.0	98
Galileo	47.4	1130

Note that:

Water boils @ 2.3 MJ/kg

Carbon vaporizes @ 60.5 MJ/kg

In each case $g_o h$ is about 1% of total
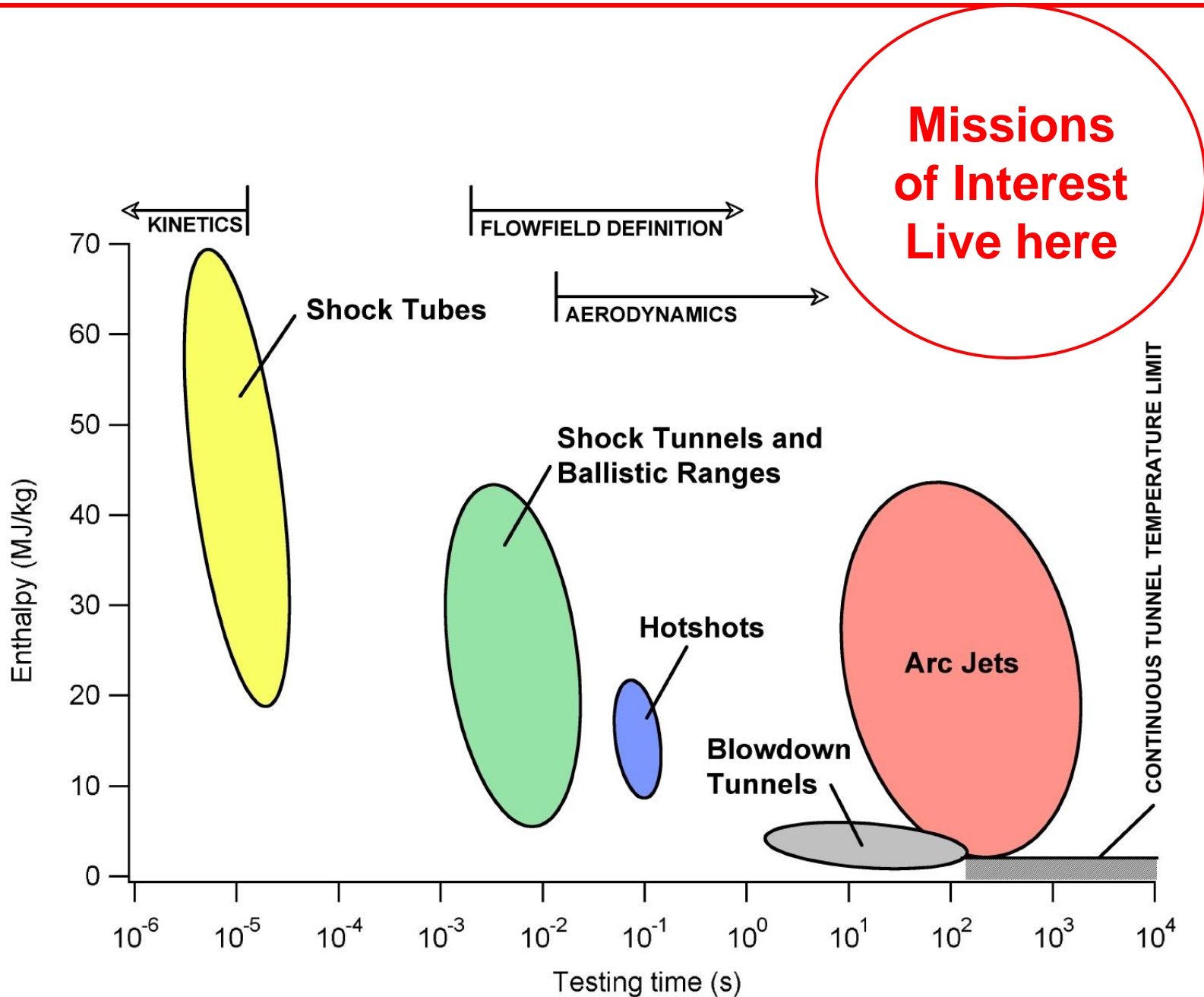
- **Why is a blunt body used for planetary entry?**
    - Slender body: low drag, highly maneuverable
    - Blunt body: high drag, not very maneuverable

- **Blunt bodies generate strong shock waves**
    - Efficient energy dissipation. Shock waves convert kinetic energy to internal energy. Result is: heating of the gas, dissociation, ionization
    - Most of this energy is convected into the vehicle wake rather than transported to the surface
    - Intuitively, blunter is better (more bluntness equals stronger shock). Hold that thought; we will come back to it…
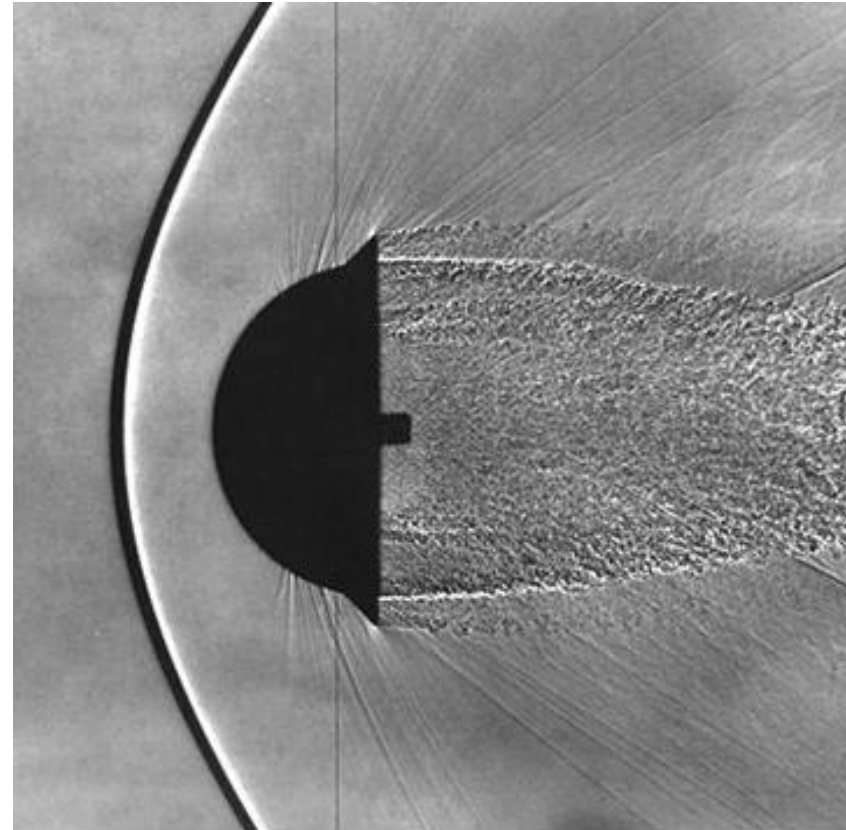
Apollo Wake Flow
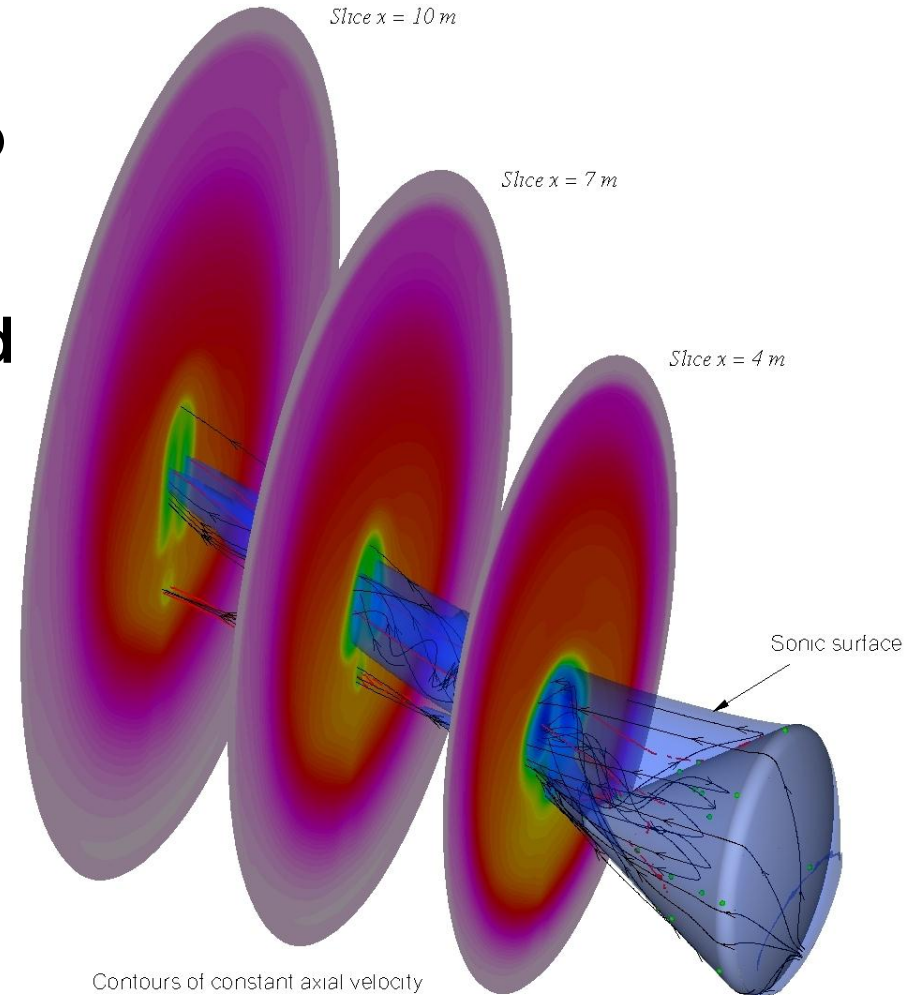
- **Normal shock heats the gas to many thousands of degrees**

- **Much of this heat is conducted into the vehicle wake and propogated downstream**

- **Can be tracked as a "velocity deficit" and persists long downstream of the vehicle**

Slice x = 10 m

Slice x = 7 m

Slice x = 4 m

Sonic surface

Contours of constant axial velocity

Definitions

- **Heat Rate (q)**
  - Instantaneous heat flux at a point on the vehicle (W/cm^2)

- **Heat Load (Q)**
  - Integration of heat rate with time over a trajectory (J/cm^2)

- **Convective Heating**
  - Heat flux to the vehicle from conduction (κ gradT)

- **Catalytic Heating**
  - Heat flux to the vehicle due to surface facilitated chemical reactions
  - Commonly lumped with convective heating by convention

- **Radiative Heating**
  - Heat flux to the vehicle from radiation produced by excited atoms and molecules in the shock layer

What is Aerothermodynamics?

- **Accurate and conservative prediction of the heating environment encountered by an Earth or planetary entry vehicle**

- **Aerothermal modeling is coupled and entwined with Thermal Protection System (TPS) design**
  - The TPS is designed to withstand the predicted environment with risk-appropriate margin
  - For ablative systems, the flowfield and TPS interact with each other in non-reversible manner; the physics themselves are coupled

- **At its core, aerothermodynamics becomes the study of an energy balance at the surface of the material**

  - ➤ **Heat flux (with pressure & shear) used to select TPS material**
  - ➤ **Heat load determines TPS thickness**

Principles of Aerothermal Models

Planetary Atmospheres
Mars&Venus: CO_2/N_2
Titan: N_2/CH_4
Giants: H_2/He
Earth: N_2/O_2

Thermal Protection System (TPS)

Hot Shock Layer (up to 20000 K)
Thermochemical nonequilibrium, Ionization, Radiation

Boundary Layer (2–6000 K)
Transport properties, Ablation product mixing, Radiation blockage

V

"Cool" Surface (2–3000 K)
Surface kinetics, Ablation

Surface Energy Balance

q_{rerad}

q_c
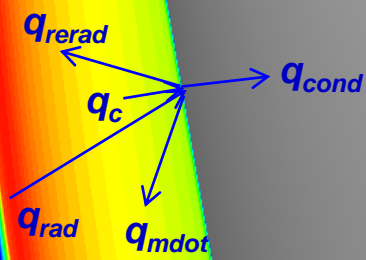
q_{cond}

q_{rad}

q_{mdot}

Design Problem: Minimize conduction into vehicle to minimize TPS mass/risk

$$q_{cond} = q_c + q_{rad} - q_{rerad} - q_{mdot}$$

Incident Aeroheating

Material Response

- **The current SOA involves the steady solution of the reacting Navier-Stokes equations via CFD or DSMC methods**
- **Full 3D simulations possible in hours to days**
- **Longer time required for the simulation of OML details (steps, gaps, seals, windows, etc.**
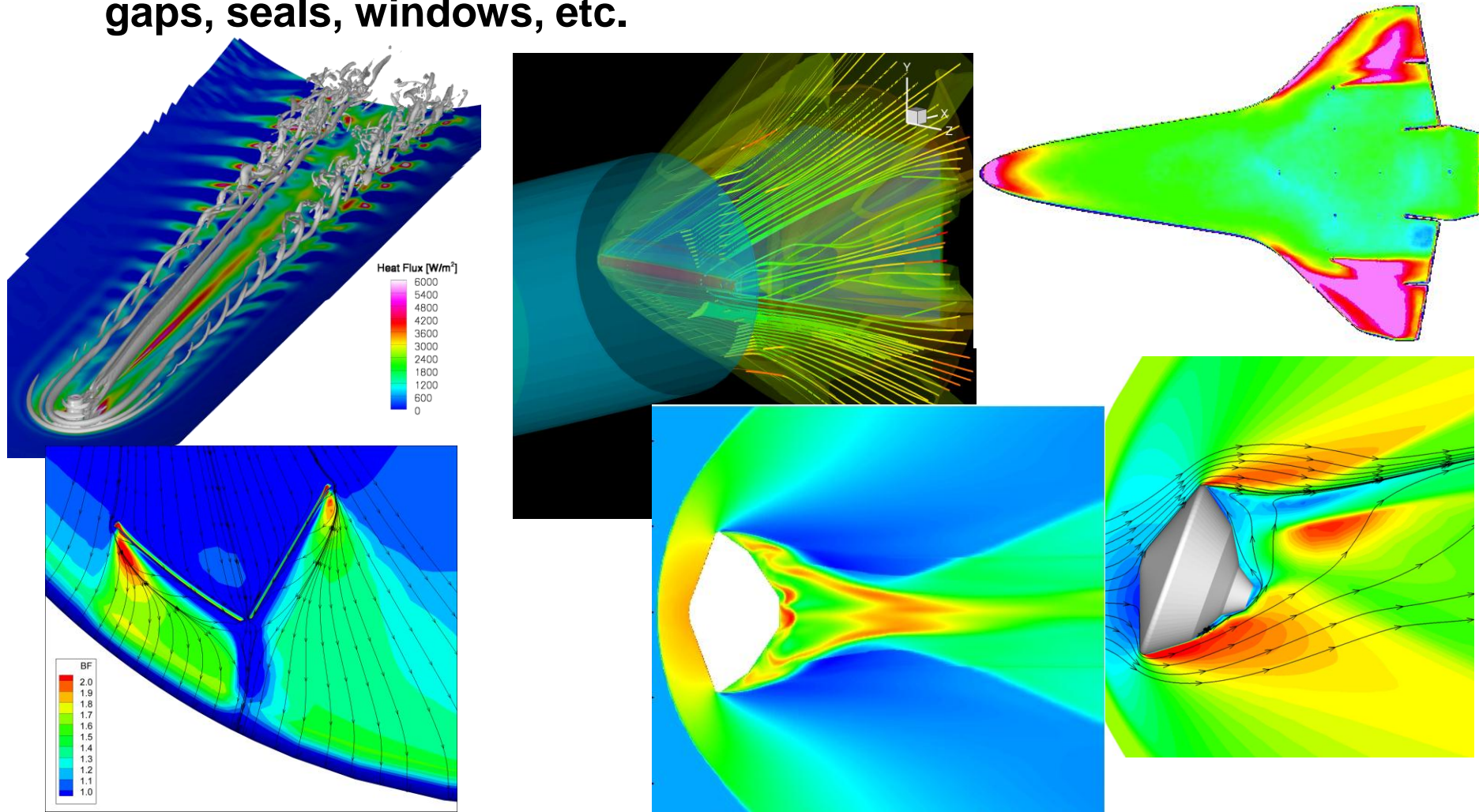
Pushing the Current State of the Art

- **DES, DNS, LES**
- **Unsteady RANS (URANS) simulations of Supersonic Retro-Propulsion flowfields; going on right now…**

LaUPWT SRP Run 165, AoA=0°
Single Nozzle, Mach 4.6, C_T 2
OVERFLOW

$\log(\|\nabla\rho\|+0.001)$: -5 -4 -3 -2 -1 0 1 2 3 4 5

Time = 0.000034 seconds

Z (diameters)

X (diameters)

NASA CFD Development Strategy
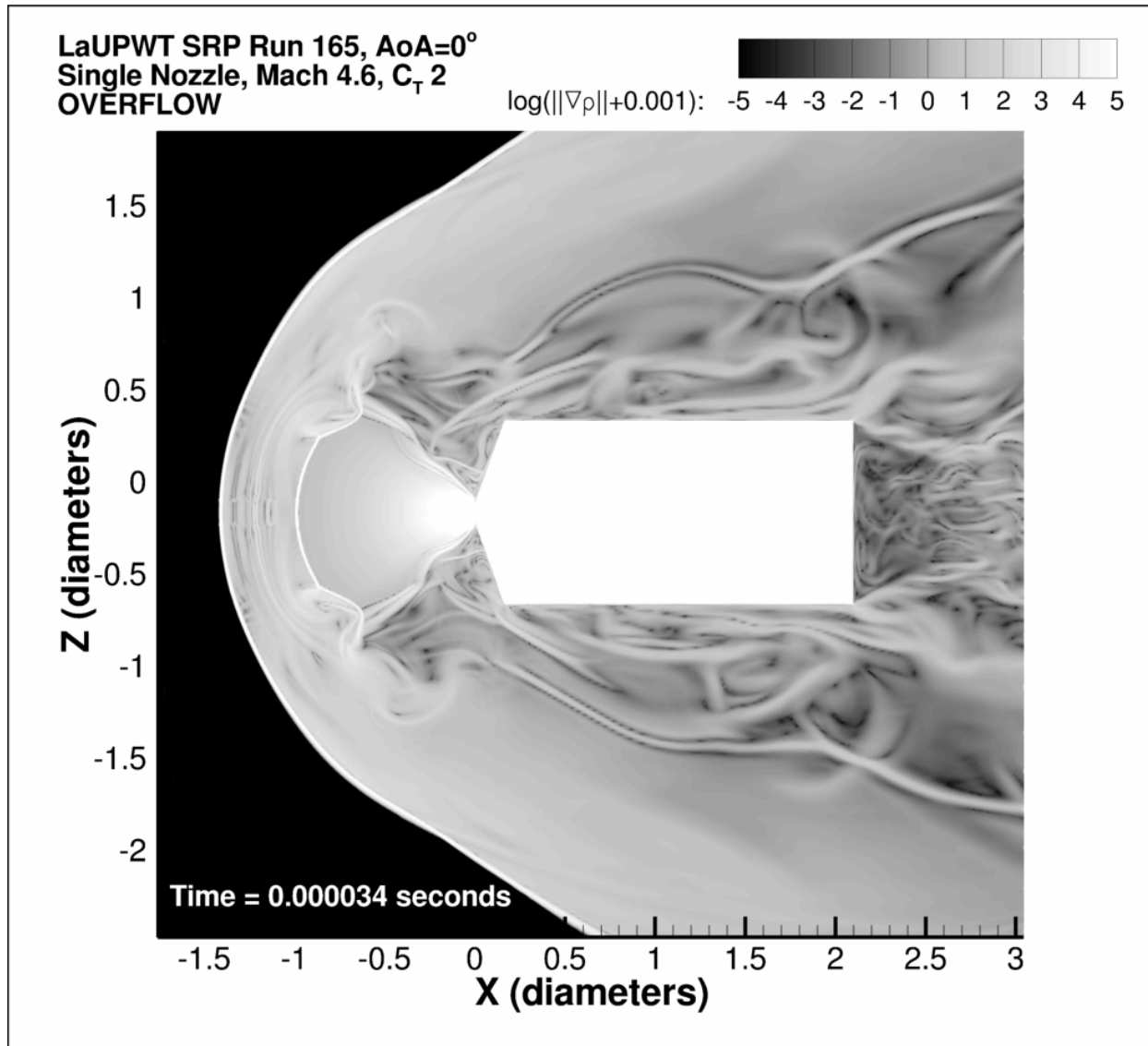
LAURA

DPLR

Today

• Structured, Finite Volume, mostly steady-state
• **Also coupled to Radiation and Ablation codes**

US3D-NASA

FUN3D (LAURA-path)

In 2-3 Years

• Unstructured, Finite Volume, low-dissipation schemes, DES/LES, DNS capability, well-balanced schemes

DG (Discontinuous Galerkin)

CESE (Conservation Element Solution Element)

In 5-10 Years

• Unstructured, higher order, unsteady, beyond finite volume

Why Engineering Methods?

With present computational abilities, why use engineering methods?

- CFD is a powerful tool, but high-fidelity simulations remain time (and resource) consuming

- Some applications of simple relationships for calculating non-ablating convective and radiative heating

  – Negligible computation time
  – Included in most atmospheric trajectory codes-stag. pt. heating
  – Initial estimates of heating rates and loads for use during conceptual design stage

- But most important:

  ➜ In this day of commodity supercomputers it is all too easy to run simulations without truly understanding the physics involved or the trends that are expected. ***The fact that it "converged" doesn't make it right***. Engineering methods are based on sound approximations to theory and provide a valuable sanity check on CFD results

- **Pioneering engineering theories were developed in the 1950's (missile technology)**

  Lees, L. "Laminar Heat Transfer Over Blunt-Nosed Bodies at Hypersonic Speeds," *Jet Propulsion*, pp. 256-269, Apr. 1956

  Fay, J.A. and Riddell, F.R., "Theory of Stagnation Point Heat Transfer in Dissociated Air," *Journal of Aeronautical Sciences*, Feb. 1958

- **Extensions to higher velocities were required to account for chemistry and ionization**

- **Many extensions and simplifications followed for specific applications, non-Earth atmospheres**

- **Early correlations for convective heating have the form:**

$$\dot{q}_s' \sim V^3 \left(\frac{\rho}{R_n} \right)^{\frac{1}{2}}$$

- **Why?**

- **At first cut, one might expect heat flux to the surface to be proportional to freestream energy <u>flux</u> ($\frac{1}{2}\rho V^3$)**

- **From previous discussion one would expect convective heat flux to decrease as bluntness (R_n) increases, but with what functionality?**

- **(insert brief derivation here)**

♦ **<u>Convective</u>: derived from boundary layer and stagnation point theories**

w = wall
e = edge

Fay & Riddell (1958):

Boundary layer eqns, similarity transformation

$$\dot{q}_w = \frac{0.763}{(\mathrm{Pr}_w)^{0.6}}(\rho_e\mu_e)^{0.4}(\rho_w\mu_w)^{0.1}\left[(h_o)_e - h_w\right]\left[1 + (Le^{0.52}-1)\frac{h_d}{(h_o)_e}\right]\left[\left(\frac{du_e}{dx}\right)_t\right]^{0.5}$$

Velocity gradient from mod. Newtonian theory $\sim(1/R_n)$

$$\frac{du_e}{dx} = \frac{1}{R}\sqrt{\frac{2(p_e - p_\infty)}{\rho_e}}$$

Significant advance, but still requires many quantities that are not readily available to designer

Allows for chemistry effects, non-unity Pr, Le (Prandtl, Lewis numbers)

Chapman Equation (Earth):

$$q_s = 1.63 \times 10^{-4} \left(\frac{\rho}{R_n} \right)^{\frac{1}{2}} V^3 \left(1 - \frac{h_w}{h_\infty} \right)$$

$$h_\infty = \int_0^T C_p T dt + \tfrac{1}{2} V_\infty^2$$

"hot wall correction" can frequently be neglected in hypersonic flow ($h_w << h_\infty$)

Sutton Graves:

$$q_s = k \left(\frac{\rho}{R_n} \right)^{\frac{1}{2}} V^3$$

k = 1.7415e-4 (Earth)
k = 1.9027e-4 (Mars)

(SI units)

- **Calculated for specific atmosphere (Earth or Mars), accounting for thermodynamics.**

- **Above assume a fully catalytic surface; equivalent expressions for non catalytic wall are available.**

Hot Wall Correction Term

- **Negligible above about 100 W/cm^2 assuming radiative equilibrium**
- **Actual effect is smaller than this for ablative TPS**

$$HWC = \left(1 - \frac{h_w}{h_\infty}\right)$$

Radiative Equilibrium

Approximate
Ablative Correction

Enthalpy Ratio

q (W/cm^2) – log scale

# Generalized Chapman Method

Generalized Chapman Method
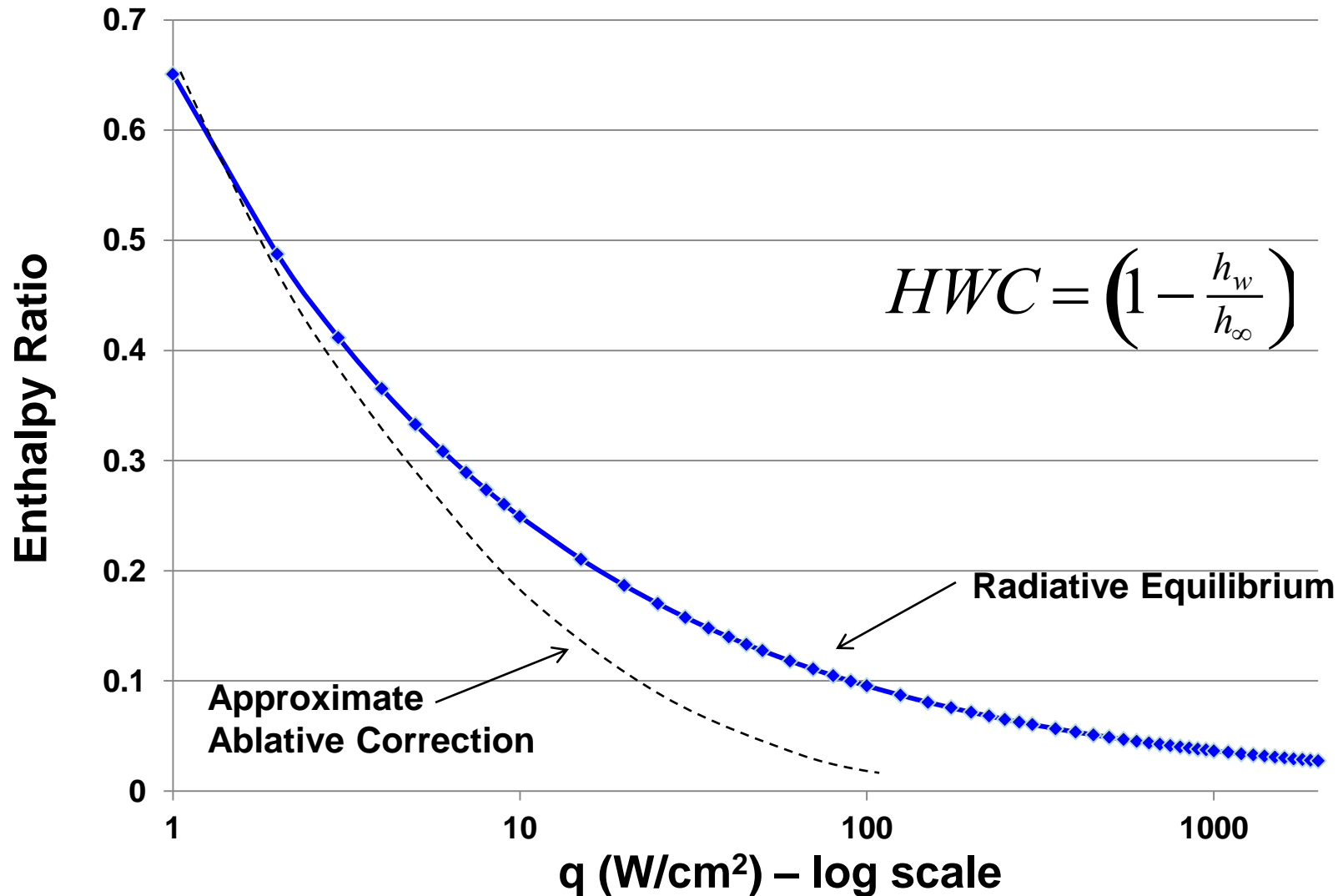
$$q_{c,0} = \frac{C}{\sqrt{R_n}} \left(\rho_\infty\right)^m \left(V_\infty\right)^n \left[1 - \frac{h_w}{h_\infty}\right];$$

Earth :   **m = 0.5,**   **n = 3**
Mars: **m = 0.5,**   **n = 3.04**

C is derived for problem of interest

Powerful design tool - can be used to approximate heating from a small number of CFD "anchor points" even away from the stagnation point by letting *C*, *m*, and *n* be curve fit coefficients

Nuance – Effective Nose Radius
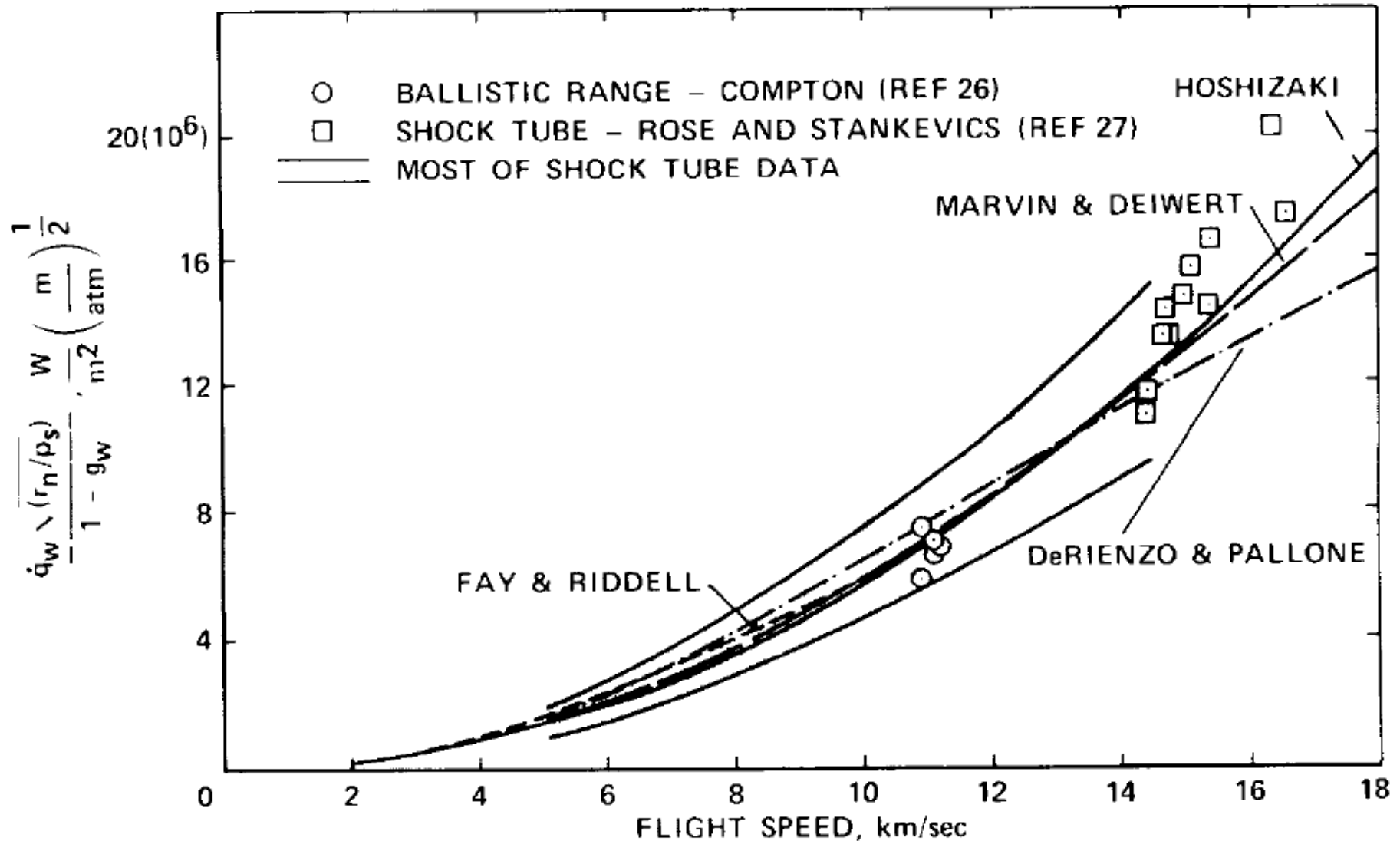
- **Prior correlations are straightforward and require only readily available quantities**

- **However, there is a nuance. All are dependent on the effective nose radius of the vehicle under investigation**

- **For a hemisphere, $R_{eff} = R_n$, but corrections are required for other vehicle shapes.**

- **For example, Apollo was a truncated sphere, with an effective radius almost twice the base radius of the capsule. MER/MSL use sphere-cones, where the conical flank increases the effective radius of the nose**

- **For bodies with a rounded corner, Zoby and Sullivan have computed tables of effective radius as a function of R_b/R_n and R_c/R_b:**

Zoby, E. and Sullivan E, "Effects of Corner Radius on Stagnation Point Velocity Gradients on Blunt Axisymmetric Bodies," Journal of Spacecraft and Rockets, Vol. 3, No. 10, 1966.

When does it matter?

    Can the flow "tell" that the nose is finite?
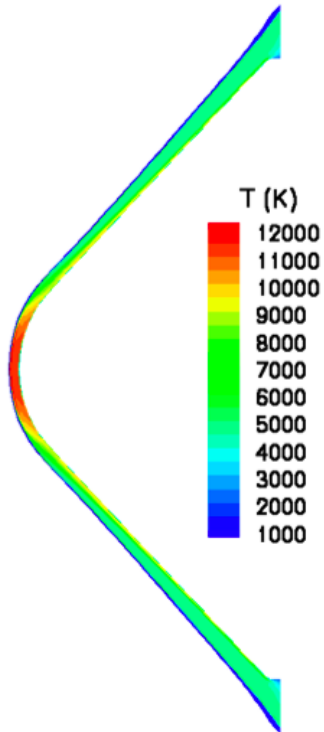
45° Sphere-Cone
Supersonic Oblique Shock
$R_{eff} = R_n$
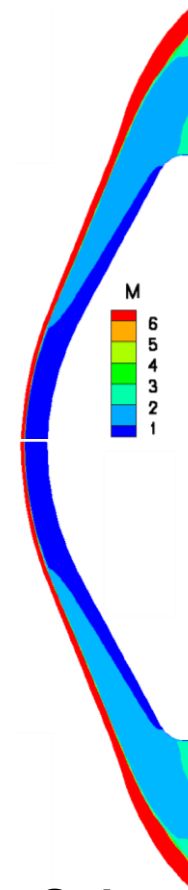
60° Sphere-Cone
Subsonic Shock
$R_{eff} > R_n$

- **Theory is less intuitive, more involved**

- **Atoms or molecules are excited by collisions. Excited species can emit a photon that carries energy with it**

- **Photons are emitted isotropically, and travel effectively instantaneously**

- **Radiative heating is the integration of those photons that hit the surface times the energy they carry; intuitively should be proportional to the size of the radiating volume**

- **Partition functions for excited states imply a near exponential dependence on temperature**

- **Radiation is coupled to the fluid mechanics for two reasons:**

  - Emitted photons carry energy out of control volume (adiabatic cooling)

  - Photons can be absorbed in the boundary layer and heat the gas

Upper Level (U)

$h\nu$

$2h\nu$ Stimulated Emission

Spontaneous Emission

$h\nu$

$$h\nu = \Delta E = E_U - E_L$$

Absorption

Lower Level (L)

$h\nu$
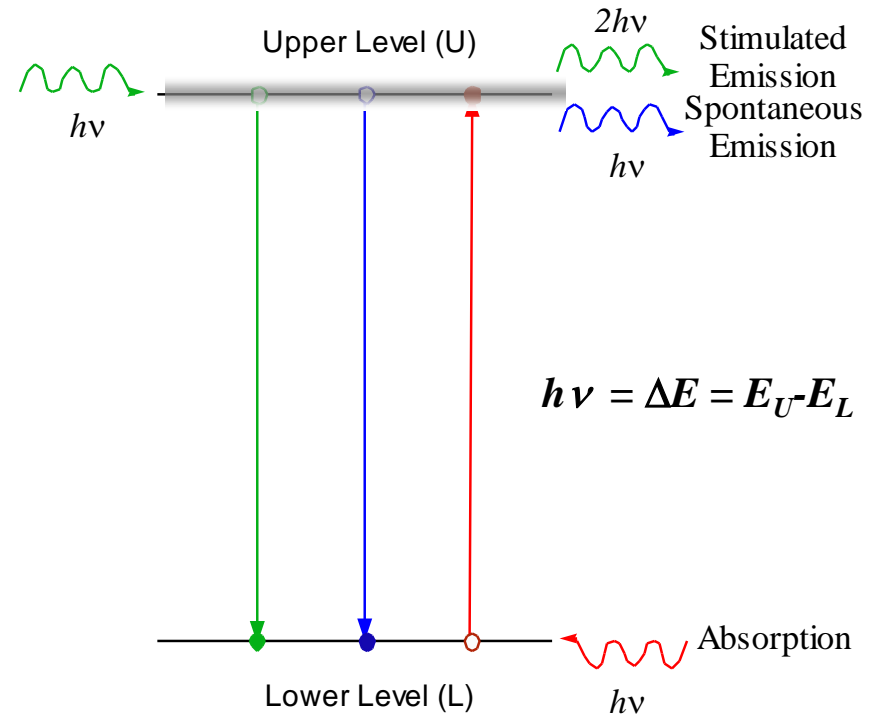
$$\frac{N_i}{N} = \frac{g_i e^{-\frac{E_i}{kT}}}{\sum_j g_j e^{-\frac{E_j}{kT}}} = \frac{g_i e^{-\frac{E_i}{kT}}}{Q}$$

LTE-Plasma

Adapted from Anderson, Hypersonic and High Temperature Gas Dynamics, Fig. 18.10
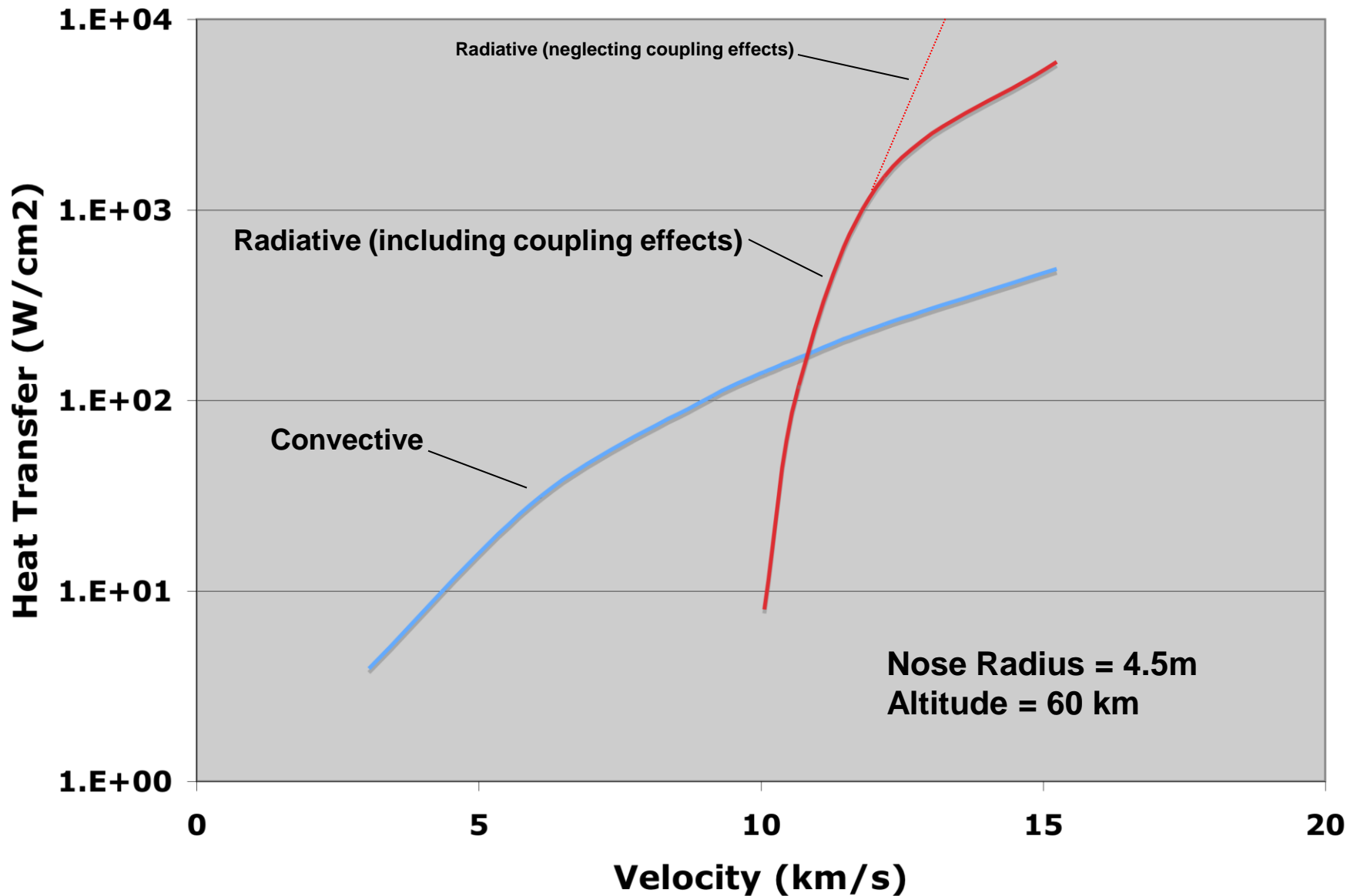
Martin:

$$\dot{q}'_r \sim r_n^{1.0} \rho_\infty^{1.6} V_\infty^{8.5}$$

♦ **Earth**

Direct dependence on R_n agrees with intuitive argument about radiating volume

Tauber-Sutton:

$$\dot{q}'_r = C_i r_n^a \rho_\infty^m f_i(V_\infty)$$

♦ **based on tabulated data, equilibrium shock theory**

Earth : a ~ 1,   m ~ 1.2
Mars: a = 0.526,   m ~ 1.2

f_i **are tabulated, near exponential at moderate velocity**

Theory is less intuitive, more involved. Typically relies on table lookups and has limited range of validity

Fortunately, radiation is not a major issue for many problems of interest: Mars (moderate velocity), LEO return, Titan

Importance of Radiative Cooling

- **The shock layer is cooled by the emission of photons. Clearly this effect will become more important as a larger fraction of the total shock layer energy is converted to photons**

- **Tabular or engineering expressions for stagnation point radiation typically _include_ the radiative cooling effect**

- **However it is very important to recognize this phenomenon when computing radiation from CFD data (inherently uncoupled operation)**

- **Goulard proposed a non-dimensional parameter that is essentially the ratio of total energy flux to that lost to radiation:**

$$\Gamma = \frac{2q_{R,unc}}{\frac{1}{2}\rho V^3}$$

- **The net radiative heating can then be computed from (Tauber-Wakefield):**

$$q_{R,coup} = \frac{q_{R,unc}}{\left(1 + \kappa \Gamma^{0.7}\right)}$$

- **Where κ is an atmosphere-specific constant**
  - κ = 2 for Titan
  - κ = 3.45 for Earth
  - $\kappa \sim$ 3 for Mars/Venus

Example - Galileo Probe

Adapted from Anderson, Hypersonic and High Temperature Gas Dynamics, Fig. 18.16
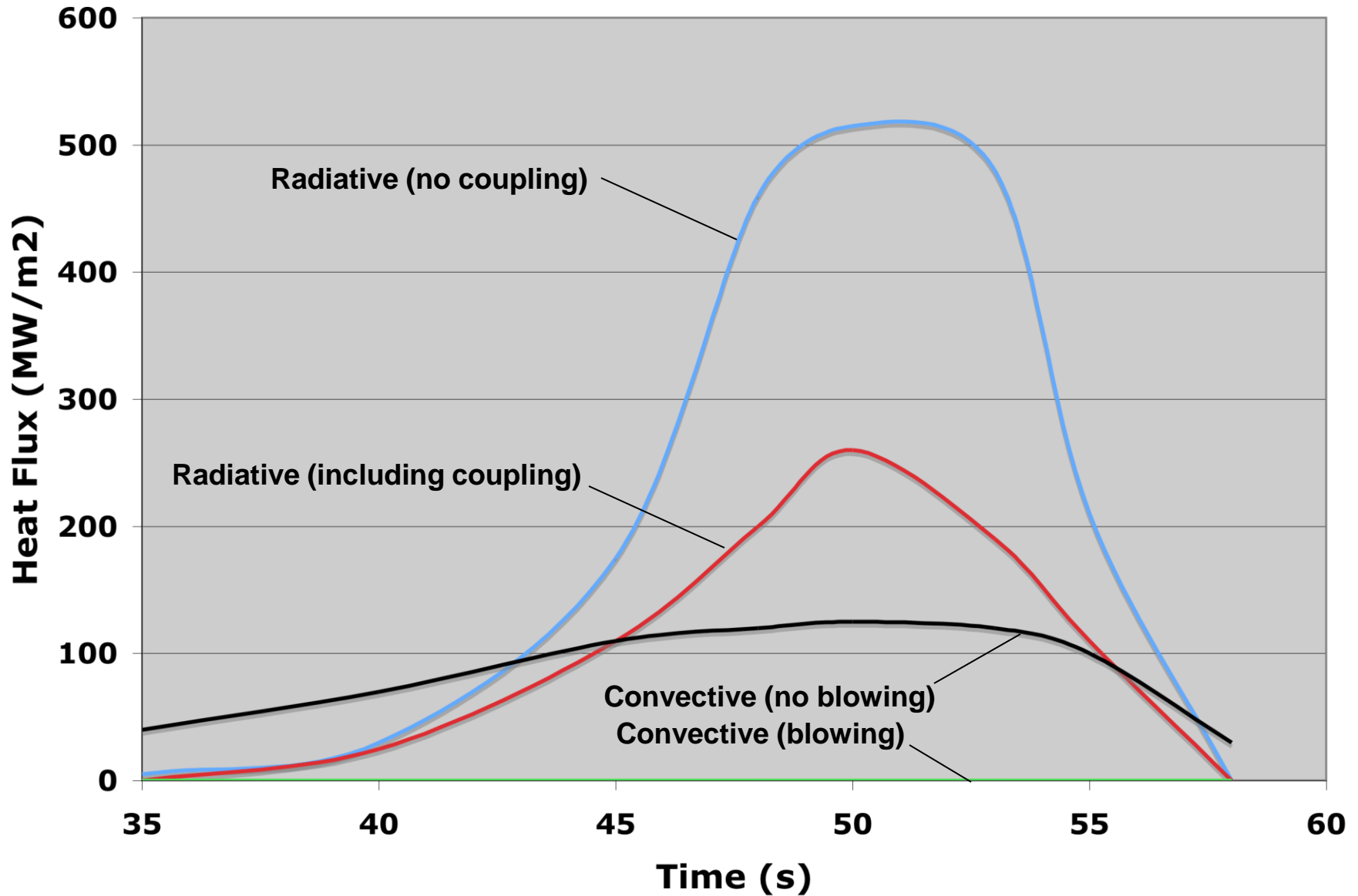
- **How hot does the TPS surface get?**

- **A body radiates heat at a rate proportional to the 4th power of its temperature**

- **Stefan-Boltzmann Law:** $q_{rerad} = \varepsilon \sigma T^4$

    - where ε is the emissivity of the TPS (ε = 1 for a blackbody), σ is the Stefan-Boltzmann constant (σ = 5.67e-8 W/m^2/K^4), and T is the wall temperature (assumes the ambient temperature is much lower)

- **The wall heat flux balance is in general given by the sum of heat into the material minus reradiation, conduction, and material response. A primary function of TPS is to minimize conduction (good insulator), and thus, neglecting material response we can assume that:**

$$q_{rerad} \sim q_{conv} + q_R$$

which can readily be solved for Tw.

- **Examples:**
    - Orbiter peak heating (Tw = 1600 K)
    - MER peak heating (Tw = 1725 K)
    - Orion peak heating (Tw = 3360 K)
        - by this point we are overpredicting by ~20% due to material response effects

- **For the Shuttle-Like entry previously studied, what is the stagnation point heating rate and the wall temperature at 60 km altitude? Assume a 1m nose radius and a TPS emissivity of 0.8**

  - ρ = 3.1459e-4 kg/m^3
  - V = 3.535 km/s
  - q_w = 1.7415e-4*(3.1459e-4/1)$^{0.5}$*(3535)^3 = 13.6 W/cm^2 (Sutton-Graves)
  - q_R = 0 (Tauber-Sutton)
  - T_w = [(13.6*1e4)/(0.8*5.67e-8)]$^{0.25}$ = 1316 K

Further Reading

Engineering Methods

- Tauber, M., "A Review of High-Speed, Convective Heat Transfer Computation Methods," NASA TP-2914, Jul. 1989.

- Tauber, M., Bowles, J., and Yang, L., "Use of Atmospheric Braking During Mars Missions," *Journal of Spacecraft and Rockets*, Sept.-Oct. 1990, pp. 514-521.

- Tauber, M., Yang, L. and Paterson, J., "Flat Surface Heat-Transfer Correlations for Martian Entry," *Journal of Spacecraft and Rockets*, March-April 1993, pp.164-169.

- Compton, D. L. and Cooper, D. M., "Free-Flight Measurements of Stagnation Point Convective Heat Transfer at Velocities to 41,000 ft/sec," NASA TN D-2871, Jun. 1965.

- Marvin, J. G. and Deiwert, G. S., "Convective Heat Transfer in Planetary Atmospheres," NASA TR R-224, Jul. 1965.

- Kaattari, G. E., "Effects of Mass Addition on Blunt Body Boundary Layer Transition and Heat Transfer", NASA TP-1139, 1978.

- Tauber, M. E. and Sutton, K., "Stagnation Point Radiative Heating Relations for Earth and Mars Entries", Journal of Spacecraft and Rockets, Jan.-Feb. 1991, pp. 40-42.

- Page, W. A. and Woodward, H. T., "Radiative and Convective Heating during Venus Entry", AIAA Journal, Oct. 1972, pp.1379-1381.

- Tauber, M. E., "Some Simple Scaling Relations for Heating of Ballistic Entry Bodies", Journal of Spacecraft and Rockets, July 1970, pp. 885-886.

- Chapman, G.T., "Theoretical Laminar Convective Heat Transfer & Boundary Layer Characteristics on Cones at Speeds to 24 km/s," NASA TN D-2463, 1964

- Sutton, K. and Graves, R.A., "A General Stagnation Point Convective Heating Equation for Arbitrary Gas Mixtures," NASA TR- R-376, 1971

- Fay, J.A, and Riddell, F.R, "Theory of Stagnation Point Heat Transfer in Dissociated Air," *J. Aeronautical Sciences*, **25**, 1958, pp. 73-85,121.

Lecture #2: Distributed Heating and Trajectory Effects

Distributed Heating - Sphere

- **It can be shown that the heat transfer rate along the body varies according to**

$$\frac{q}{q_{stag}} \approx \cos\theta$$

   for angles as large as 45° (in theory) and 70° (in practice)

- **This expression permits us to integrate the total heat flux into a spherical nose as**

$$\int q\,dA = q_{stag} \int \cos\theta\,dA$$

$$dA = 2\pi y R_n\,d\theta = 2\pi R_n^2 \sin\theta\,d\theta$$

$$\int q\,dA = 2\pi R_n^2 q_{stag} \int_0^{\pi/2} \sin\theta \cos\theta\,d\theta = \pi R_n^2 q_{stag}$$

- **For a laminar boundary layer, the heat input to a hemisphere is ~ equal to the product of stag. point heating times the projected area**

Distributed Heating - Sphere (2)
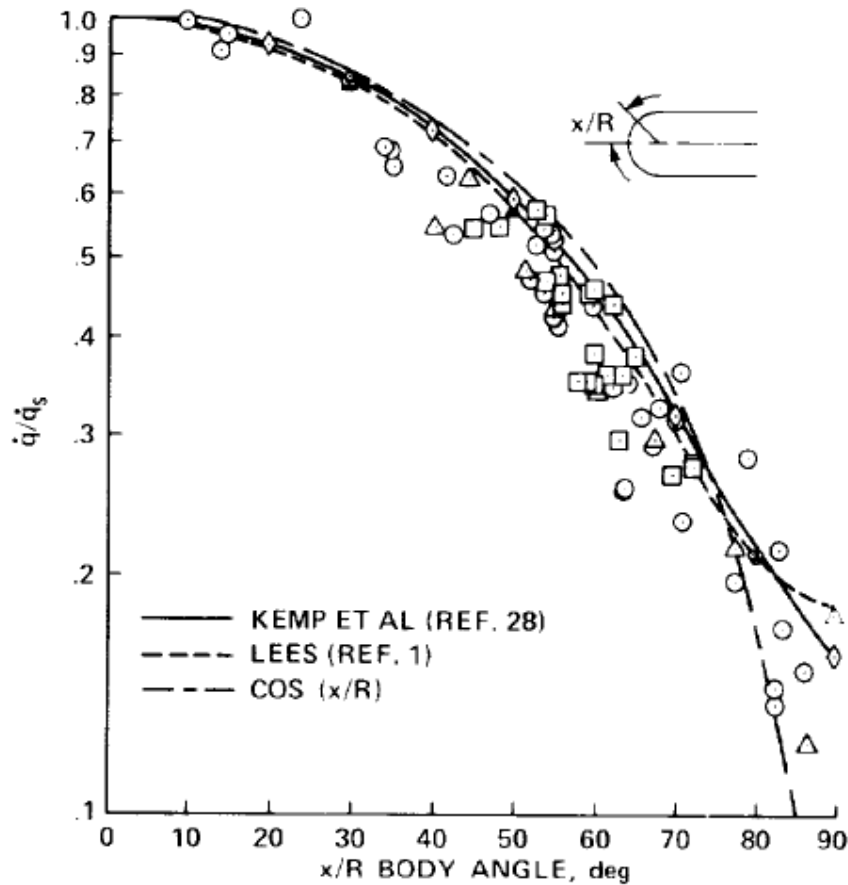
Figure 5.– Heat-transfer distribution on hemisphere cylinder. (From ref. 28; reprinted with permission of The American Institute of Aeronautics and Astronautics.)
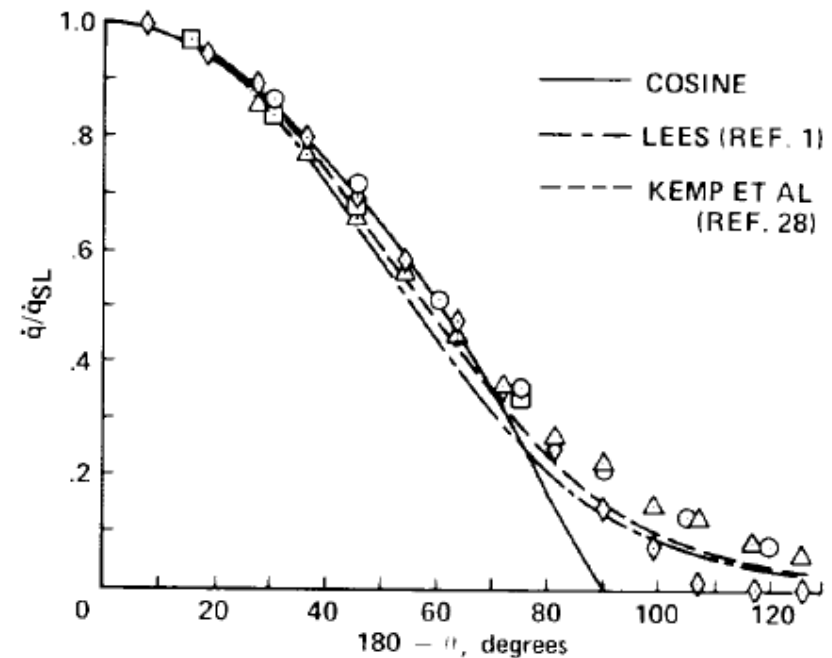
Figure 6.– Comparison of predicted and measured heat flux distributions on a circular cylinder normal to a stream.

Local Similarity - Flat Faced Cylinder

- **Local similarity methods (see e.g. Anderson) can be extended to other geometries**

- **Take for example a flat-faced cylinder with a rounded corner**

- **For this case, local similarity theory (and more sophisticated methods) show that the stagnation point is not the highest heating location; rather heating is higher on the corner**

  – Physically, the large favorable pressure gradient causes the boundary layer to thin. This increases the magnitude of ∇h, which increases heat transfer per previous arguments. The magnitude of increase is inversely related to the radius of curvature.

Distributed Heating - FF Cylinder (2)
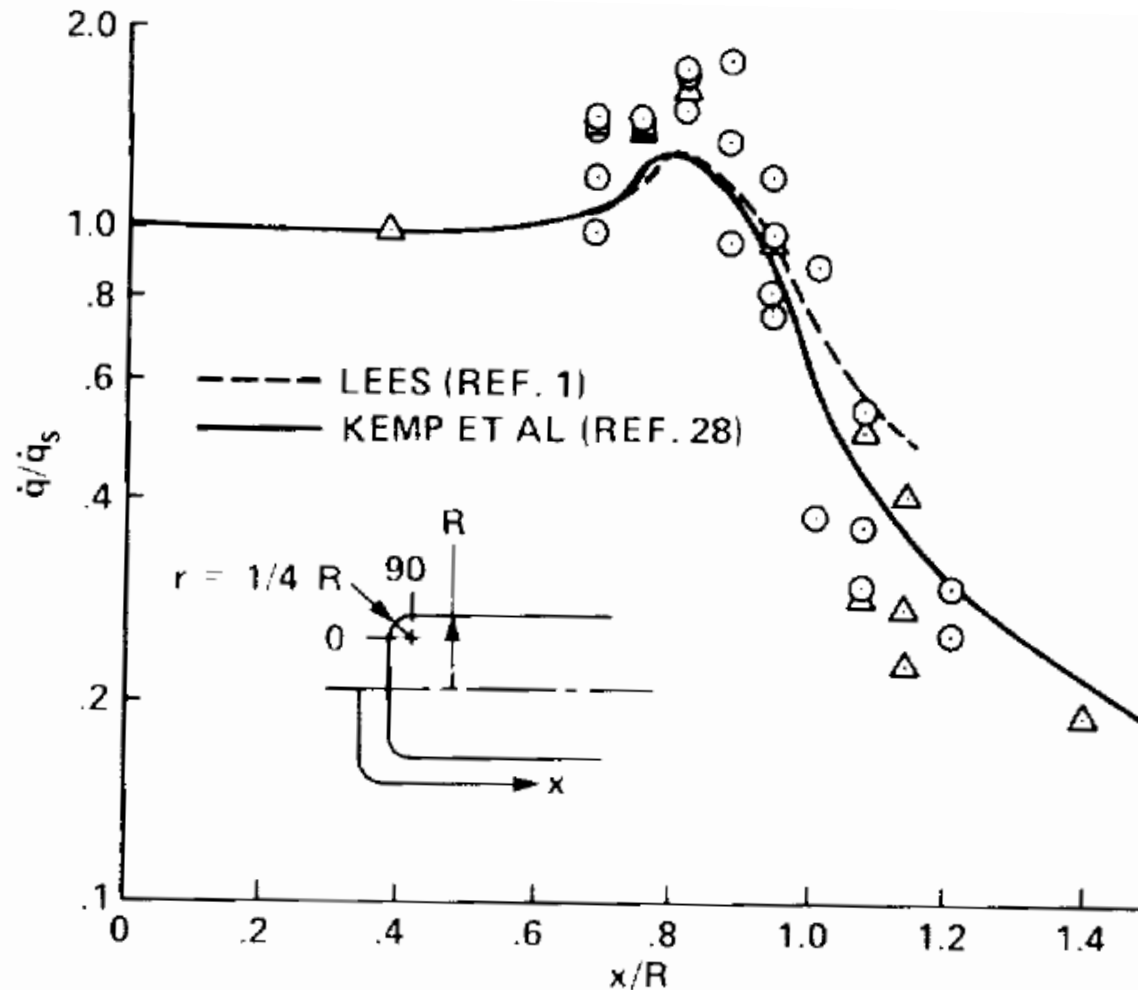
Figure 7.– Heat-transfer distribution on flat-nosed body. (From ref. 28; reprinted with permission of The American Institute of Aeronautics and Astronautics.)

Distributed Heating - Approximate Methods

- **Many other approximate methods have been developed for the calculation of heating on other geometries, e.g. wings, attachment lines.**

- **Detailed assessment is beyond the scope of these lectures, but the interested student can read further in:**

Tauber, M.E., "A Review of High Speed Convective Heat Transfer Computation Methods," NASA TP 2914, 1989

which is included as a handout for this course.

Real World Examples -
Laminar Flow

MSL Shape in T5
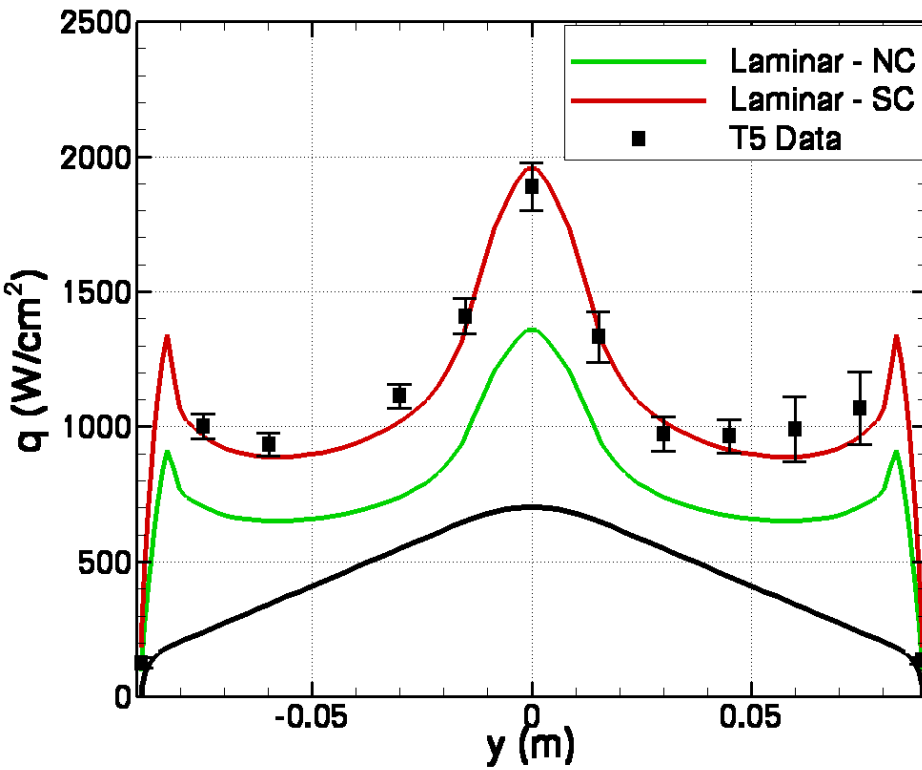
Predicted Stardust Heating
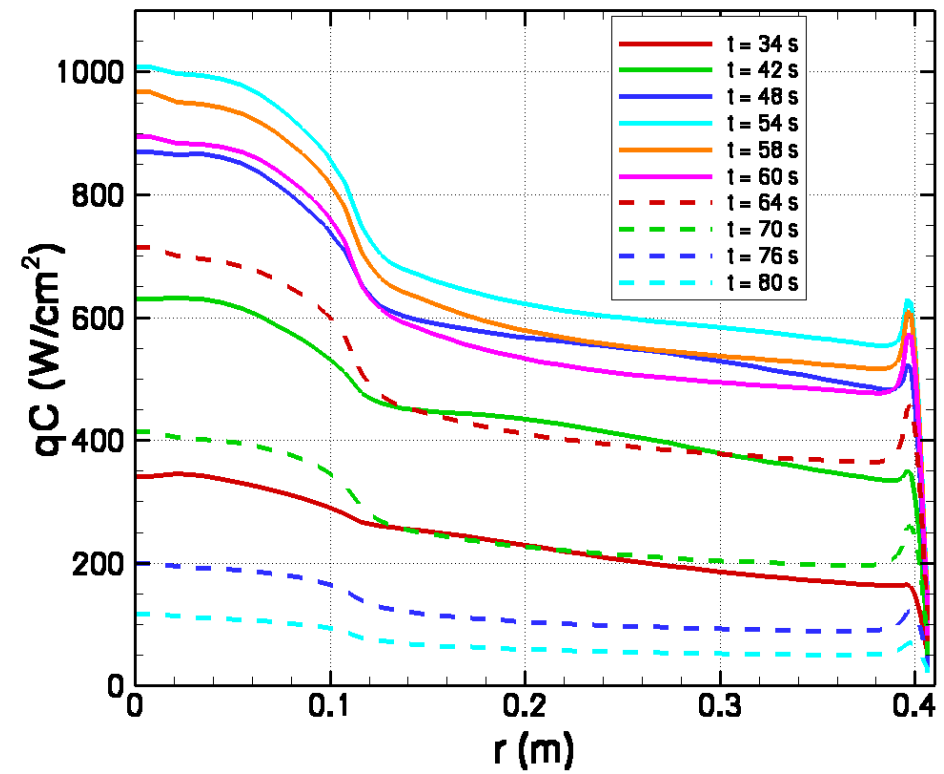
Trajectory Effects

- **The discussion up to now has focused on the calculation of an instantaneous heat flux (primarily at the stagnation point).**

- **However, the heating on the vehicle is obviously coupled to the trajectory flown, and thus it is important to develop expressions that quantify the relationship between heating and trajectory.**

- **You have already learned two basic trajectory equations (Allen-Eggers and Equilibrium Glide); lets start with Allen-Eggers**

- **For simplicity, lets use the simplest of convective heating relationships:**

$$q_s \sim (\rho)^{\frac{1}{2}} V^3$$

Intuition (1)

- **Two identical ballistic vehicles enter the atmosphere. One is on a steep entry trajectory and one is on a shallow entry trajectory. Which has the higher peak heat flux? Load?**

shallow γ

steep γ
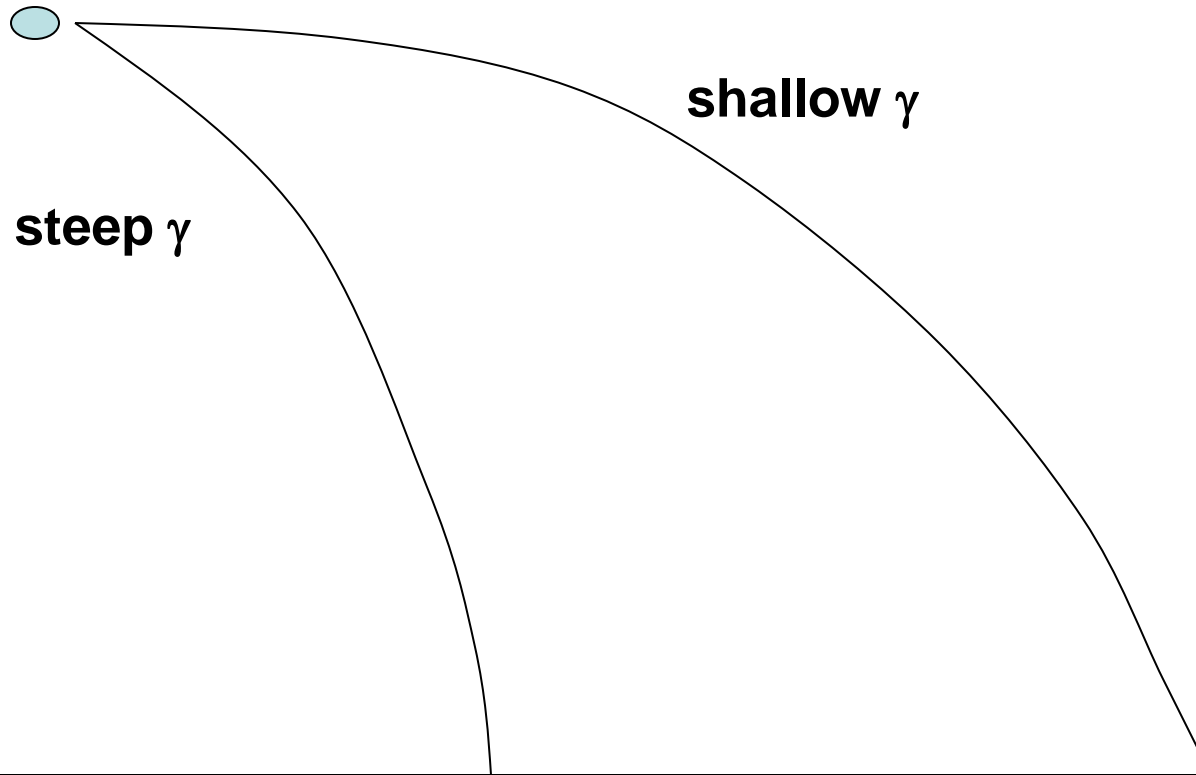
Intuition (2)

- **Two ballistic vehicles enter the atmosphere on an identical flight path angle. One has a higher ballistic coefficient. Which has the higher peak heat flux? Load?**

high β

low β
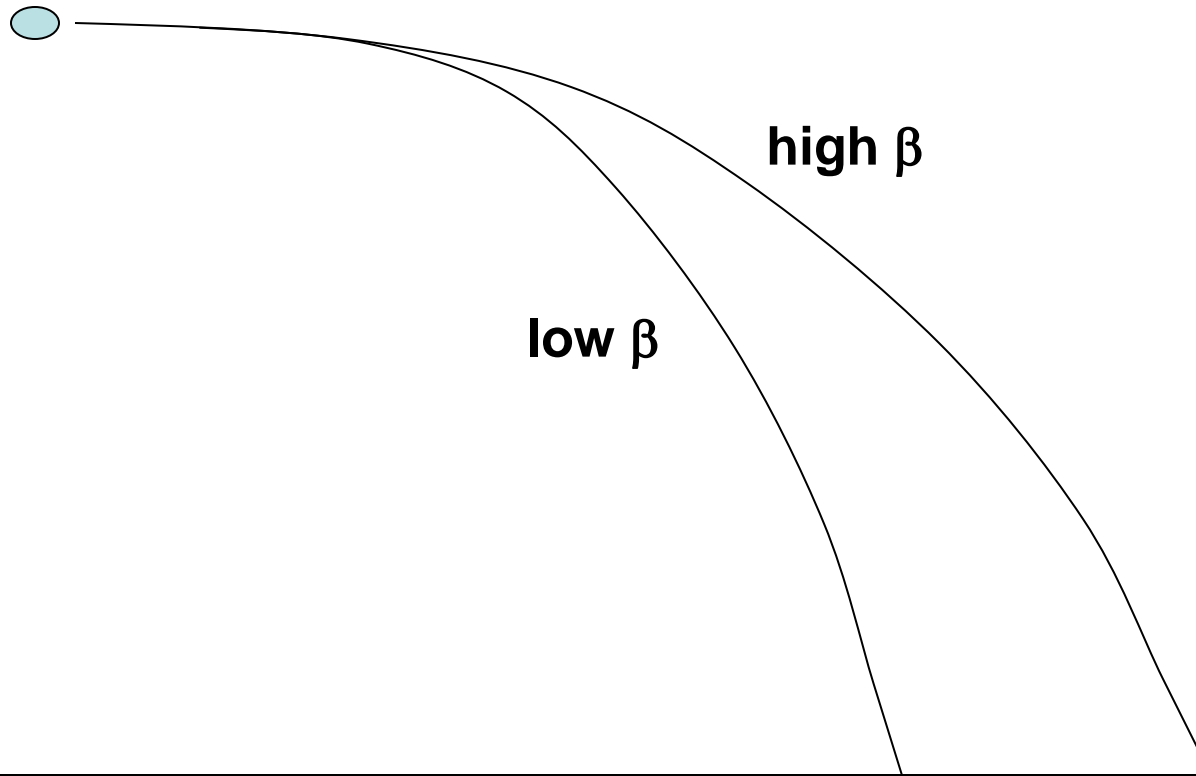
Allan-Eggers Trajectory Equation

$$V = V_{atm} \exp\left[Ce^{-h/H}\right] = V_{atm} \exp\left[C\frac{\rho}{\rho_o}\right]$$

$$C = \frac{H\rho_0}{2\beta\sin\gamma}$$

V_{atm} = Velocity at atmospheric interface
$\beta = m/C_D A$
Exponential atmosphere assumed
Ballistic entry

- **Substitute above for V into approximate heating equation:**

$$q_s \sim (\rho)^{\frac{1}{2}}\left(V_{atm}^3 \exp\left[3C\frac{\rho}{\rho_o}\right]\right)$$

- **Differentiate w.r.t density:**

$$\frac{1}{2}(\rho)^{-\frac{1}{2}}\left(V_{atm}^3 \exp\left[3C\frac{\rho}{\rho_o}\right]\right) + (\rho)^{\frac{1}{2}}\left(\frac{3C}{\rho_o}\right)\left(V_{atm}^3 \exp\left[3C\frac{\rho}{\rho_o}\right]\right) = \frac{dq_s}{d\rho}$$

Allan-Eggers Trajectory Equation (2)

- Looking for a maximum of q_s, which should occur when $dq_s/q\rho = 0$:

$$1 + 6C\frac{\rho}{\rho_o} = 0$$

- So the density of maximum convective heating is:

$$\rho^*_{q\,max} = -\frac{\rho_o}{6C} = \frac{\beta\sin\gamma}{3H}$$

- For a given atmospheric scale height, the density (altitude) of peak heating increases with ballistic coefficient and flight path angle

Allan-Eggers Trajectory Equation (3)

- **So, in the exponential atmospheric model**

$$\frac{\beta \sin\gamma}{3H} = \rho_o e^{-h^*/H}$$

$$-\frac{h^*}{H} = \ln\left(\frac{\beta \sin\gamma}{3H\rho_o}\right)$$

- **The altitude and velocity of peak heating are given by:**

$$h^*_{q\,\text{max}} = -H\ln\left(\frac{\beta \sin\gamma}{3H\rho_o}\right)$$

$$V^*_{q\,\text{max}} = V_{atm}\exp\left[\frac{C}{\rho_o}\left(\frac{-\rho_o}{6C}\right)\right] = V_{atm}e^{-1/6} = 0.846 V_{atm}$$

Allan-Eggers Trajectory Equation (4)

- As in the case of the previously derived expression for the velocity at peak deceleration, the velocity at peak heating is a function only of the entry velocity.

- Recall that $V_{gmax} = 0.606V_{atm}$. Therefore, peak heating occurs earlier in the entry than peak deceleration. In fact, it can be shown that

$$h^*_{q\,max} \approx 1.1 h^*_{g\,max}$$

- We are now in the position of being able to calculate the peak stagnation point convective heat rate for a ballistic entry vehicle

- Substitute the evaluated expressions for V_{qmax} and ρ_{qmax} into the Sutton-Graves Equation:

$$q_{s,max} = k\left(\frac{1}{R_n}\right)^{\frac{1}{2}}\left(\frac{\beta\sin\gamma}{3H}\right)^{\frac{1}{2}}\left(.6055V^3_{atm}\right)$$

- In addition to the nose radius dependence shown earlier, we now see that peak heating rate increases with increasing ballistic coefficient and flight path angle

Heat Load

- **Stagnation point heat load is just the time integration of the heat flux**

$$Q_s = \frac{k}{\sqrt{R_n}} \int \rho^{\frac{1}{2}} V^3 dt$$

- **How do we convert this to an integral that we now how to evaluate (redefine *dt* through change of variables)? Lets borrow some logic from the Equations of Motion:**

$$\sin\gamma = -\frac{dh}{ds} \; ; \qquad V = \frac{ds}{dt}$$

$$dt = \frac{ds}{V} = -\frac{dh}{V\sin\gamma}$$

- **Using the exponential atmosphere model we can write this in terms of dρ**

Heat Load (2)

- **Exponential atmosphere model**

$$\rho = \rho_o e^{-h/H}$$

- **Differentiate:**

$$\frac{d\rho}{dh} = -\frac{\rho_o}{H} e^{-h/H} = -\frac{\rho}{H}$$

- **Substitute into dt:**

$$dt = \frac{Hd\rho}{\rho V \sin\gamma}$$

- **Now we can substitute into the heat load integral:**

$$Q_s = \int q_s dt = \frac{k}{\sqrt{R_n}} \frac{V_{atm}^2 H}{\sin\gamma} \int_0^{\rho_o} \rho^{-\frac{1}{2}} \exp\left[\frac{2C\rho}{\rho_0}\right] d\rho$$

$$Q_s \sim k V_{atm}^2 \left[\frac{\beta}{R_n \sin\gamma}\right]^{\frac{1}{2}}$$

After some manipulation…

Heat Rate vs Heat Load

- **Quantitative expression can be derived from approximate evaluation of the integral:**

$$Q_s \approx k V_{atm}^2 \left[\frac{\beta}{\rho_o} \left(\frac{\pi H}{R_n \sin\gamma} \right) \right]^{\frac{1}{2}}$$

k is the Sutton-Graves constant

- **Compare the derived expressions for heat rate and heat load:**

$$q_{s,\max} = k \left(\frac{1}{R_n} \right)^{\frac{1}{2}} \left(\frac{\beta \sin\gamma}{3H} \right)^{\frac{1}{2}} \left(.6055 V_{atm}^3 \right)$$

$$Q_s = k V_{atm}^2 \left[\frac{\beta}{\rho_o} \left(\frac{\pi H}{R_n \sin\gamma} \right) \right]^{\frac{1}{2}}$$

- **Heat rate increases with both β and γ, while heat load increases with β, but decreases with γ**

- **This leads to a second mission design trade (the first was R_n and its impact on drag, convective heating, and radiative heating):**

- **The selection of γ becomes a trade between peak heat rate (TPS material selection), and total heat load (TPS thickness and mass)**

So, Did you get it Right? (1)

- **Two identical ballistic vehicles enter the atmosphere. One is on a steep entry trajectory and one is on a shallow entry trajectory. Which has the higher peak heat flux? Load?**

shallow γ Higher Peak Heat Load

steep γ

Higher Peak Heat Flux
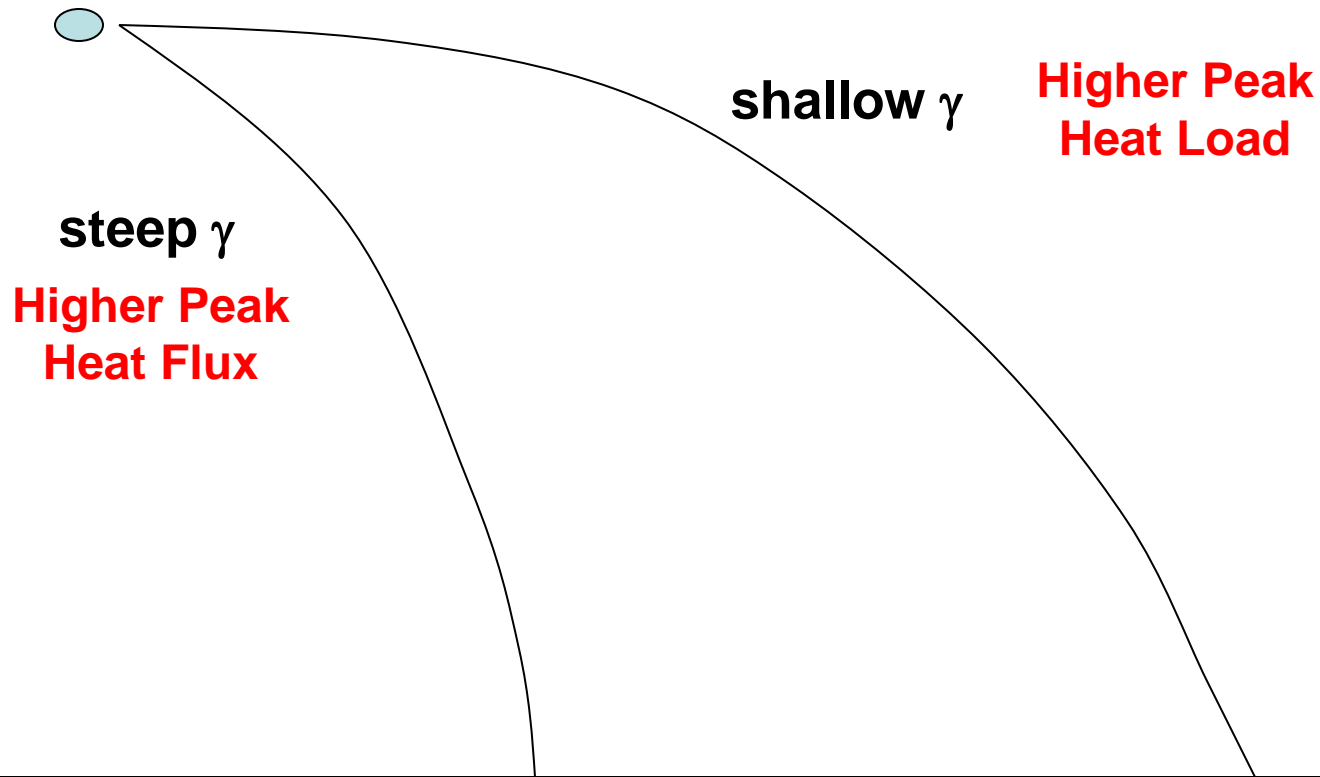
So, Did you get it Right? (2)

- **Two ballistic vehicles enter the atmosphere on an identical flight path angle. One has a higher ballistic coefficient. Which has the higher peak heat flux? Load?**

high β

Higher Peak Heat Load

Higher Peak Heat Flux

low β
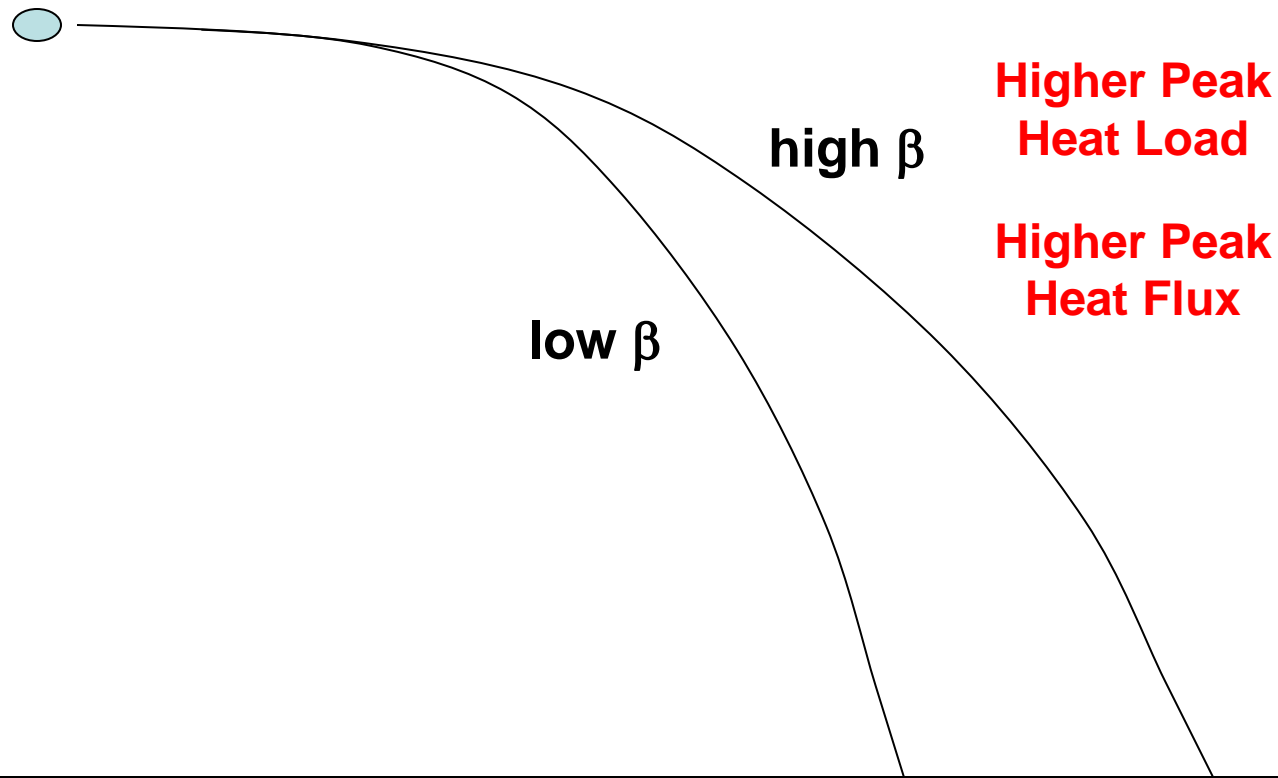
Mars Entry Heating - Example

Entry Flight Path Variation
$\beta = 90$ kg/m^2; $V_i = 5.5$ km/s
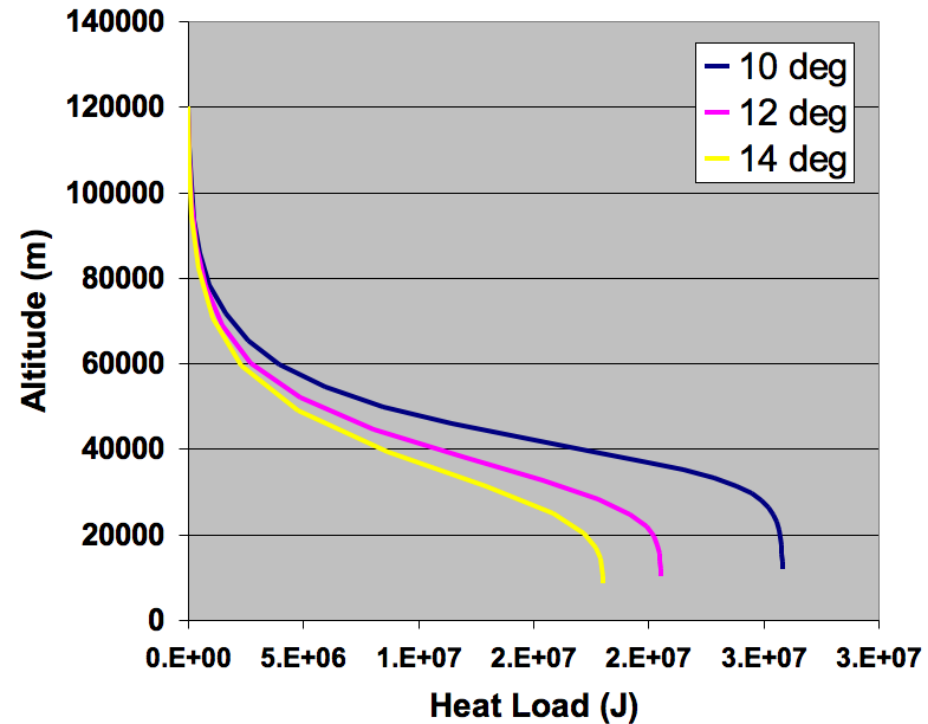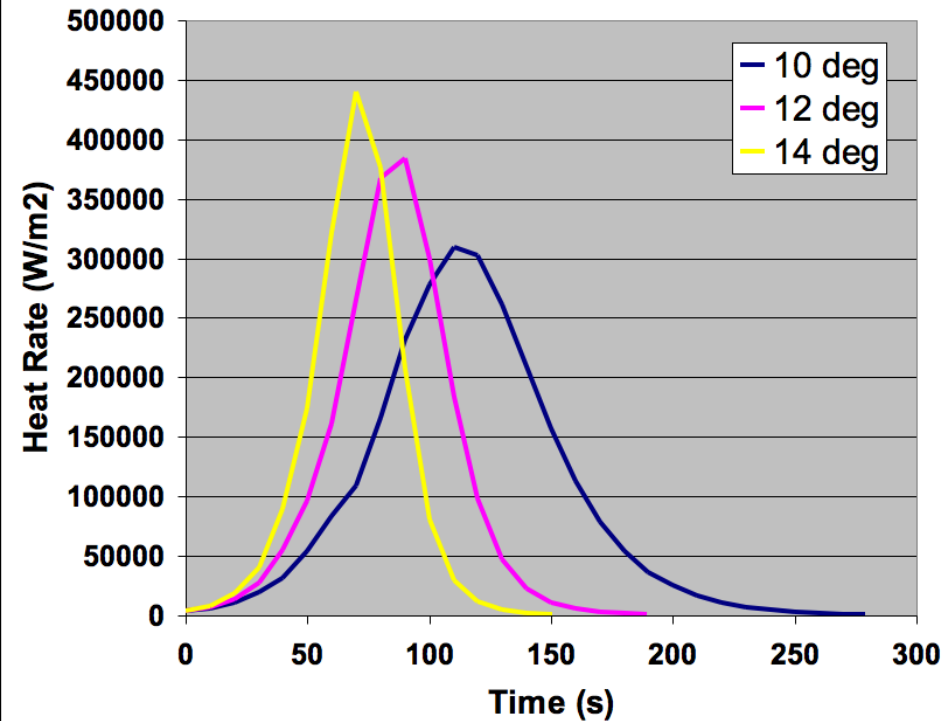
Heat rate falls and heat load grows as FPA decreases

Mars Entry Heating - Example

Ballistic Coefficient Variation

$\gamma = -12$ deg; $V_i = 5.5$ km/s
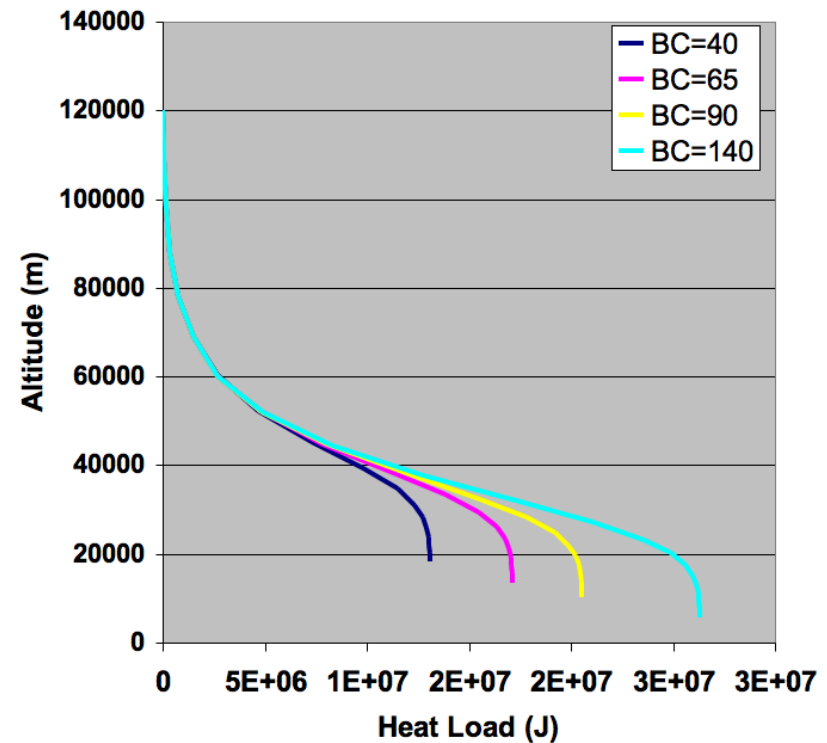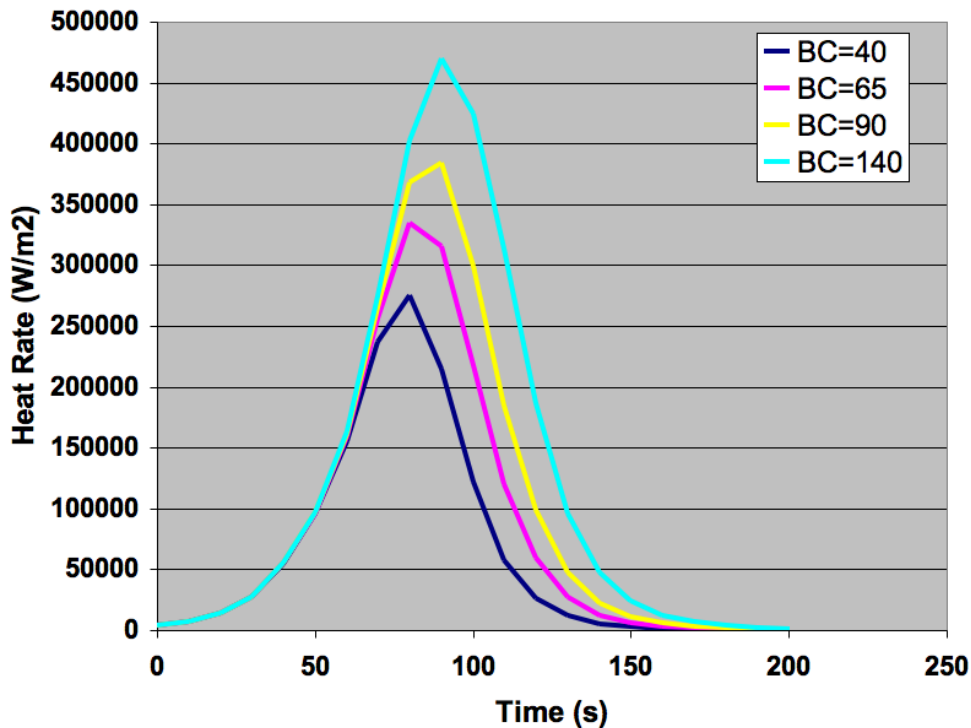
Rising ballistic coefficient raises heat rate and load

Equilibrium Glide Entry

- **Can perform the same analysis of an equilibrium glide (lifting) entry**

- **Details are left as an exercise for the student**

$$V_{q\,\max}^{*} = \sqrt{\tfrac{2}{3}}\,V_c \qquad \text{(for } V_{atm} \geq \sqrt{\tfrac{2}{3}}\,V_c)$$

$$q_{s\,\max} = 1.94 \times 10^4 \left[\frac{1}{R_n}\left(\frac{\beta}{L/D} \right) \right]^{\frac{1}{2}}$$

$$Q_s \approx 2.05 \times 10^7 \left[\frac{\beta}{R_n}\left(\frac{L}{D} \right) \right]^{\frac{1}{2}} \left[\sin^{-1}\left(\frac{V_{atm}}{V_c} \right) - \frac{V_{atm}}{V_c}\left(1 - \left(\frac{V_{atm}}{V_c} \right)^2 \right)^{\frac{1}{2}} \right]$$

- **Compare to Allen-Eggers; similar dependence on β, but a lifting body (L/D > 1) will have heat flux inversely dependent on L/D and heat load directly dependent on L/D**

Numerical Example: MER

- **What is the peak stagnation point heating for the MER example previously examined ($R_n = 0.5R_b$)?**

- **At peak heating:**

  V_{qmax} = 0.846*5.45 = 4.61 km/s

  R_n = 2.65/4 = 0.6625 m

  h = 40.87 km

  ρ = 3.11e-04 kg/m³

- **From the Allen-Eggers expressions derived herein:**

$$q_s = k\left(\frac{\rho}{R_n}\right)^{\frac{1}{2}} V^3 = 1.9027 \times 10^{-4}\left(\frac{3.11 \times 10^{-4}}{0.6625}\right)^{\frac{1}{2}} (4610)^3 = 40.4 \text{ W/cm}^2$$

$$T_w = \left(\frac{q_w}{\varepsilon\sigma}\right)^{\frac{1}{4}} = \left(\frac{40.4 \times 10^4}{0.8 \cdot 5.67 \times 10^{-8}}\right) = 1727K$$

(literature quoted values range from 40-44 W/cm² based on CFD)

Other Trajectory Effects

- **Prior discussion focused on impact of trajectory on stagnation point heating**

- **However, trajectory selection has other aerothermal impacts as well**

- **Transition to turbulence**
    - Can dramatically increase heating levels away from stagnation point (4-6 times laminar levels)
    - Governed by Reynolds number ($\rho u L/\mu$), therefore exacerbated by large entry bodies, steeper flight path angle, higher entry velocity, higher ballistic coefficient

- **Heat soak**
    - Longer trajectory time increases the amount soak of energy into the TPS, which increases the amount of TPS required to protect the structure (a given TPS tends to be less efficient as peak heat flux drops but heat load stays constant)

Orbiter Thermal Imagery

Stagnation Point (Laminar)

Turbulent flow from wing BLT protuberance

Turbulent flow from unknown origin

STS-119
Mach ~ 8.5
Mar 28, 2009
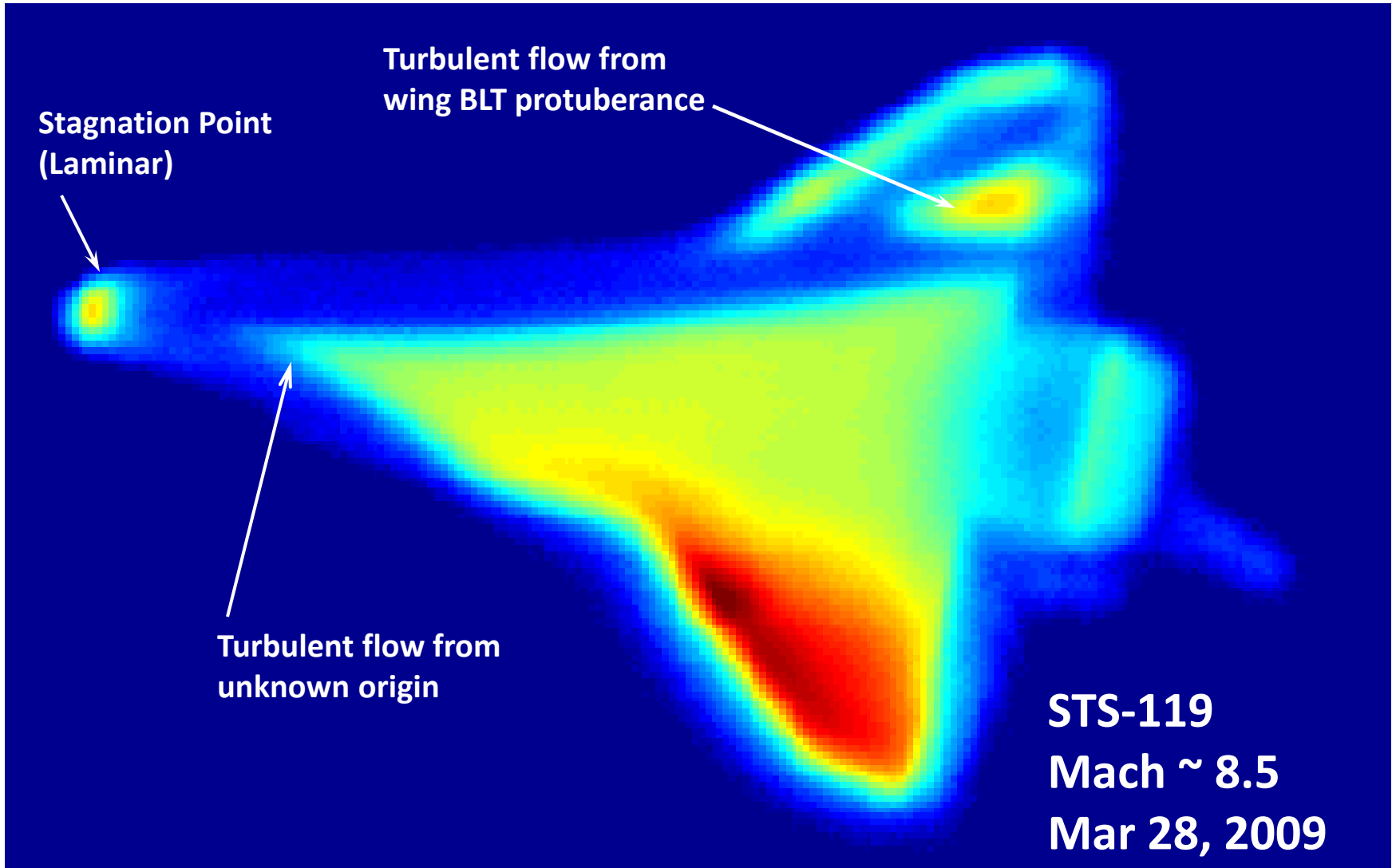
Review: 20 minutes of Peter Parameter

Lecture #3: Advanced Topics

CFD Process for Entry Vehicle Design

➤ **High fidelity CFD tools based on 20-year old methodologies**

➤ **Recent advances in parallel computing, efficient implicit algorithms have enabled rapid turnaround capability for complex geometries**

➤ **Full body three-dimensional CFD is an integral part of the design of all planetary and Earth entry TPS**

Shuttle RCC Repair Concept Evaluation

T_i 2200 2300 2400 2500 2600 2700 2800 2900 3000 3100 3200

$T_{max} = 3115.1\ °F$

Centerline Cavity

Acreage Cavity
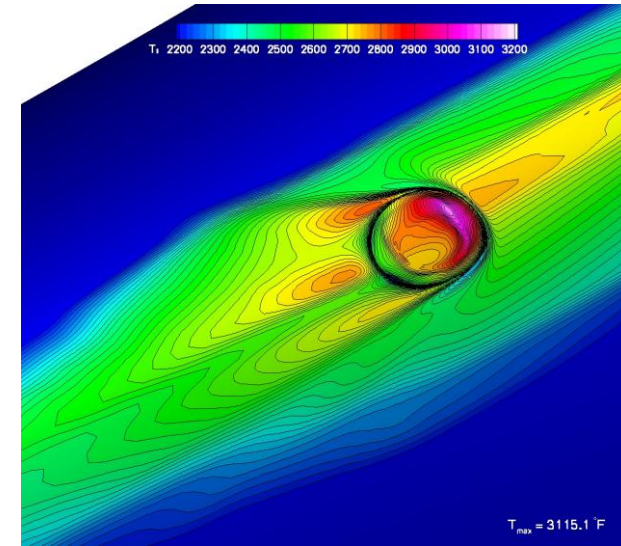
Genesis Penetration Analysis

$q\ (W/cm^2)$
200
190
180
170
160
150
140
130
120
110
100
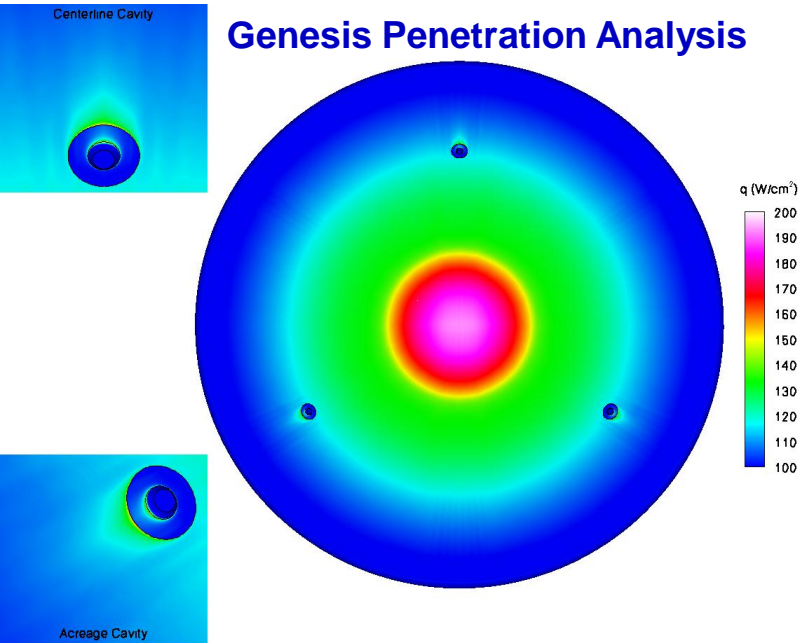
Arc Jet Model Simulation

Test model

Inlet conditions

Nozzle flow CFD simulation

Model CFD simulation

Arc jet test
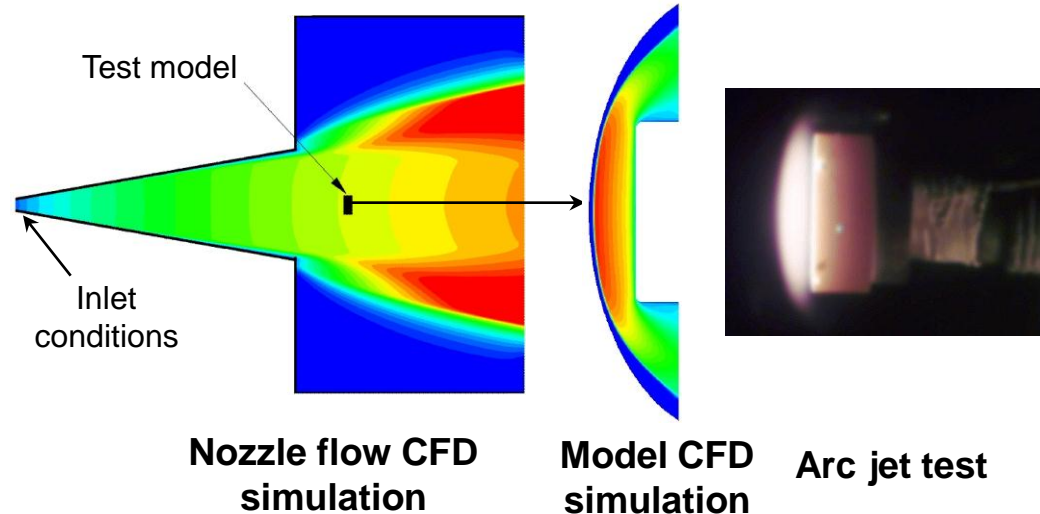
Identification of Aerothermal Modeling Needs for Entry Missions

♦ **Needs are both physics and process driven**
- process improvements are important for modeling complex geometries - not covered in this presentation
- physical model improvements are important across the spectrum of NASA missions

♦ **Gaps are destination <u>and</u> mission specific**
- shock layer radiation in particular will dominate aeroheating for some missions and be unimportant for others
- sensitivity analysis must be performed for each candidate mission

♦ **Gaps can be divided into general categories**
- reacting gas physical models
- surface kinetics
- transition and turbulence
- afterbody heating
- shock layer radiation modeling
- coupling between radiation/material response/fluid dynamics/aerodynamics
- unsteady separated flows (wakes, control surface shock-BL interaction)
- geometry effects

Turbulence: The Eyeball…

70° Sphere-Cone:

Hypersonic Flight in Ballistic Range

Orbiter Thermal Imagery

Stagnation Point (Laminar)

Turbulent flow from wing BLT protuberance

Turbulent flow from unknown origin

STS-119
Mach ~ 8.5
Mar 28, 2009
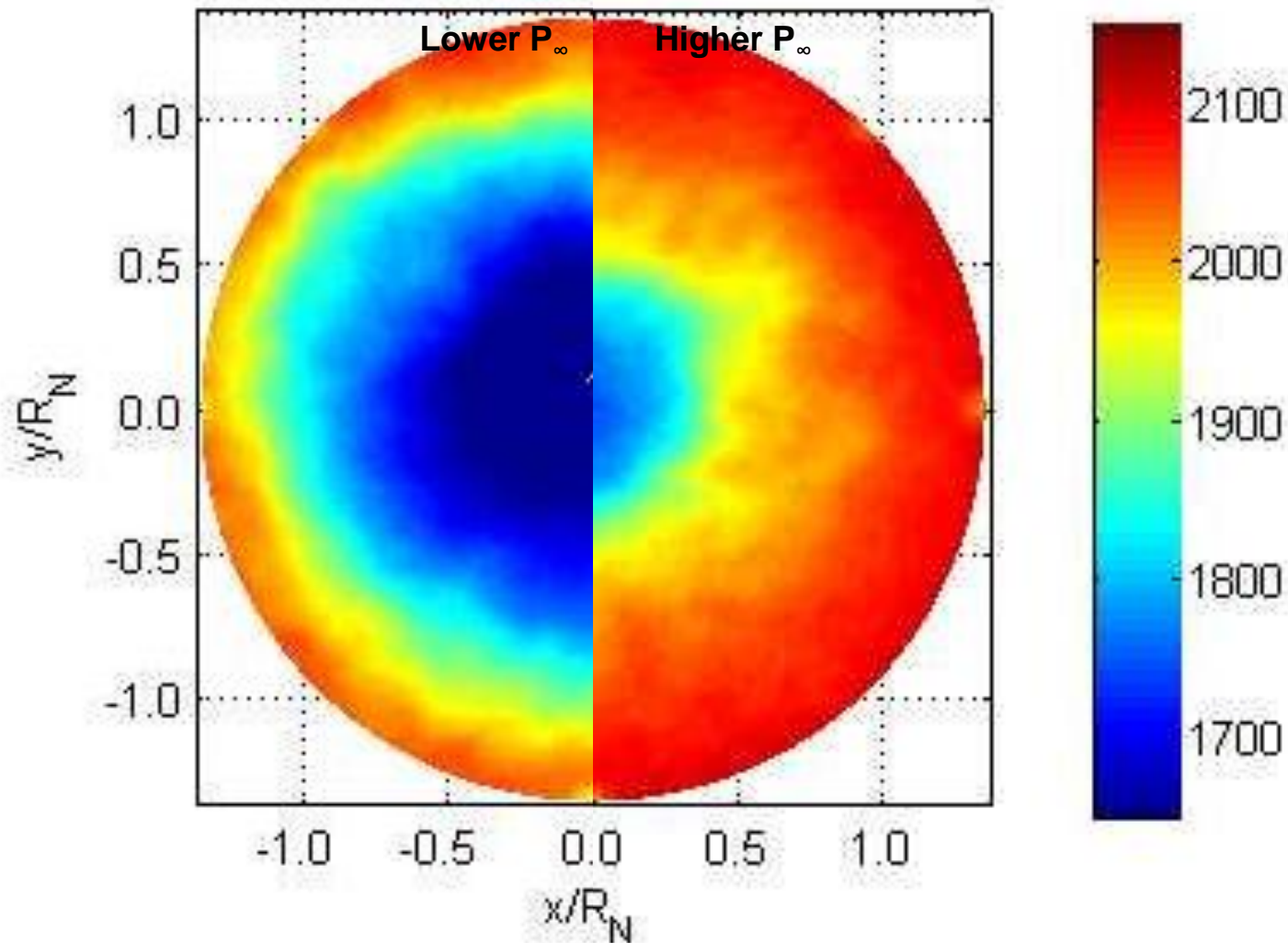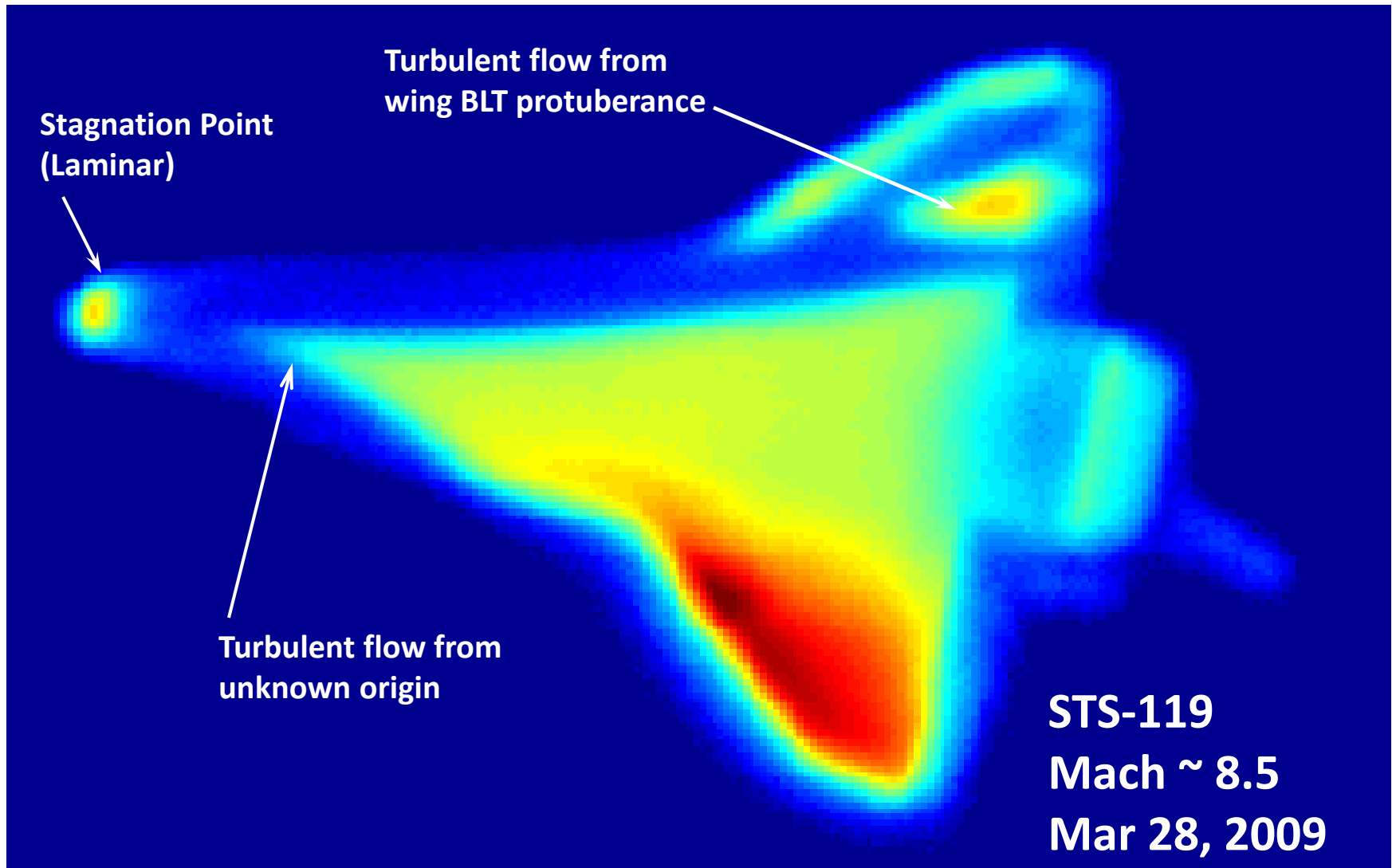
Status and Remaining Gaps

70° Sphere-Cone:

Hypersonic Flight in Ballistic Range

Transition Front
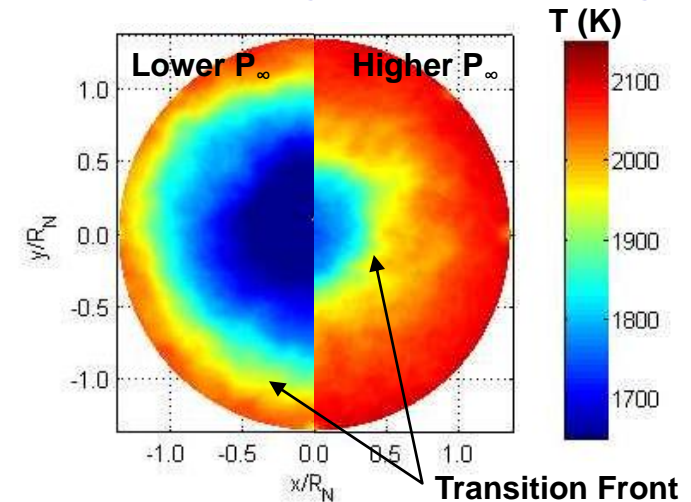
Mars Science Laboratory
Peak Heating Condition

Laminar   Turbulent

Stagnation Point
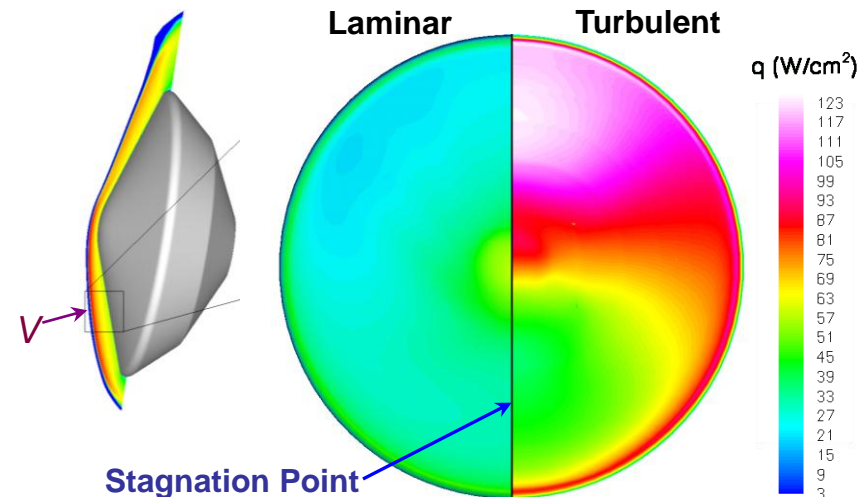
➤ **Transition is less of a concern for blunt capsules**
- shorter trajectories, smaller surface area leads to less heat load augmentation
- single use ablative TPS can withstand heating if mass penalty not large – design to fully turbulent

➲ **Conclusion: Transition cannot be accurately predicted for most problems of interest. Designs must rely on testing and conservatism.**

➤ **Acreage turbulent heating predictions generally within 25% for orbital Earth entries (RANS), but additional developments are required for chemistry, blowing, roughness**

➤ **DNS, LES, DES type models under development to replace current RANS**

Turbulent Heating:
Effects of Surface Roughness

- **Previous discussion centered on smooth wall turbulence**
- **However, all ablators develop a roughness pattern that can augment heating**
- **Analysis for MSL based on correlations from WT experiments and DoD RV data**
  - 1mm roughness → potential for up to 50% augmentation to baseline smooth wall predictions
  - if true, roughness has eaten up entire turbulent heating uncertainty!
- **Roughness can also lead to a positive feedback loop → vortical structures are generated that augment roughness**

Effects of Roughness on Heating

Smooth Wall Heating

Rough Wall Heating

qw (W/cm^2)

240
220
200
180
160
140
120
100
80
60
40
20
0

1.4

1.3

1.2

from Brown, ARC
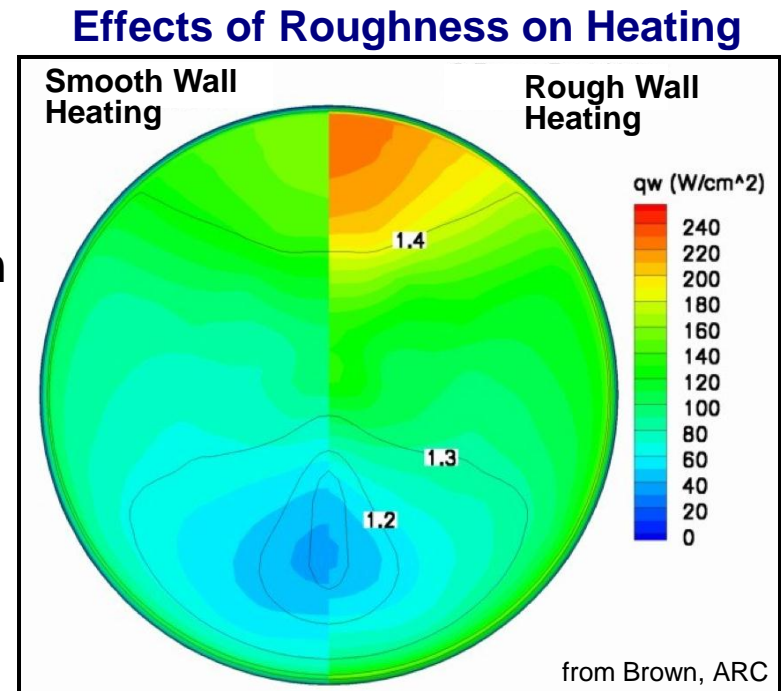
Surface Catalysis

➢ **No validated model exists for Mars:**

   $CO + O; \quad O + O; \quad CO + O_2$
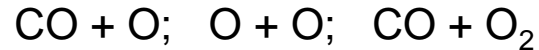
➢ **As a consequence, Mars entry vehicles are designed assuming a worst case scenario**
   – so called "supercatalytic" wall

➢ **For MSL there is a factor of four difference in heating between the various models**

Parametric Analysis of Catalytic Heating

Impact of Catalysis Model on Heating
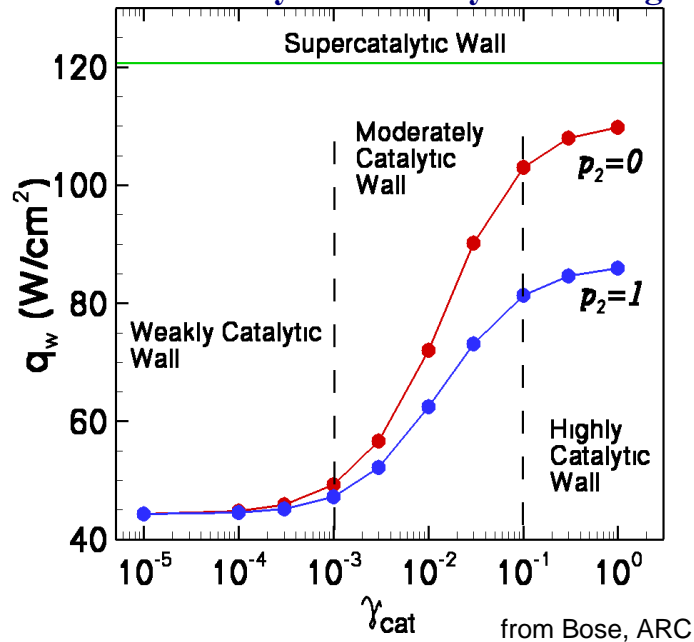
➢ **What are the key gaps?**
   – quantum chemistry to determine reaction rates (gas phase and gas-surface)
   – MD simulations of key GSI processes
   – experimental data on TPS materials at relevant conditions

Afterbody Heating

➢ **Wake flows are much harder to simulate than forebody**
  – separated, low density, unsteady, nonequilibrium flowfield
  – significant code-to-code differences still exist

➢ **Current uncertainty levels ~50-300%**
  – primary reason: lack of validation; we have not quantified how good (or bad) we are

MSL Afterbody Heating

from Edquist, LaRC

CFD Validation with AS-202 Flight Data
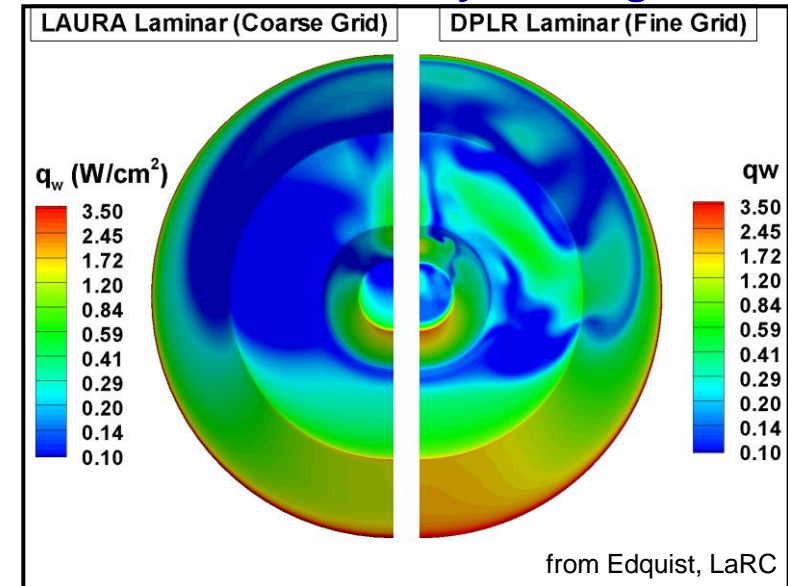
➢ **What are the key gaps?**
  – additional ground test data (including free flight or stingless models)
  – explore advanced methods (DES, LES) for hypersonic separated flows
  – advocate for additional flight data

Singularity Heating

➢ **Now throw OML singularities (such as RCS thrusters) into the wake flow**

– does not make things easier!

➢ **MSL is actively guided; thrusters must fire during hypersonic entry**

– predicted locally high heating rates necessitated a late change in backshell TPS for MSL (with significant cost and mass penalty)

RCS Thruster Impingement Heating (No Margin)

q_{max}=33 W/cm^2

q_w (W/cm^2)
33.000
18.478
10.347
5.794
3.244
1.817
1.017
0.570
0.319
0.179
0.100

from Dyakonov, LaRC

MSL RCS Thruster Design (Preliminary)
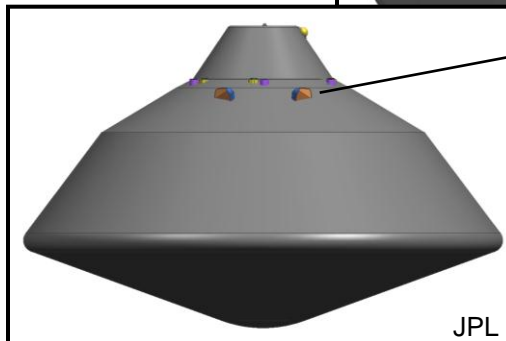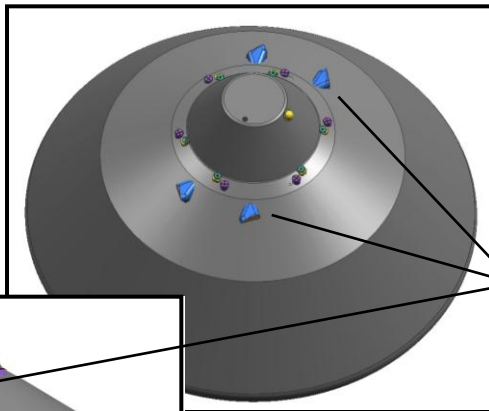
JPL

➢ **MSL backshell design requires canted thrusters for control authority**

➢ **Thrusters sticking into the flow; must be designed to withstand aerothermal environment**

– no validation of our methods for this application
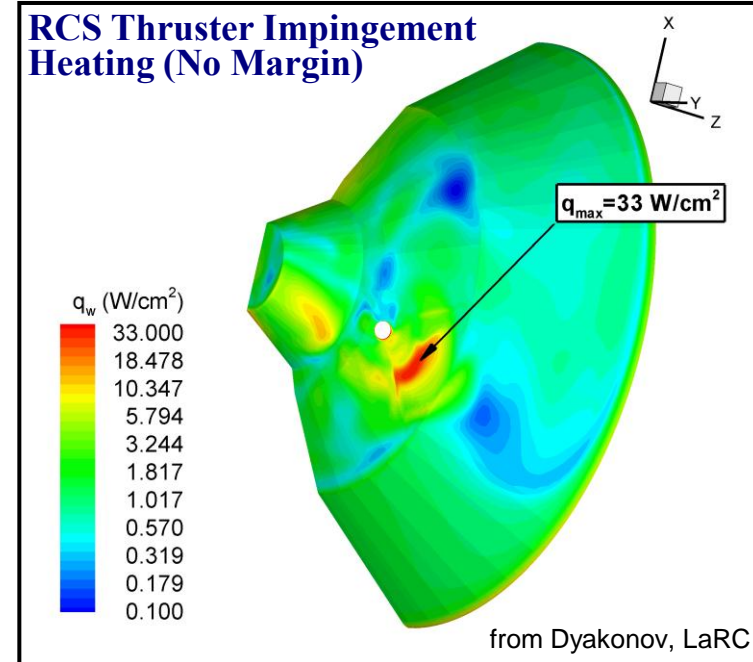
Shock Layer Radiation

➢ **Shock layer radiation is highly non-equilibrium, non-blackbody**
  – Titan analysis showed order of magnitude differences between equilibrium&accurate model

➢ **Not important for Mars missions to date, but critical for HMMES**
  – importance increases with velocity & vehicle size
  – primary radiator, CO(4+) emits in UV
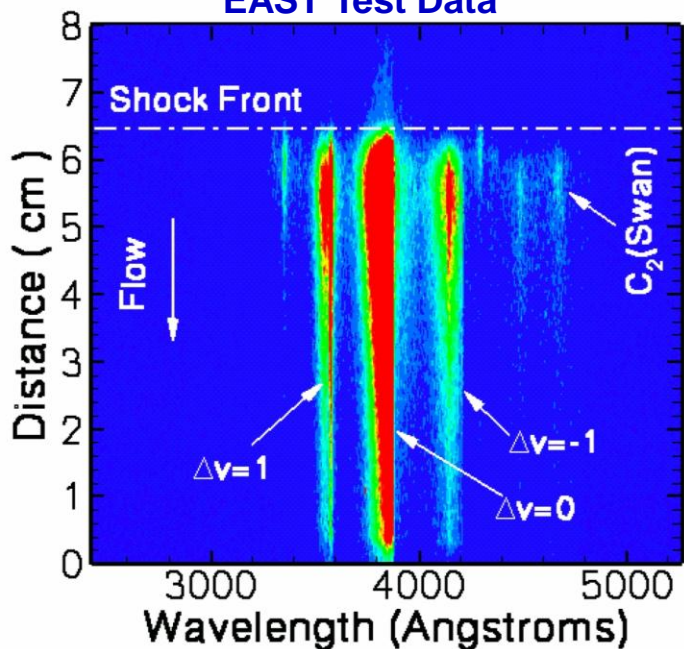
CN Radiation Model Validation

2%CH$_4$/98%N$_2$
5.15 km/s, 0.1 Torr
Spec. Range: 400-430 nm

Boltzmann

CR-Models

Experiment

Solid: NASA Ames
Dashed: Ecole Centrale
DashDot: EADS

EAST Test Data

Shock Front

Flow

$\triangle v = 1$

$\triangle v = 0$

$\triangle v = -1$

C$_2$(Swan)

from Bose, ARC
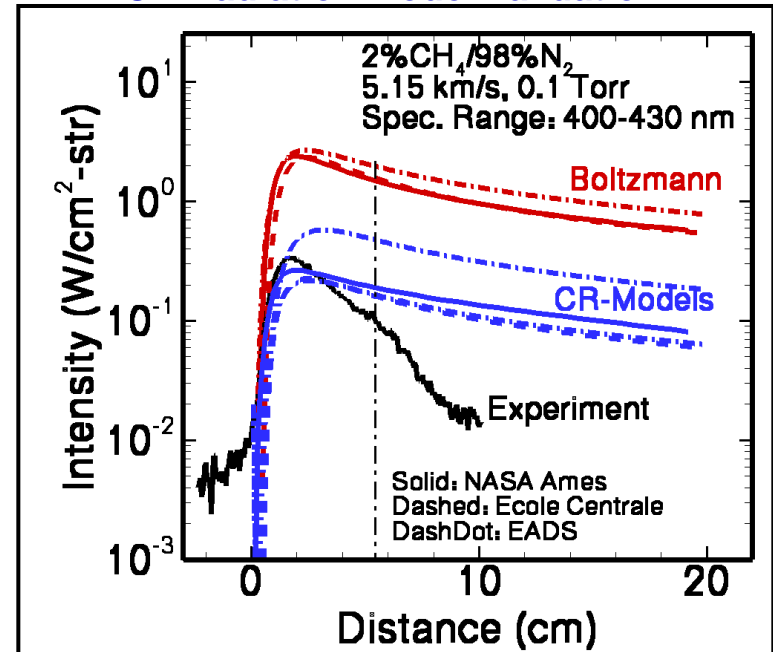
➢ **What are the key gaps?**
  – obtain additional shock tube data for Mars entries
  – build collisional-radiative models for all atomic and molecular radiators
  – compute excitation rates from QM
  – develop medium-fidelity methods for design
  – develop models for coupling to fluid dynamics

Flowfield-Radiation-Ablation Coupling

Titan Radiation Coupling
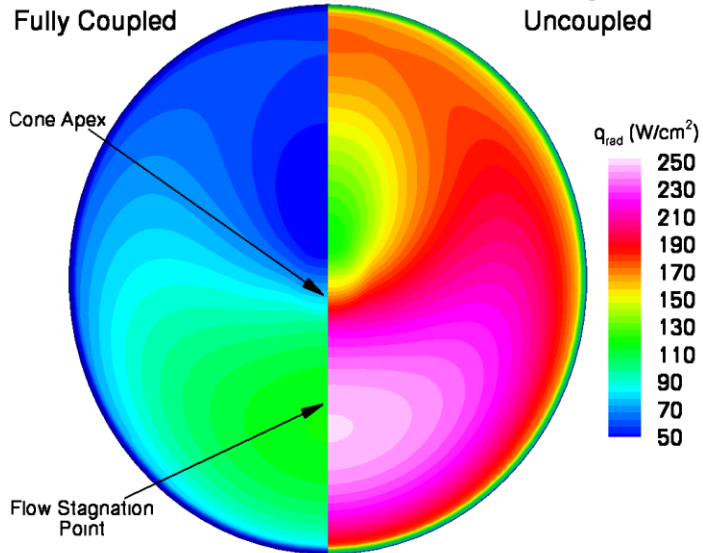
Stardust Ablation Coupling
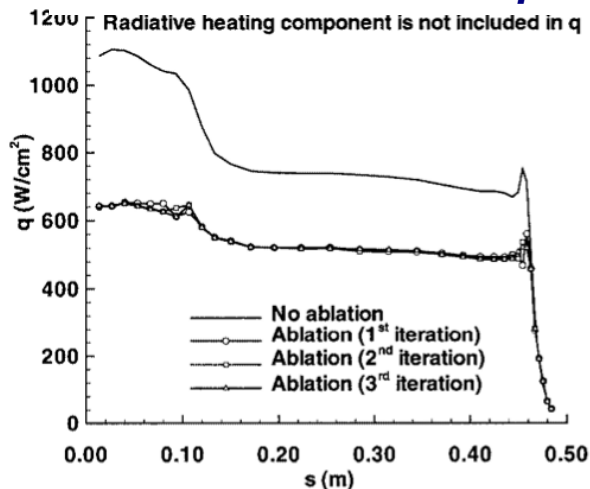
➢ Flowfield-Radiation (adiabatic cooling)
- Engineering approximation

$$\Gamma = 2q_{rad}/(\tfrac{1}{2}\rho_\infty V_\infty^3) \qquad q_{coup}/q_{unc} = 1/(1 + \upsilon\Gamma^{0.7})$$

- Loose coupling is also possible
- More accurate answer requires simultaneous solution of the Navier-Stokes and radiative transfer equations; not possible except for limiting cases

➢ Flowfield-Ablation
- Blowing reduces heat transfer
- Ablation products mix with boundary layer gases
- Typically solved via loose-coupling approximation

➢ Radiation-Ablation
- Injected ablation products can absorb/emit radiation

➢ Ablation-Trajectory
- Significant ablation can lead to changes in aerodynamics/trajectory/GN&C
- Primarily a concern for RV's

TPS – Boundary Layer Interaction

➤ **We have already discussed gas-surface and ablation coupling, but other interactions are important**

➤ **Ablation induced distributed roughness**
- Surface roughness generated on TPS surface as a consequence of ablation.
- Strong interaction with boundary layer - increased heating and shear stress result
- Heating augmentation from zero to factor of three possible over turbulent smooth wall

➤ **Discrete roughness**
- Due to gaps, repairs, geometrics singularities, etc.
- Generate local heating and shear augmentation factors which must be accommodated

➤ **For MSL:**
- Distributed roughness adds about 20% to heating (pattern roughness not expected)
- Discrete roughness adds another 40% locally in areas of gaps or repairs)

Pattern Roughness on RV Nosetip

Protruding Gap Filler in Arc Jet Test

TPS – Boundary Layer Interaction

➤ Melt layer interactions

- One class of ablators uses a glassy substrate material
- Energetically favorable; glass vaporization is highly endothermic
- Can cause strongly coupled instabilities in environments where glass melts but does not vaporize
- Interactions or instabilities can range from minor to catastrophic

➤ What to do?

- Simple solution: don't fly glassy ablators in such environments
- Better long term solution: develop models of the boundary layer surface interaction

Melt Flow induced by stream wise vortices

Flow
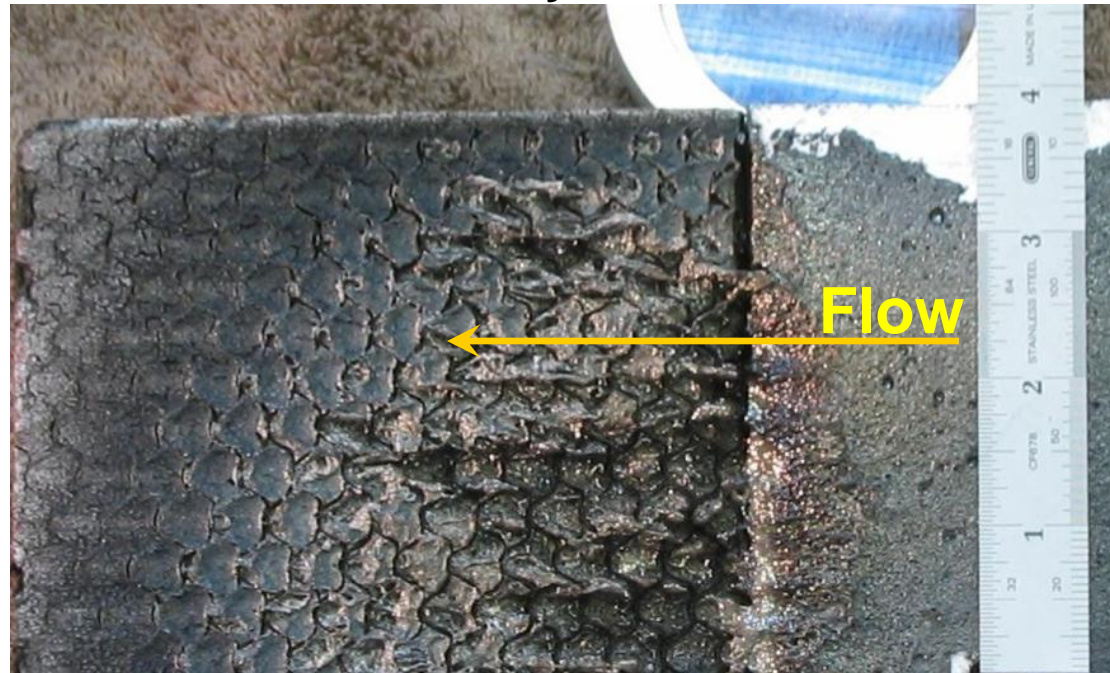
Research topic: Better models for all aspects of material / fluid interactions

Shape Optimization

➢ **The primary reason we continue to use 70° sphere cones for Mars entry is "heritage"**
  – argument is weak: clear finding of MSL aerothermal peer review last summer

➢ **Non-optimal from aerothermal perspective**
  – expansion around nose leads to boundary layer instabilities, early transition, high heating levels

➢ **Modified ellipsoid aeroshell has significant advantages with same aerodynamics**
  – for Mars aerocapture this shape led to 50% lower heat flux, potential 67% TPS mass savings
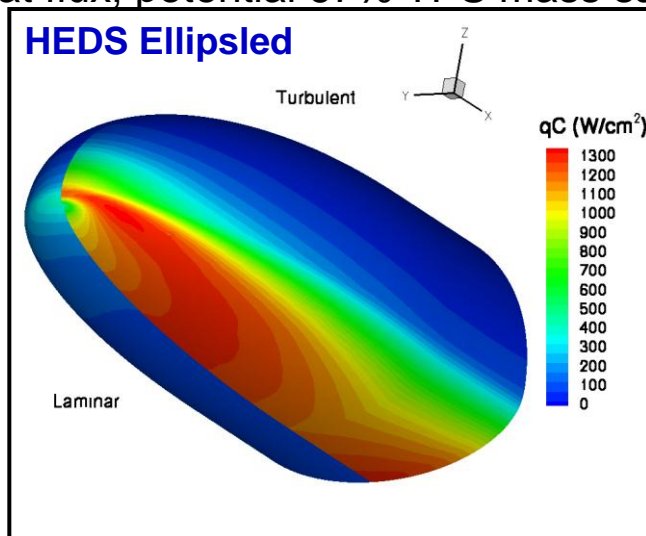
70° Sphere Cone vs. Ellipsoidal Aeroshell

from Brown, ARC
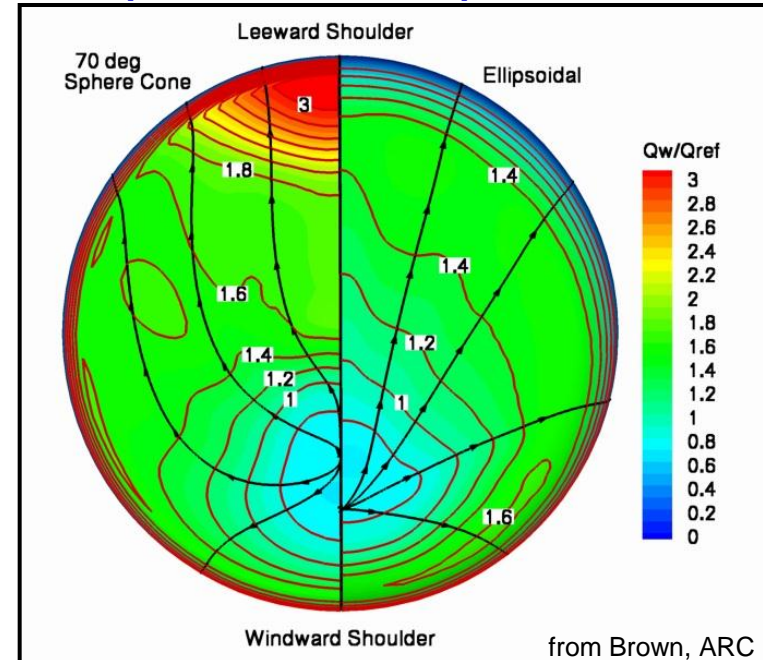
HEDS Ellipsled

➢ **For large entry masses other shapes (e.g. ellipsled, biconic, bent biconic) should be explored as well**

➔ **A full shape optimization study should be part of any future Mars systems analysis**

Validation:
AS-202 Flight Data

Afterbody Calorimeter Placement
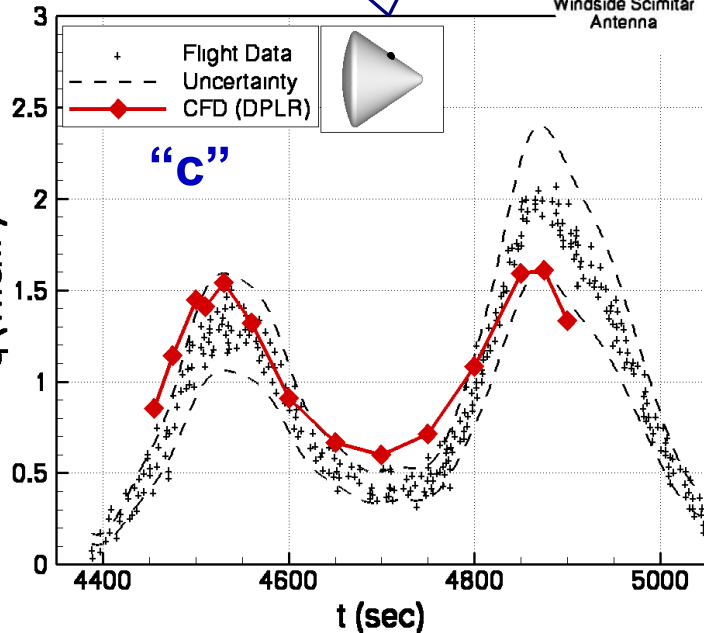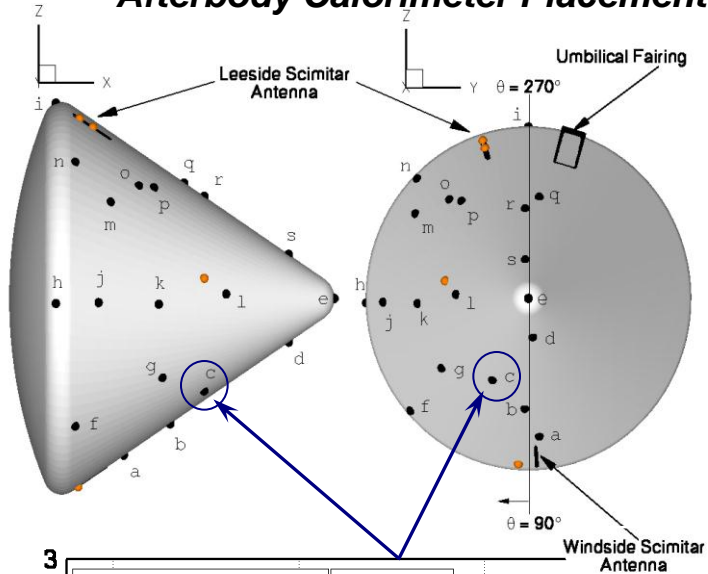
- **Problem:** Current uncertainty on afterbody heating predictions is very high

- **Goal:** reduce uncertainty levels by validation with flight data

Surface Oilflow
$t= 4900 \ s, Re_D = 7.6 \times 10^5$

T_w, K
200 300 400 500 600 700 800 900 1000 1100 1200
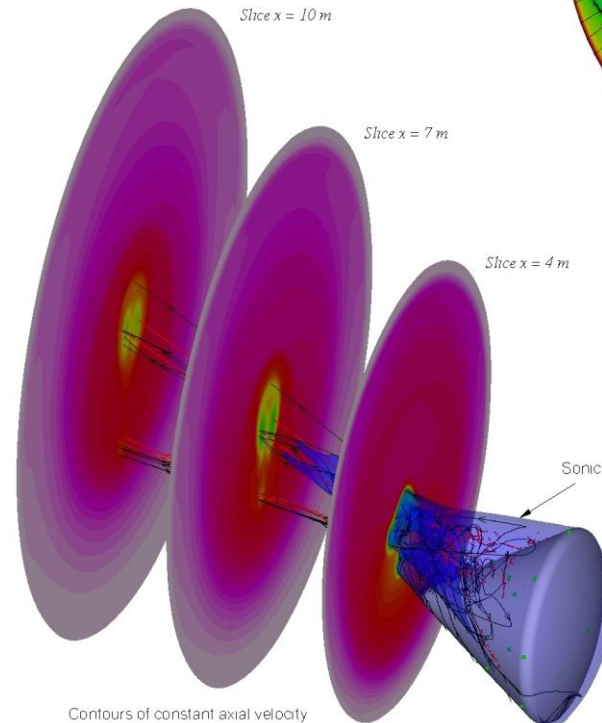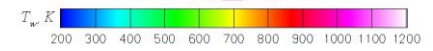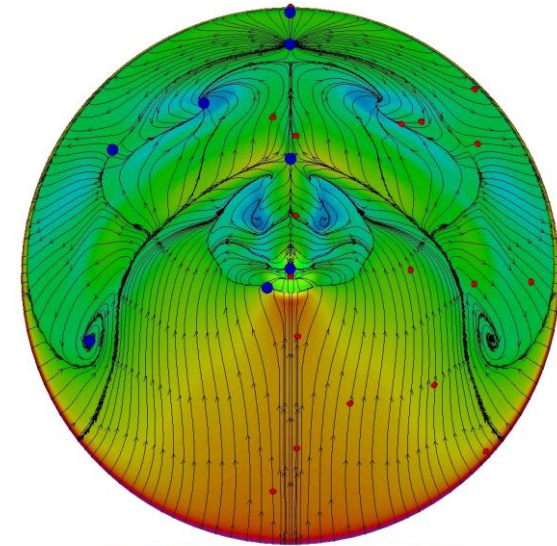
$\Rightarrow$**Computations generally agree with flight data to within $\pm$20% uncertainty at 15 of 19 calorimeter locations.**

Slice x = 10 m
Slice x = 7 m
Slice x = 4 m
Sonic surface
Contours of constant axial velocity

"C"

q (W/cm²) vs t (sec)

Legend:
+ Flight Data
-- Uncertainty
— CFD (DPLR)

Flight Data: MER-B Heatshield

- ➢ **Unique opportunity to observe in-situ flight hardware during Opportunity extended mission**

- ➢ **Multiple images of (inverted) heatshield made with cameras and micro-imager**

- ➢ **Work ongoing to compare visualized material response to predictions**
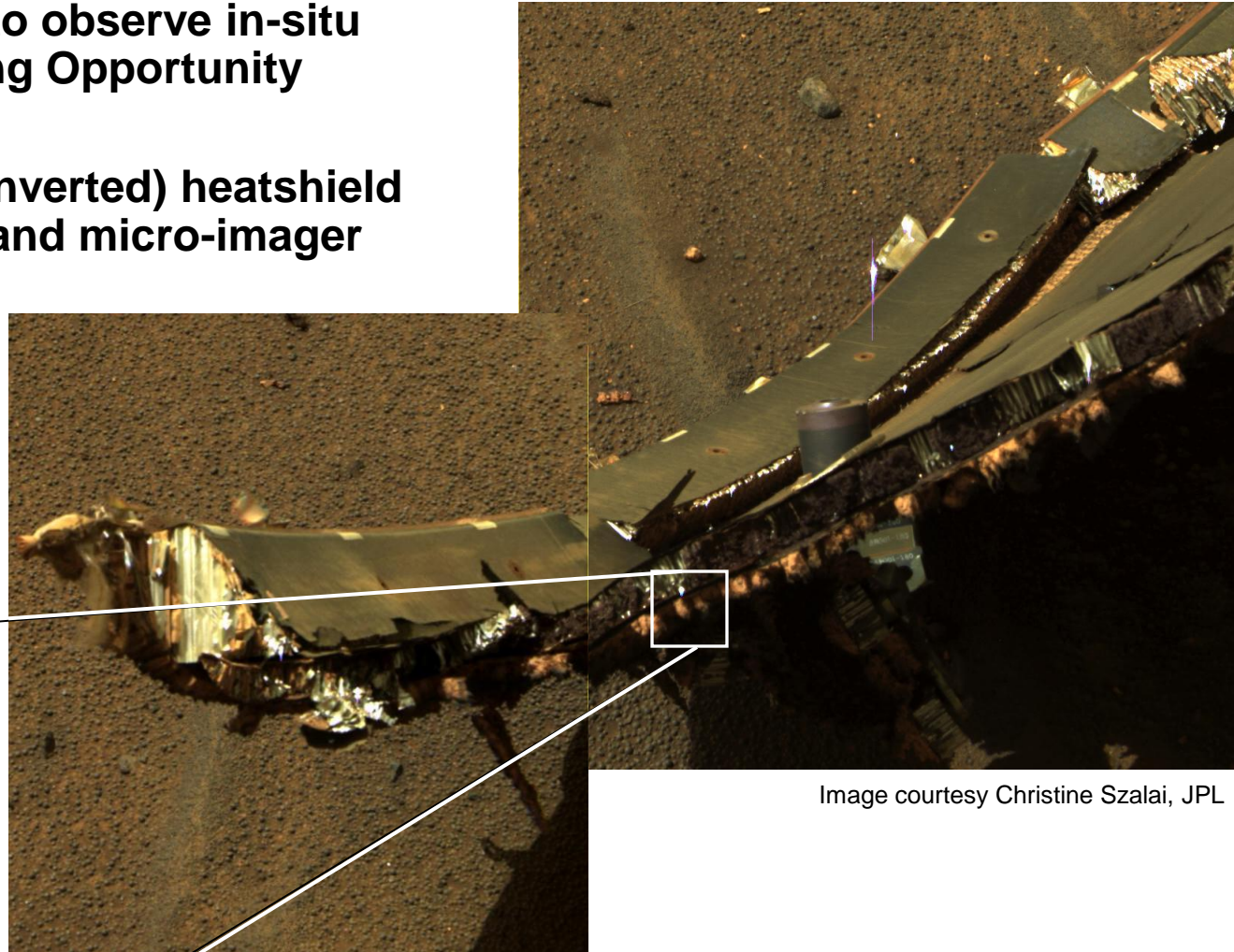
Image courtesy Christine Szalai, JPL

➔ **Flight data are the gold standard for final model validation**

Flight Data: MEDLI

MSL Heatshield Layout

- ➢ **HQ approval for MSL instrumentation suite!**
- ➢ **High TRL sensors to be installed in seven locations on heatshield**
- ➢ **Flight data obtained will go a long way toward validating ARMD-developed tools to drive down uncertainties discussed herein**
- ➢ **No backshell instrumentation (backshell is on critical path)**

Recession Sensor

Wound resistive wire

Outer kapton layer (tube or coating)

Hollow kapton tube

Thermocouple Plug

Pressure Sensor

ARC Sensor Lab

Question and Answer Period

Thermal Protection Systems
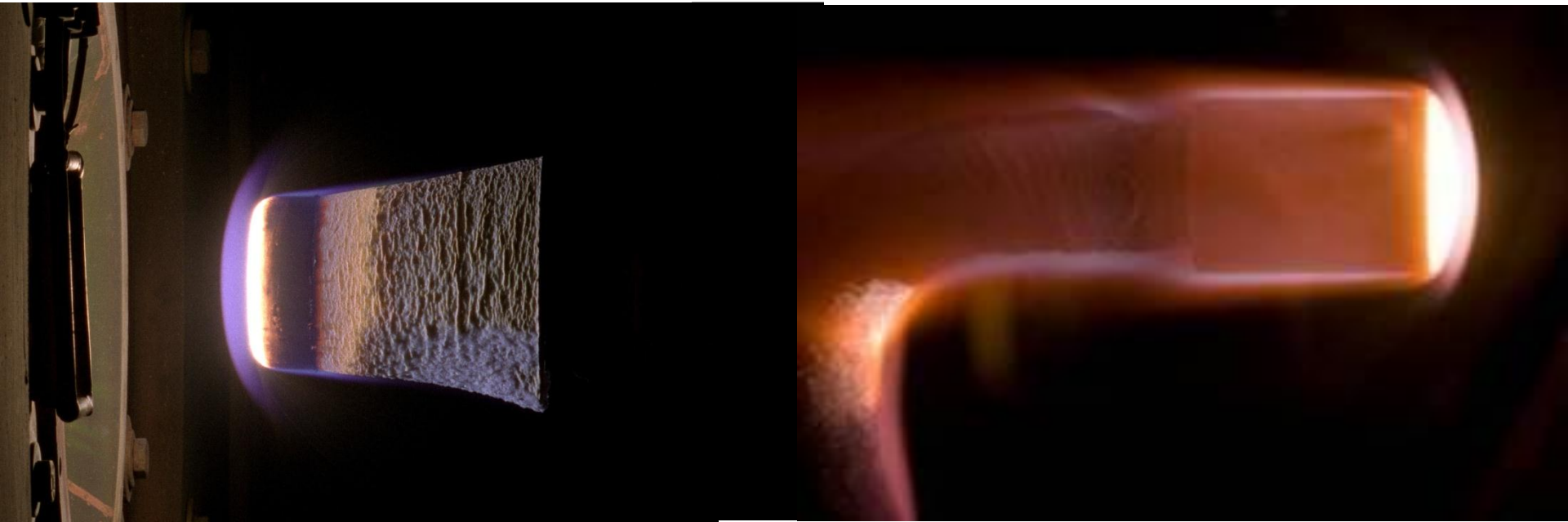
John A. Dec
NASA Langley Research Center

Outline

♦ **Background Information**
- – What is TPS?
- – Selecting the Right Material for the Mission

♦ **Ablative TPS Modeling**
- – Ablator Characteristics
- – Surface Recession
- – In-Depth Models

♦ **TPS Sizing and Margin**

♦ **TPS Testing**

♦ **Look to the Future**

Passive (Reusable)

Rely on reradiation to reject heat, low thermal conductivity to limit penetration

Coatings to increase emissivity, reduce catalycity

Limited by reusable temperatures of common materials

Uses: Shuttle Orbiter, X33, X34

Active (Reusable)

Rely on active cooling for heat rejection

Plumbing systems, active transpiration

Very complex; seldom considered; very low technology readiness

Ablative (Non-Reusable)

Combine reradiation with ablation and pyrolysis for heat rejection

Can be considered passive transpiration cooling

Ideal for high heat flux/load entries, particularly when reusability not required

The focus of today's lecture is on ablative systems; baseline for all planetary EDL to date

Ablation

- Definition:
  - The term ablation is encountered in many fields of science and engineering
    - In the medical field it refers to the surgical removal of a body part or tissue
    - In glaciology it refers to the removal of ice and snow from the surface of a glacier

  - In space physics, ablation is the process of absorbing energy by removal of surface material by melting, vaporization, sublimation, or chemical reaction

Why Ablative Materials?

Courtesy Bernie Laub, NASA Ames
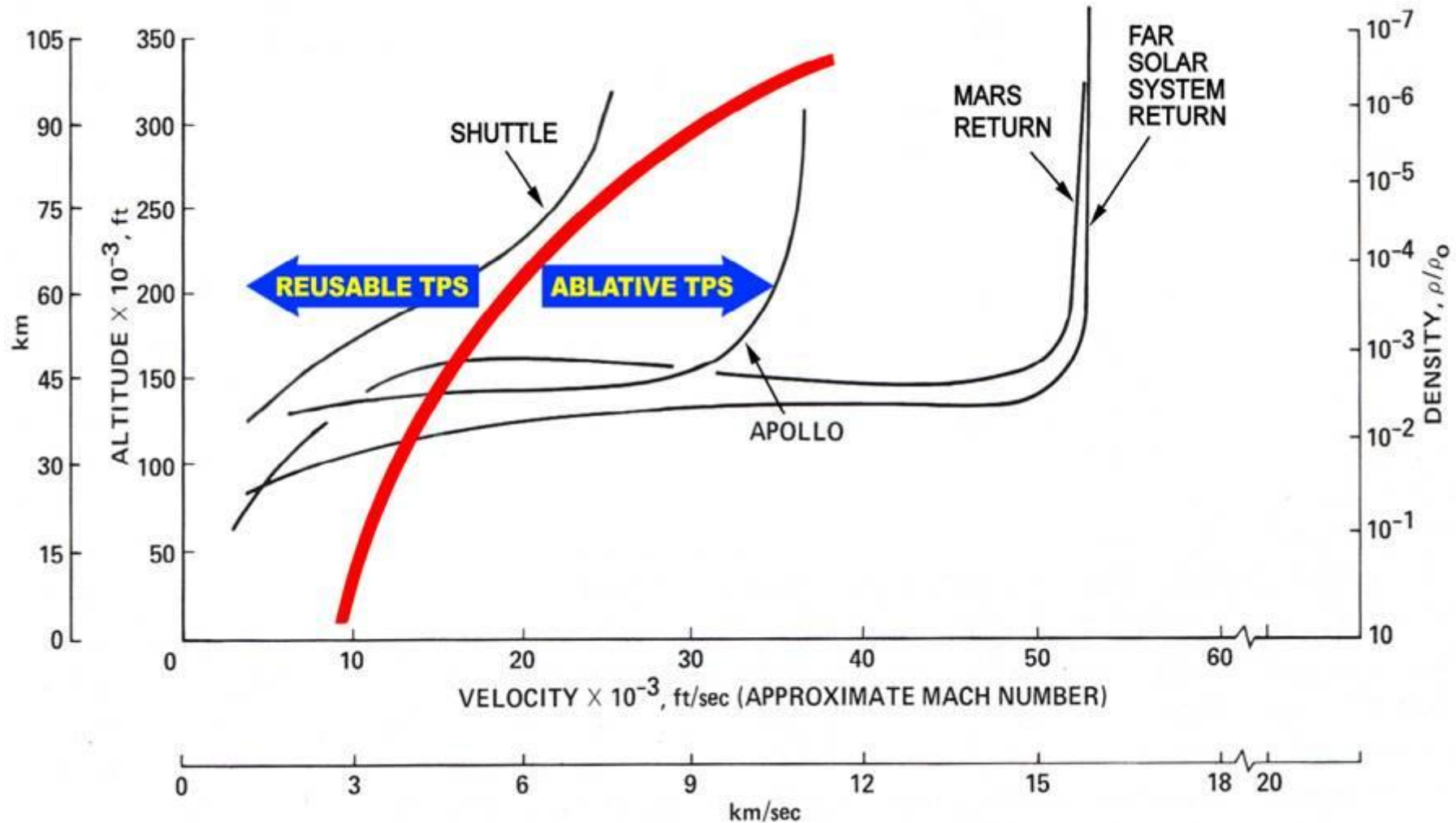
How is TPS Chosen?

- **Heat rate, along with pressure and shear, determine type of TPS to employ**
  - Material classes have clear performance limits marked by poor performance/material failure

- **Heat load determines overall thickness of TPS material**

- **Other design features play a role**
  - Need for tiles, forebody penetrations, compression pads, structural loads, etc. can impact material selection and TPS design
  - RF transparency for materials that protect antennae

Ablative TPS:
History of Success, Little Recent Development

Ablative TPS Chronology (forebody)
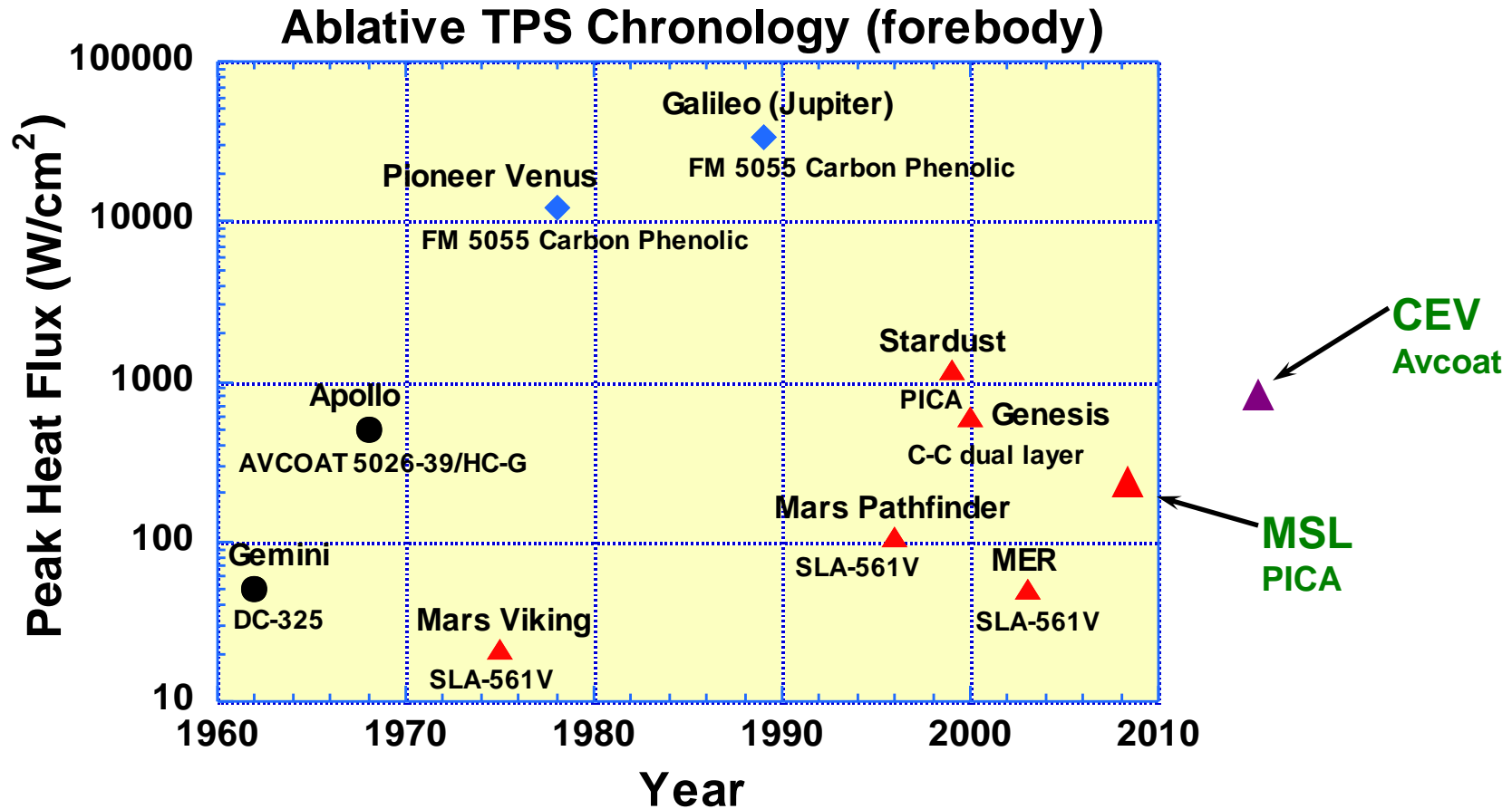
No Human Rated Ablative TPS Available Today!
CEV/Orion is working to develop Avcoat, for a human rated
system - Very Close to Achieving This Goal!

Courtesy Bernie Laub, NASA Ames

Available Materials

Material Name	Manufacturer	Density (kg/m³)	Limit (W/cm²)	
SLA-561V	Lockheed-Martin	256	~ 200	Not viable for high shear
FM 5055 Carbon Phenolic	Fibercote (formerly US Polymeric), Hitco Inc.	1450	> 10,000	No source of heritage Rayon
MX4926N Carbon Phenolic	Cytec (pre-preg), ATK, HITCO	1450	> 10,000	Flown on Shuttle SRM, never as a heat shield
PhenCarb-20,24,32	Applied Research Associates (ARA)	320-512	~ 750	Never flown
PICA (Phenolic Impregnated Carbon Ablator)	Fiber Materials, Inc. (FMI)	265	> 1500	Must be tiled above 1m diameter
Avcoat 5026 (Apollo)	Textron Systems	513	~1000	Recreated for CEV
ACC	Lockheed-Martin	1890	~ 1500	Heavy, not readily extendible above 2m

TPS Mass Fraction Requirements

TPS Mass Fraction for prior missions

TPS MF=0.091*(Heat Load)$^{0.51575}$

Galileo

Stardust
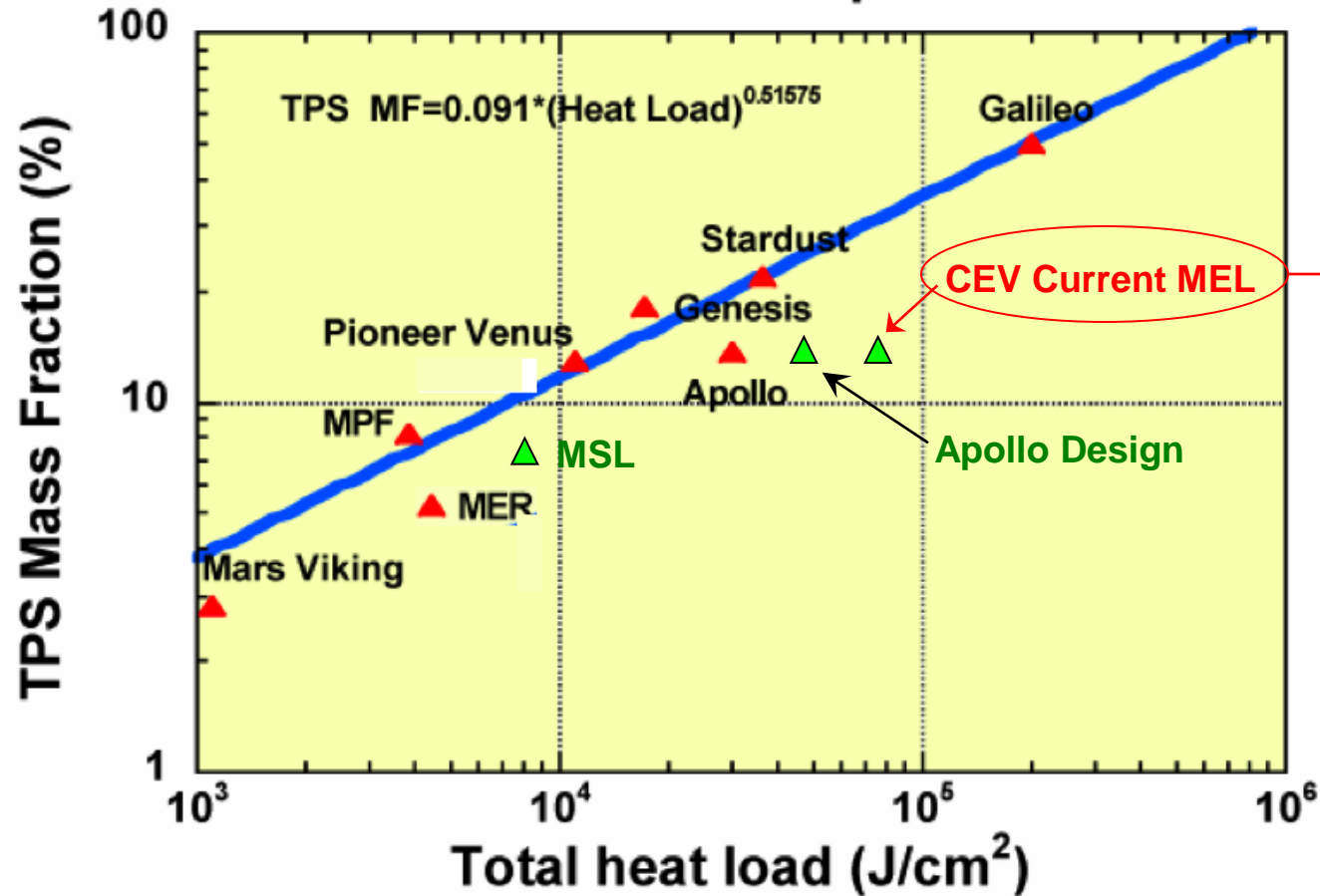
CEV Current MEL → **Wow! This is going to be hard w/o a significant improvement to the state of the art**

Genesis

Pioneer Venus

Apollo

Apollo Design

MPF

MSL

MER

Mars Viking

TPS Mass Fraction (%)

Total heat load (J/cm^2)

What Are They Made Of?

Large Cell Phenolic Honeycomb
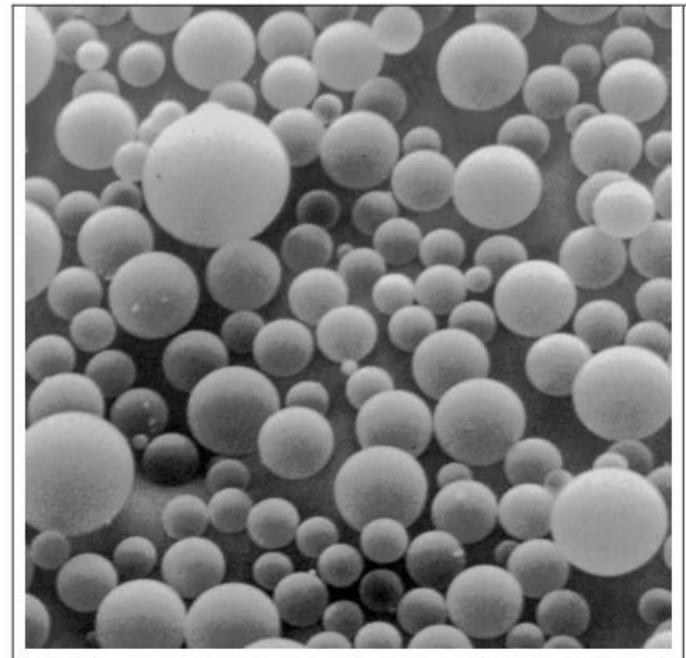
Organic Fiber Reinforced Phenolic

Silica Microballoons

Largest ~100 Microns
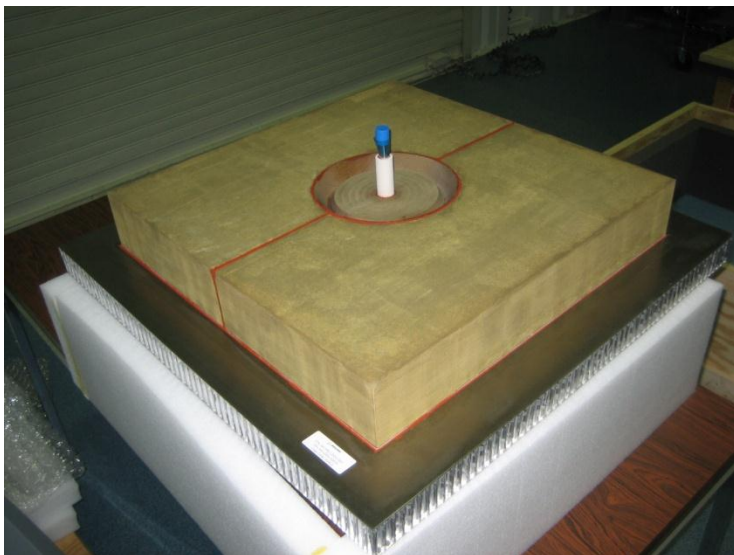
Pyrolyzing Ablators

Substrate Material (e.g. fibers, cloth)
- **Desire ability to withstand high temperatures (reradiation)**
- **Carbon is best; glass also good (heat of vaporization)**

Organic Resins (e.g. phenolics)
- **Pyrolyzing ablators only**
- **When heated resin generates gas and leaves carbon residue**
- **What are they good for?**
    - in-depth and surface transpiration
    - endothermic reactions absorb energy
    - carbon char for reradiation

Additives (e.g. microballoons, cork)
- **Density & thermal conductivity control**

Added Reinforcement (e.g. honeycomb)
- **Structural integrity, bond verification (adds mass)**

How do they Work?
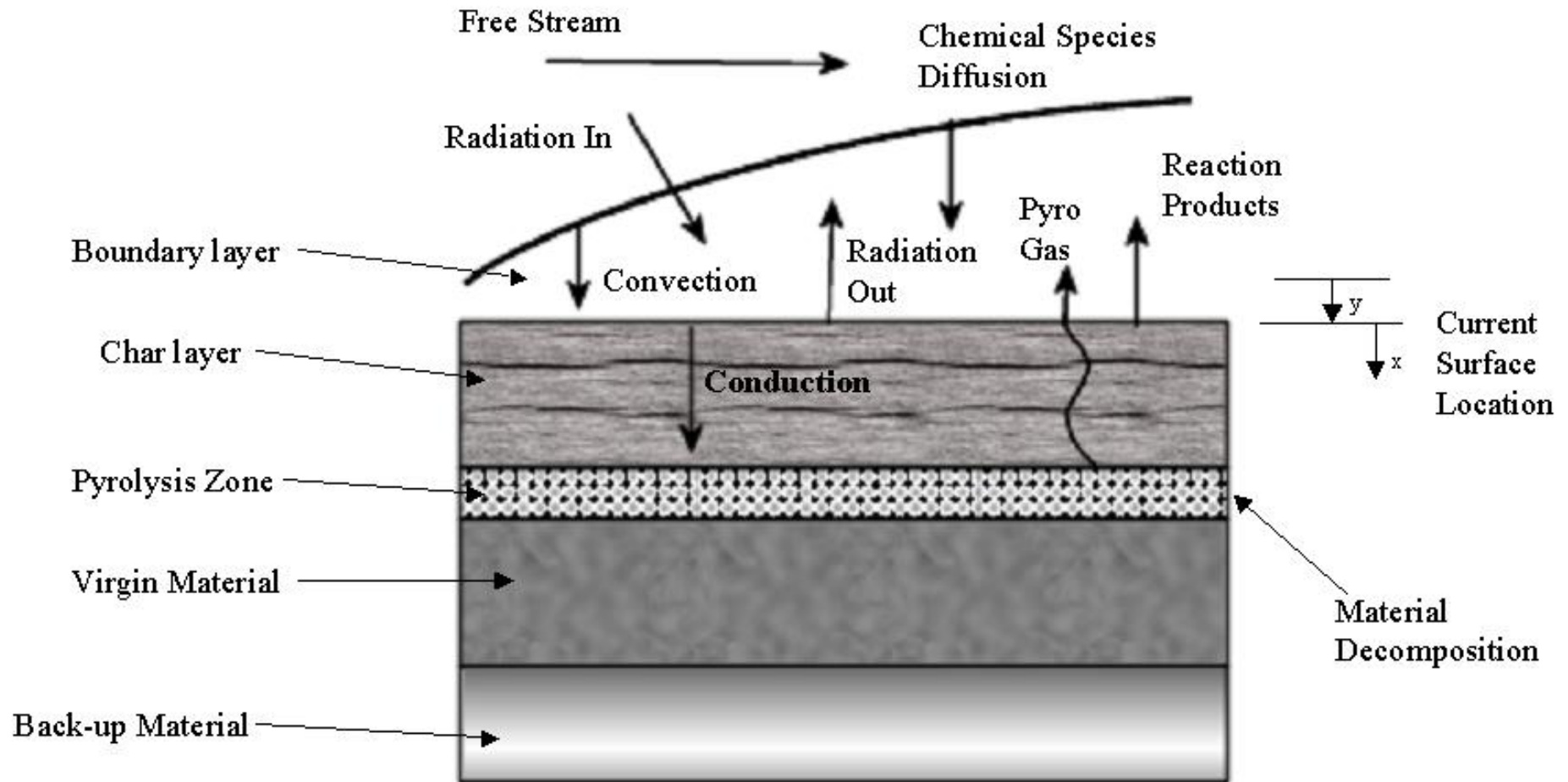
Surface Ablation Mechanisms

- Melting – common ablation mechanism, but doesn't absorb much energy

- Vaporization – absorbs significant amount of energy

- Oxidation – exothermic process that adds energy

- Sublimation – Can be significant energy absorber

- Spallation – Mass loss with minimal energy absorption (Thermostructural Failure – HIGHLY UNDESIRABLE)

Oxidation

- Oxidation is an *exothermic* process
- Example:

$$2C(s) + O_2(g) \rightarrow 2CO(g)$$

$$\Delta H_{comb} \approx -4170 \ kJ/g_{carbon}$$

- Note: the B' curve for carbon in air was generated with assumptions of thermochemical equilibrium, equal diffusion coefficients, etc.
- The "equilibrium" assumption allows the diffusion-limited plateau to extend to *unrealistically low* surface temperatures

Graphite in air Thermochemical equilibrium

- 1.0 atm
- 0.1 atm
- 0.01 atm
- 0.001 atm

Sublimation

Diffusion-limited oxidation

B'$_c$ (y-axis)

Surface temperature (K) (x-axis)
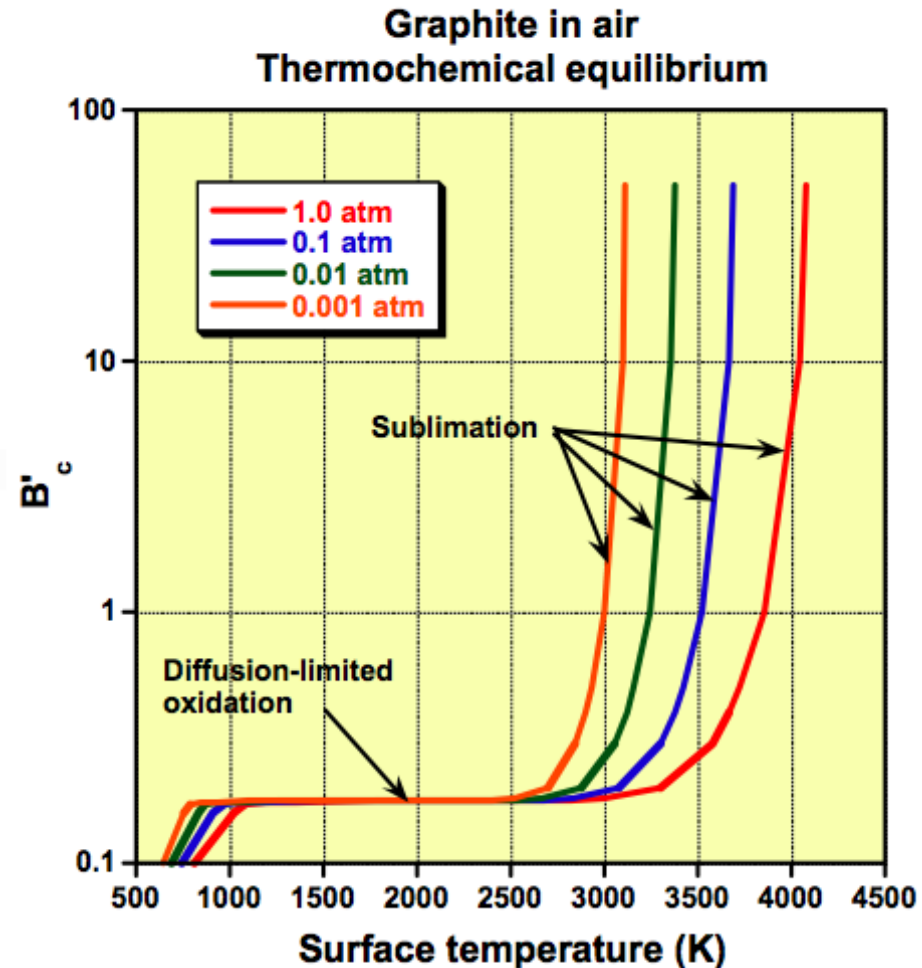
Other exothermic surface chemistry is possible ("nitridation" and "hydridation") but these are not typically significant players

Courtesy Bernie Laub, NASA Ames

Other Mechanisms

- Material decomposition …aka pyrolysis
  - Endothermic reactions absorb energy
  - Convection of pyrolysis gas through the char
- Conduction through the material
  - Transfer energy to structure or heat sink
- Re-radiation from the surface
  - Largest percentage of energy is dissipated through this mechanism

Modeling Approach

- In the mid to late 1960's, Kendall, Rindal, and Bartlett, and Moyer and Rindal extended the work by Kratsch et. al.
  - Included unequal heat and mass transfer coefficients
  - Non-unity Lewis and Prandtl numbers
  - Corrected in-depth energy equation:
    - to account for the energy of the pyrolysis gas convection and generation within the solid
    - to account for grid motion due to a coordinate system that is attached to the receding surface

$$\rho c_p \frac{\partial T}{\partial t} = \frac{\partial}{\partial x_S}\left(k\frac{\partial T}{\partial x_S}\right) + \left(h_g - \bar{h}\right)\frac{\partial \rho}{\partial t}\bigg|_x + \dot{S}\rho c_p \frac{\partial T}{\partial x_S} + \dot{m}_g \frac{\partial h_g}{\partial x_S} \qquad (12)$$

$$-k\frac{dT}{dx} = \rho_e U_e C_H \left(H_{sr} - h_{sw}\right) + \rho_e U_e C_M \left(\sum_i \left(Z_{ie}^* - Z_{iw}^*\right)h_i^0 + B'_c h_c + B'_g h_g - B' h_w\right) - q^* + q_{rad_{out}} - \alpha q_{rad_{in}} \qquad (13)$$

- If the diffusion coefficients are assumed equal and the Le=Pr=1.0, the surface energy balance simplifies to

$$-k\frac{dT}{dx} = \rho_e U_e C_H \left(H_{sr} - h_{sw} + B'_c h_c + B'_g h_g - B' h_w\right) - q^* + q_{rad_{out}} - \alpha q_{rad_{in}} \qquad (14)$$

Example: SLA-561V Failure

Derivation of the Governing Differential Equations

- 1-Dimensional control volume

$$\left(\dot{m}_g h_g + \dot{m}_g \frac{u^2}{2} + \dot{m}_g gZ \right)_x$$

$$m_{cv}$$

$$\dot{E}_{st}$$

$$\left(\dot{m}_g h_g + \dot{m}_g \frac{u^2}{2} + \dot{m}_g gZ \right)_{x+dx}$$

$$\dot{m}_{g_x}$$

$$\dot{m}_{g_{x+dx}}$$

$$q_x$$

$$q_{x+dx}$$

$$dx$$

x
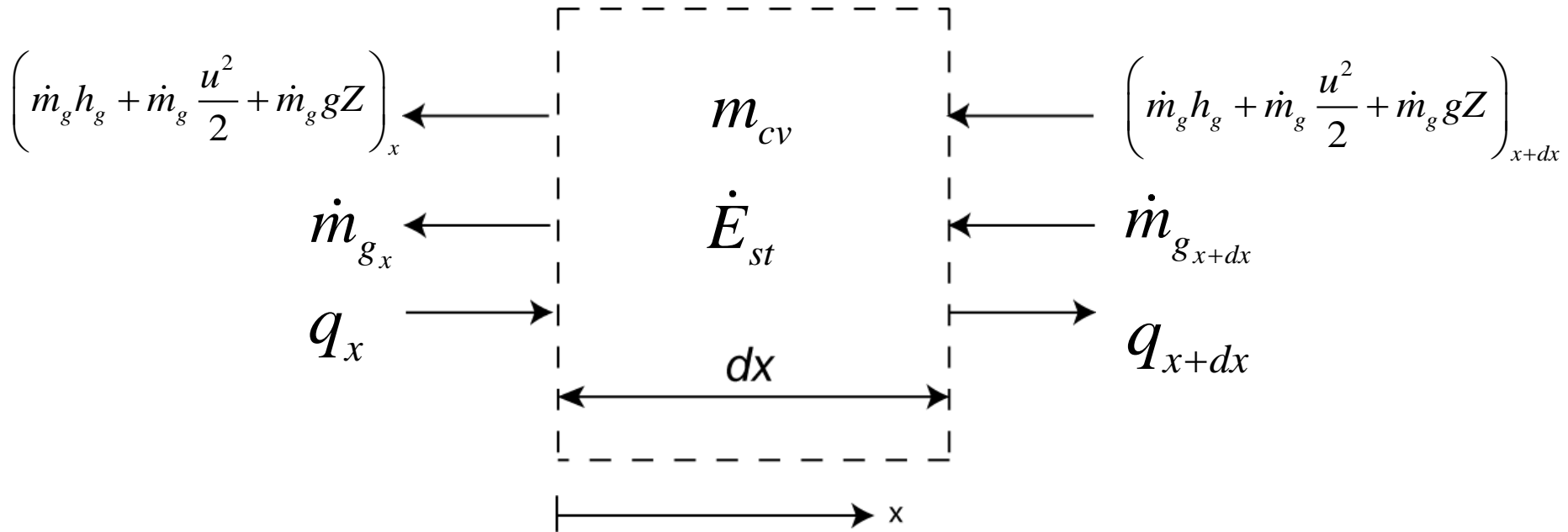
Conservation of Mass

- Pyrolysis gas flows from the pyrolysis zone through the porous char to the heated surface

  - Assume gas flow is 1-D and normal to the heated surface

  - Assume dp~0 across the char (neglect the momentum eqn)
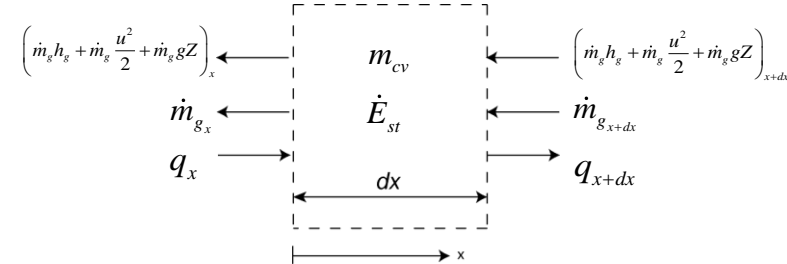
$$\frac{\partial m_{cv}}{\partial t} = \dot{m}_{in} - \dot{m}_{out} \qquad (15)$$

Where $\quad m_{cv} = \rho A dx \quad (16) \qquad \dot{m}_{g_{x+dx}} = \dot{m}_{g_x} + \frac{\partial \dot{m}_{g_x}}{\partial x} dx \quad (17)$

$$A \frac{\partial \rho}{\partial t} dx = \left(\dot{m}_{g_x} + \frac{\partial \dot{m}_{g_x}}{\partial x} dx \right) - \dot{m}_{g_x} \qquad \Longrightarrow \qquad \boxed{\frac{\partial \rho}{\partial t} = -\frac{\partial \dot{m}_{g_x}''}{\partial x}} \qquad (18)$$

$\frac{\partial \rho}{\partial t}$ Determined experimentally and modeled with an Arrhenius fit

$\dot{m}_{g_x}'' = $ Mass flow rate per unit area

Conservation of Energy

- Two energies associated with this control volume

  - Pyrolysis gas flow
  - Heat conduction.
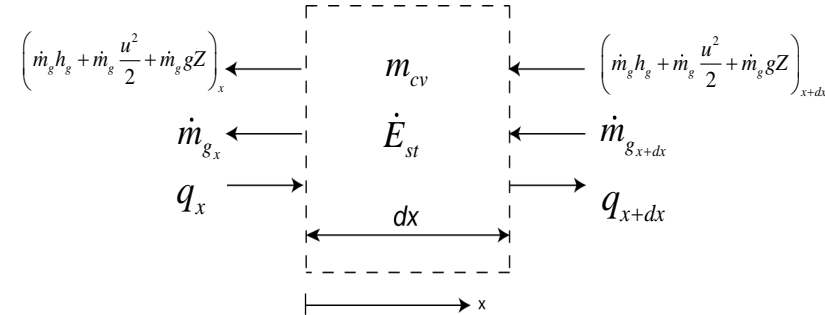
- Pyrolysis gas flow assumptions

  - Pyrolysis gas is in thermal equilibrium with the charred material within the control volume

  - Pyrolysis gas residence time within the control volume is small.

  - Potential energy of the pyrolysis gas may be neglected since the change in height across the control volume is negligible.

  - The kinetic energy of the pyrolysis gas may be neglected since it is of small magnitude relative to its enthalpy

Conservation of Energy

- 1st Law of Thermodynamics

$$\frac{dE_{cv}}{dt} = \dot{Q}_{cv} - \dot{W}_{cv} + \left[\dot{m}_{in} \left(e + Pv \right)_{in} - \dot{m}_{out} \left(e + Pv \right)_{out} \right]$$ (19)
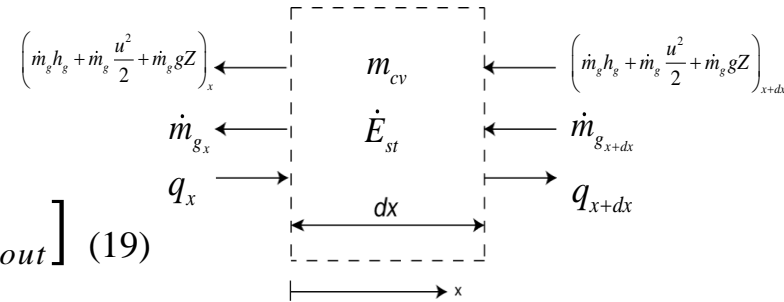
Where *e* is the total energy per unit mass and includes kinetic, potential, and internal energy

The internal energy and flow work may be expressed in terms of the enthalpy by, $h = u + Pv$

Rewriting equation 19 in a simplified form gives,

$$\frac{dE_{cv}}{dt} = \dot{E}_{in} - \dot{E}_{out}$$ (20)

Conservation of Energy

- The energy entering and leaving the control volume can be expressed as

$$\dot{E}_{in} = q_x + \left(\dot{m}_g h_g \right)_{x+dx}$$

$$\dot{E}_{out} = q_{x+dx} + \left(\dot{m}_g h_g \right)_x \qquad (21)$$
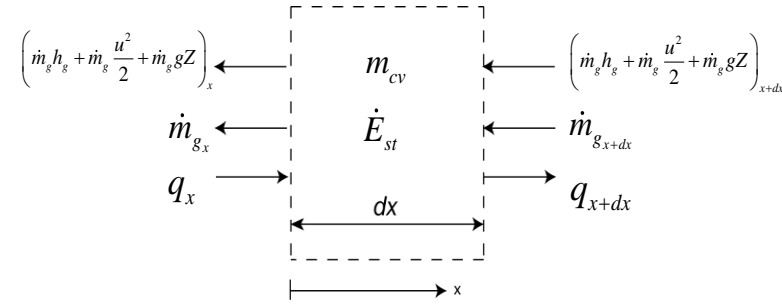
- Expressing the incremental heat conduction leaving and the convection of energy by the pyrolysis gas entering the control volume as Taylor series expansions gives, dropping H.O.T

$$q_{x+dx} = q_x + \frac{\partial q_x}{\partial x} dx$$

$$\left(\dot{m}_g h_g \right)_{x+dx} = \left(\dot{m}_g h_g \right)_x + \frac{\partial}{\partial x} \left(\dot{m}_g h_g \right)_x dx \qquad (22)$$

Conservation of Energy

- The rate of energy storage within the control volume can be expressed in terms of the density and enthalpy of the solid as

$$\frac{dE_{cv}}{dt} = \frac{\partial}{\partial t}\left(\rho h\right)A dx \qquad (23)$$
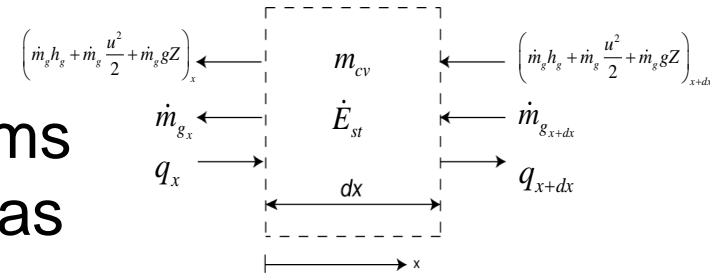
- Substituting eq 21 into eq 20, and using the definitions in eqns 22 and 23 gives

$$\frac{\partial}{\partial t}\left(\rho h\right)A dx = \left[q_x + \left(\dot{m}_g h_g\right)_x + \frac{\partial}{\partial x}\left(\dot{m}_g h_g\right)_x dx\right] - \left[q_x + \frac{\partial q_x}{\partial x}dx + \left(\dot{m}_g h_g\right)_x\right] \qquad (24)$$

Conservation of Energy

- Canceling like terms, dividing by *Adx,* and using Fourier's law of heat conduction eqn 24 reduces to,

$$\underbrace{\frac{\partial}{\partial t}(\rho h)}_{\text{I}} = \underbrace{\frac{\partial}{\partial x}\left(k_x \frac{\partial T}{\partial x}\right)}_{\text{II}} + \underbrace{\frac{\partial}{\partial x}\left(\dot{m}''_{g_x} h_g \right)}_{\text{III}} \quad (25)$$

Where,

ρ : density of the solid

h : enthalpy of the solid

h_g : pyrolysis gas enthalpy

k_x : thermal conductivity in the x-direction

T : temperature

$\dot{m}_{g_x}$: local gas flow rate in the x-direction

x : coordinate direction

- Physically,
  - Term I represents energy storage
  - Term II represents conduction through the material
  - Term III represents convection due to pyrolysis gas flow

Transforming the Governing Equations to a Moving Coordinate System

- The control volume is not fixed in space, it is tied to the receding surface
  - Requires transforming eqns 18 and 25 into a moving coordinate system
  - After some elaborate calculus and algebraic manipulation we arrive at,
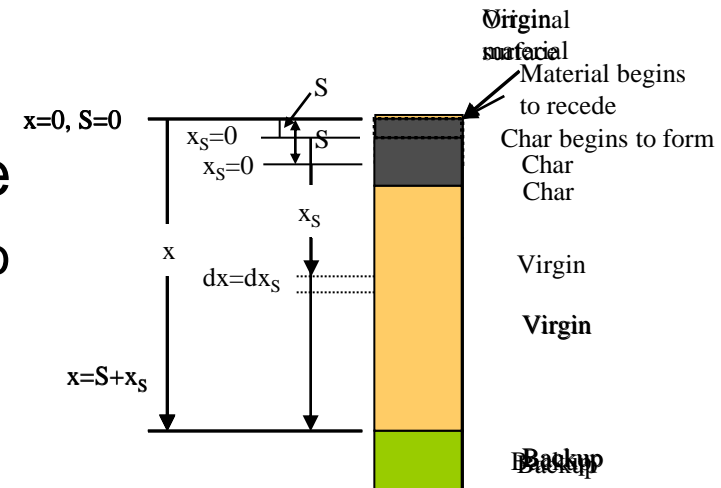
Conservation of mass in a moving coordinate system

$$\left.\frac{\partial \rho}{\partial t}\right|_{x_S} = \dot{S}\left.\frac{\partial \rho}{\partial x_S}\right|_t + \left.\frac{\partial \rho}{\partial t}\right|_x \qquad (26)$$

Conservation of energy in a moving coordinate system

$$\underbrace{\left.\frac{\partial}{\partial t}(\rho h)\right|_{x_S}}_{I} = \underbrace{\left.\frac{\partial}{\partial x_S}\left(k_x \frac{\partial T}{\partial x_S}\right)\right|_t}_{II} + \underbrace{\left.\frac{\partial}{\partial x_S}\left(\dot{m}''_{g_x} h_g\right)\right|_t}_{III} + \underbrace{\dot{S}\left.\frac{\partial}{\partial x_S}(\rho h)\right|_t}_{IV} \qquad (27)$$

Where terms I-III are the same as in eqn 25 and term IV is the convection of energy due to coordinate system movement

Final Form of the Energy Equation

- It is convenient to express the (ρh) terms in equation 27 in terms of material properties rather than the thermodynamic quantity of enthalpy

- Performing some algebra and defining a new quantity, $\bar{h}$, the energy equation takes the following form

$$\underbrace{\rho c_p \frac{\partial T}{\partial t}}_{I} = \underbrace{\frac{\partial}{\partial x_S}\left(k_x \frac{\partial T}{\partial x_S}\right)}_{II} + \underbrace{\left(h_g - \bar{h}\right)\frac{\partial \rho}{\partial t}\bigg|_x}_{III} + \underbrace{\dot{S}\rho c_p \frac{\partial T}{\partial x_S}}_{IV} + \underbrace{\dot{m}''_{g_x}\frac{\partial h_g}{\partial x_S}}_{V} \qquad (28)$$

where

$$\bar{h} = \left[\frac{\rho_v H_v - \rho_c H_c}{\rho_v - \rho_c}\right]$$

$$H_v = h_v^0 + \int_0^T c_{p_v}\, dT$$

$$H_c = h_c^0 + \int_0^T c_{p_c}\, dT$$

ρ_v : virgin material density

ρ_c : charred material density

H_v : total enthalpy of the virgin material

H_c : total enthalpy of the charred material

Final Form of the Energy Equation

$$\underbrace{\rho c_p \frac{\partial T}{\partial t}}_{I} = \underbrace{\frac{\partial}{\partial x_S}\left(k_x \frac{\partial T}{\partial x_S}\right)}_{II} + \underbrace{\left(h_g - \bar{h}\right)\frac{\partial \rho}{\partial t}\bigg|_x}_{III} + \underbrace{\dot{S}\rho c_p \frac{\partial T}{\partial x_S}}_{IV} + \underbrace{\dot{m}_{g_x}\frac{\partial h_g}{\partial x_S}}_{V} \qquad (28)$$

- Each term in equation 28 has physical significance
  - Term I
    - rate of sensible energy storage
  - Term II
    - net conduction through the material
  - Term III
    - creation of sensible energy due to pyrolysis (ie the heat of decomposition)
  - Term IV
    - energy convected due to coordinate system movement
  - Term V
    - energy convected away due to pyrolysis gas generation at that point

TPS Sizing Approach

- **Baseline (zero-margin) sizing computed assuming nominal environments and response model to hit given bondline temperature limit**

- **Margin process then applied to account for various sources of uncertainty**

- **Appropriate factors of safety be applied to trajectory dispersions, aerothermal loads, initial conditions, and material variabilities**

- **Primary (thermal) margin is applied directly to the TPS design criterion (e.g. maximum bondline temperature)**
  - The impact of this margin on TPS thickness is material-dependent since the sensitivity of bondline temperature to thickness is material-dependent

- **Secondary (recession) margin is also employed**
  - Bondline is insensitive to excessive recession until it is too late

- **Various independent sources of error are RSS'ed to avoid stacked conservatism**

- **Additional program imposed thickness factor of safety is recommended to account for unknown unknowns**

- **Other factors (e.g. thermal stress, CTE mismatch, adhesive failure) should also be tracked as possible limiting cases**
  - Adhesive failure accounted for by maintaining conservative bondline temperature limit

Simplified Approach

- Return to the simplest form of the in-depth energy equation

$$\rho c_p \frac{\partial T}{\partial t} = \frac{\partial}{\partial x}\left(k \frac{\partial T}{\partial x} \right) \qquad (1)$$

- Here we neglect the affects of decomposition, pyrolysis gas flow and surface recession.

- Additionally, if it is assumed that the solid extends to infinity in all but one direction and is characterized by a single identifiable surface, if a sudden change in conditions is imposed at this surface, transient, one-dimensional conduction will occur within the solid. This is known as the semi-infinite solid approximation

- This approach is for illustrative purposes only and should not be used beyond conceptual design

Simplified Approach

- Using the semi-infinite solid approximation, closed-form analytical solutions to the in-depth energy equation can be derived.

- For a thick slab which has a constant surface temperature at any instant in time, the temperature at a depth **x** within the solid at time **t** is given by,

$$T(x,t) = erf\left(\frac{x}{2\sqrt{\alpha t}}\right)(T_i - T_s) + T_s \qquad (29)$$

where,

T_i is the initial temperature $\qquad\qquad$ $k = thermal\ conductivity$

T_s is the surface temperature $\qquad\qquad$ $c_p = specific\ heat$

erf is the gaussian error function $\qquad$ $\rho = density$

α is the thermal diffusivity $= \dfrac{k}{\rho c_p}$

Simplified Approach

- In this simplified approach, the amount of material required for insulation and the amount of material required for recession are calculated separately

- To calculate the recession in an approximate way, use the data correlation parameter known as the heat of ablation (Q^*) and solve for recession rate

$$\dot{s} = \frac{\dot{q}_{cw}\left(\dfrac{H_r - H_{air}^{T_w}}{H_r}\right) - \sigma\varepsilon T_w^4}{\rho Q^*} \qquad (5)$$

Simple Finite Difference Approach

- To increase the fidelity, a finite difference approximation of equation 1 can be written incorporating a simplified surface energy balance

$$\rho c_p \frac{\partial T}{\partial t} = \frac{\partial}{\partial x}\left(k \frac{\partial T}{\partial x} \right) \qquad (1)$$

$$\dot{q}_{conv} + \alpha \dot{q}_{rad} - \dot{q}_{cond} - \varepsilon\sigma T_w^4 = 0 \qquad (30)$$

$$\left(1 + \frac{2k\Delta t}{\rho c_p \Delta x_i^2} \right) T_i^{n+1} - \frac{2k\Delta t}{\rho c_p \Delta x_i^2} T_{i+1}^{n+1} = T_i^n + \alpha \dot{q}_{rad} \frac{2\Delta t}{\rho c_p \Delta x_i} + \dot{q}_{conv} \frac{2\Delta t}{\rho c_p \Delta x_i} - \varepsilon\sigma T_i^{n4} \frac{2\Delta t}{\rho c_p \Delta x_i} \qquad (31a)$$

$$T_i^n = -\frac{k\Delta t}{\rho c_p \Delta x_i^2} T_{i-1}^{n+1} + \left(1 + \frac{2k\Delta t}{\rho c_p \Delta x_i^2} \right) T_i^{n+1} - \frac{k\Delta t}{\rho c_p \Delta x_i^2} T_{i+1}^{n+1} \qquad (31b)$$

Stagnation Point Sizing Example

- ## Ballistic Earth entry
  - Ballistic coefficient = 60 kg/m² , entry velocity = 12.6 km/s
  - 60° sphere cone, 0.8 m diameter, r_n= 0.23 m
  - At the stagnation point, H_r can be approximated by $\dfrac{V^2}{2}$

Stagnation Point Sizing Example
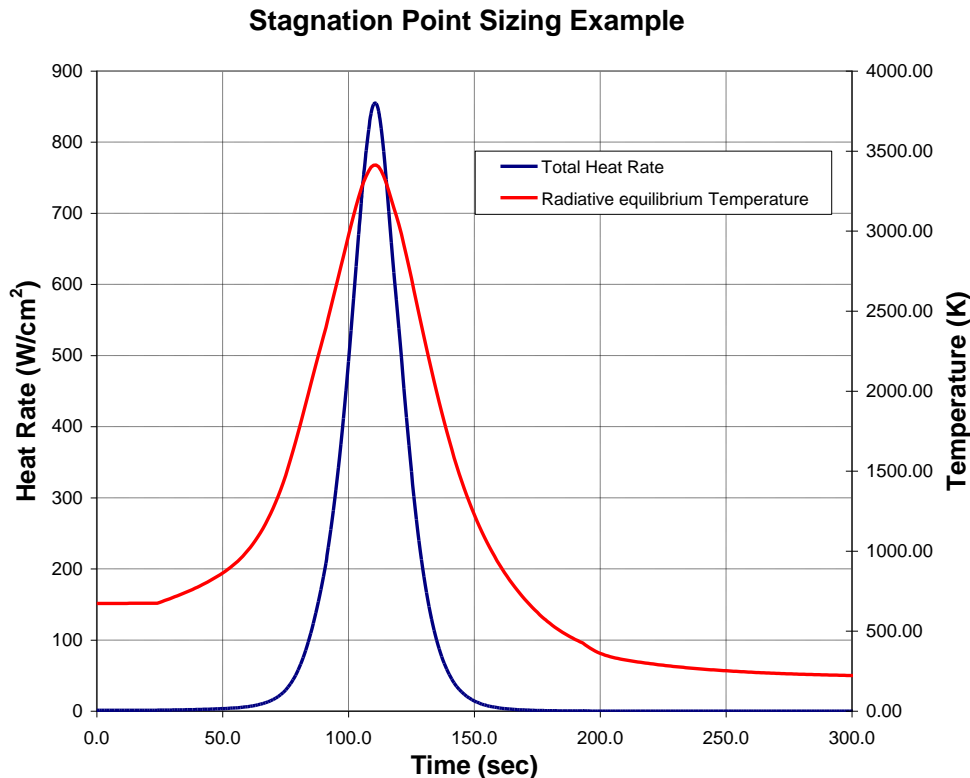
- ## PICA heat shield

$$\rho = 265.0 \; \frac{kg}{m^3}$$

$$k = 1.6 \; \frac{W}{m \cdot K}$$

$$C_p = 1592.0 \frac{J}{kg \cdot K}$$

- ## Radiative equilibrium temperature

$$T_w = \sqrt[4]{\left(\frac{\dot{q}_{cw}}{\varepsilon \sigma} + T_{surr}^4 \right)}$$

Stagnation Point Sizing Example

- Comparing the simplified approach, the simple FD approach, and the high fidelity code CMA

Typical Approach to Modeling Materials
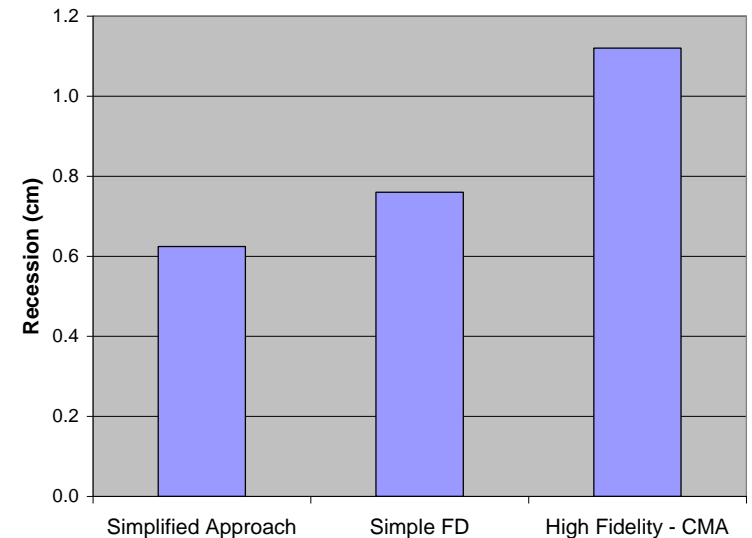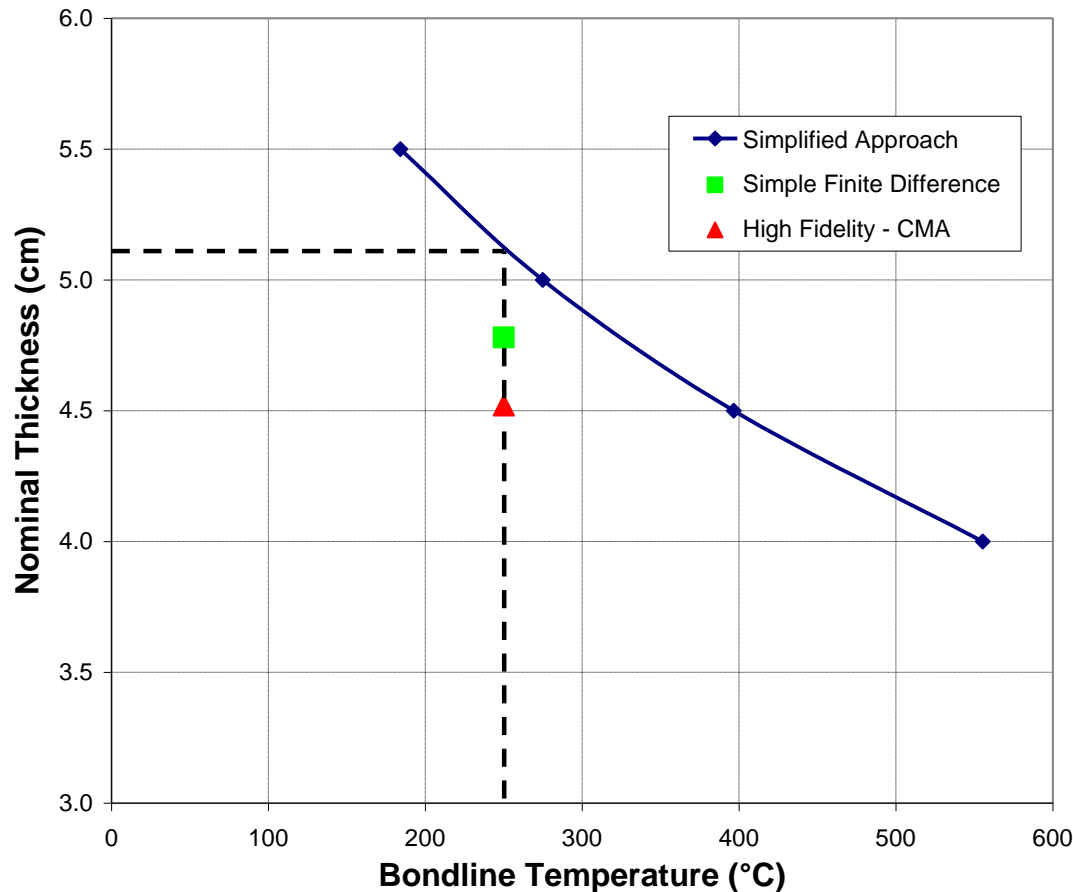
- **Decouple surface recession from in-depth conduction**
  - Use steady-state surface energy balance expression
  - Employ equilibrium thermodynamic tables for surface recession, corrected as required for finite-rate chemistry, spallation, melt flow
  - Validate surface model with arc jet data

- **Once recession model is working, develop in-depth pyrolysis model**
  - Thermochemical data from materials testing
  - Validate model by arc jet data; use first thermocouple as "truth model" boundary condition
  - Tweak char thermal conductivity as required

- **Add additional physics as required for the problem**
  - Multi-dimensional conduction, Darcy's Law, etc.

Material Modeling

Thermochemical Properties:

1. Conduct Thermogravimetric Analysis (TGA experiments) in inert gas, low temperature rise rates, usually 10° C/min. Residual mass fraction defines *char yield*. Data fits provide decomposition kinetic constants for the Arrhenius equation.

2. Conduct digital scanning calorimeter (DSC experiments) in inert gas, low temperature rise rates, 10° C/min. Data provides heat of reaction for pyrolysis reactions as function of temperature.

3. Measure elemental composition of virgin material, by mass spectrometry.

4. Measure heat of combustion of virgin material and derive heat of formation.

5. Derive elemental composition of char from known constituents and char yield data. Can be problematic to measure thermal conductivity (explained later).

6. Derive heat of formation of char from known constituents and existing data

7. Derive elemental composition of pyrolysis gases. Develop model(s) for pyrolysis gas enthalpy using combination of thermochemical equilibrium calculations and measured heat of pyrolysis data.

Material Modeling

8. Measure specific heat of virgin material as function of temperature.

9. Measure thermal conductivity of virgin material as function of temperature (and orientation, if appropriate).

10. Derive specific heat of char from known (or derived) composition using method of mixtures.

11. Measure optical properties of virgin material

12. Derive optical properties of char from known composition and properties of similar materials (or determine experimentally)

13. Measure thermal conductivity of char as function of temperature (and orientation, if appropriate).

Assertion: the thermal conductivity of the char cannot be measured in standard lab facilities!

Char Thermal Conductivity

Traditional practice has been to bake the material in an oven and measure the thermal properties of the resulting "char." Studies conducted under the Apollo heat shield program (and re-validated in other programs) demonstrated that the cellular structure of "oven chars" was different than the cellular structure of chars formed in ground test or flight.
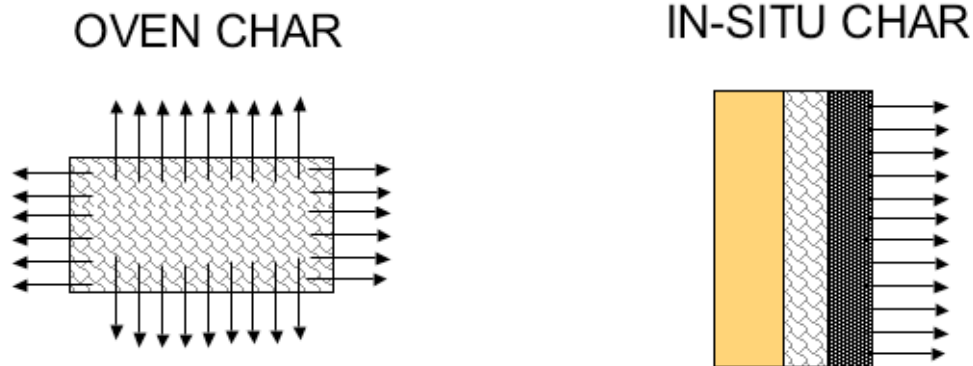
OVEN CHAR

IN-SITU CHAR

Example

Courtesy Bernie Laub, NASA Ames
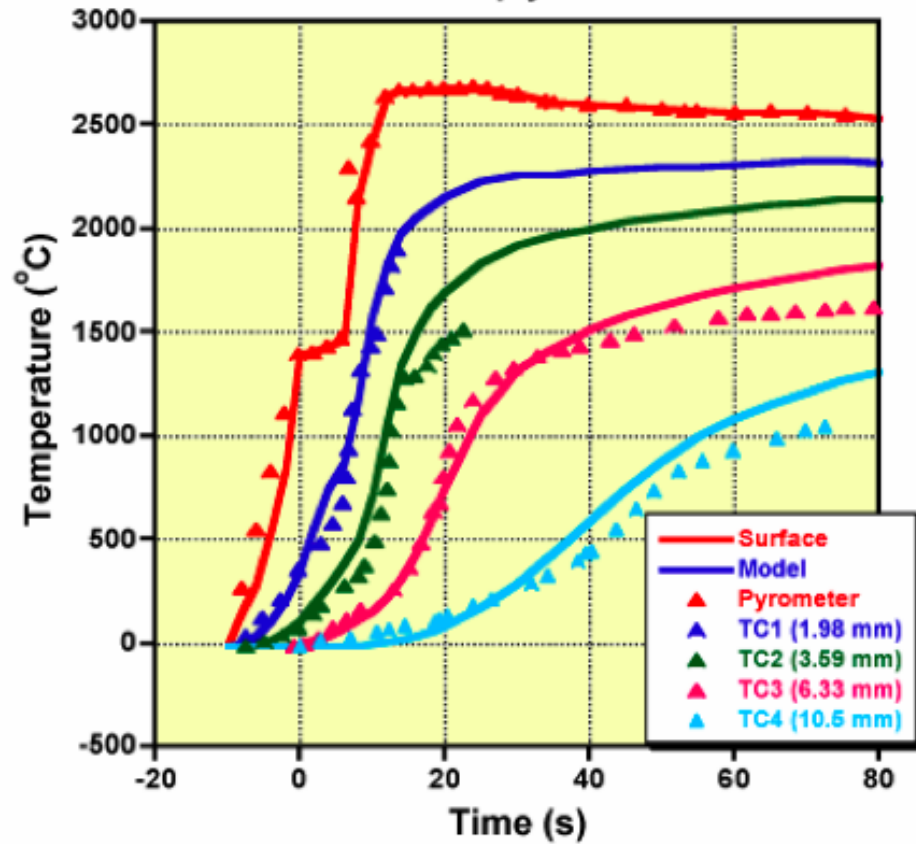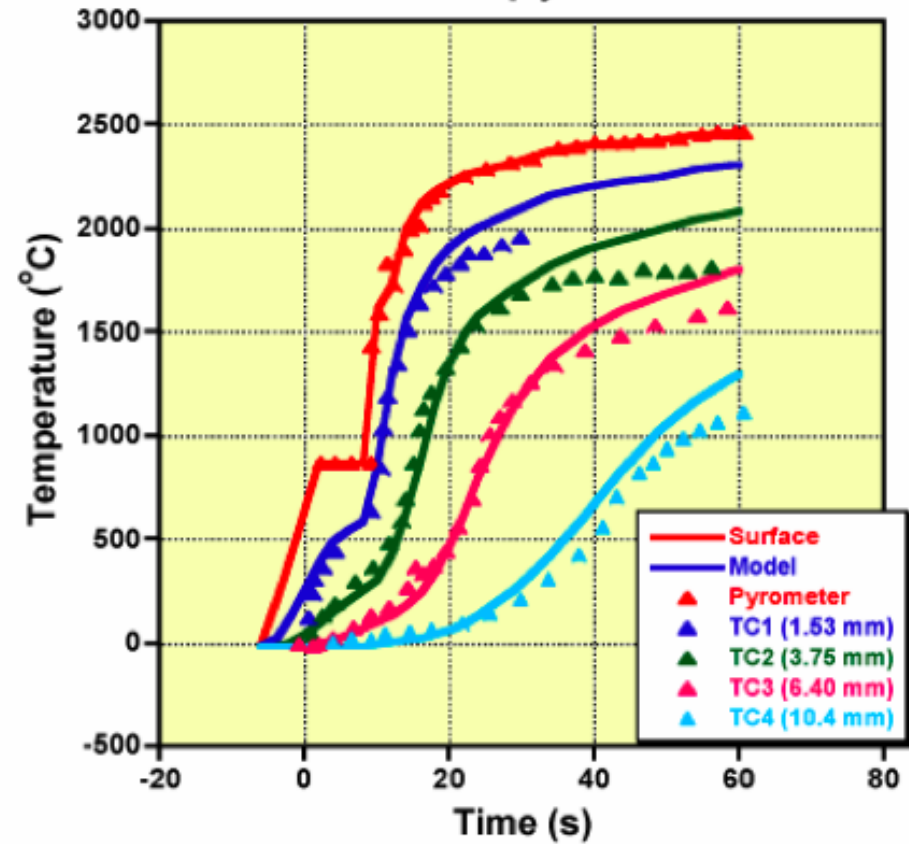
Margin vs Nominal (Zero Margin)

- **The purpose of the TPS thickness margin is to capture two things:**
  - Uncertainties in operating conditions
  - Uncertainties in baseline (nominal) sizing required to meet operational requirements (including abort)

- **As such, the TPS margin captures implicitly the fidelity and level of uncertainty in the underlying TPS design tools employed to determine the baseline sizing**

- **Research is underway to calculate TPS margins probabilistically, this requires knowledge of the uncertainties in the input parameters for all analysis codes being used; aerothermal, trajectory, thermal response**

Excess Recession Lien

Localized Application

Material Property Uncertainty
Arc-Jet Statistics
Ground-to-Flight Traceability

Recession Margins

Aerothermal Margins

Thermal Margins

Trajectory Dispersions

Excess Recession Lien
Bondline Temperature Limit
Initial Cold Soak Temperature
Material Thermal Properties
Roughness Augmentation
Transitional Database
Gap and Seam Design
Excess Erosion Behind Penetrations
Radiation Absorption

Base (Zero Margins)

Result from incomplete knowledge of operating environment, inability to test in flight environment, and/or deficiencies in underlying physical models

Courtesy Mike Wright, NASA Ames

Testing

- **No ground facility can reproduce all aspects of the flight environment; every test is a compromise**

- **Facility classes: arc jets, combustion plasma, lasers, radiant lamps, the atmosphere of the Earth (flight tests)**

- **Best facility for a given test depends upon the objectives:**
  - Materials screening
  - Materials characterization and model development
  - Performance limit evaluation (failure modes)
  - Materials qualification
  - Material interface evaluation (gaps, seals, etc.)
  - System level testing

Diagnostic Instrumentation

- **Instrumentation is critical to the success of the test**
- **Possible Types:**
  - Flowfield diagnostics (calorimetry, null points, LIF)
    - absolutely essential in arc jets to characterize freestream
  - Surface temperature (pyrometry)
    - validate recession model, detect local anomalies; global result
  - Film or video
    - evaluate transient performance, detect failures, recession (PRM)
  - In-situ
    - thermocouples, both bondline (qualification) and in-depth (material characterization
    - recession sensors
    - strain gauges (system level testing)

Arc Jets

- **Workhorse facility for TPS testing**

- **Can put flight-like q,h,p,τ on sample for long duration (but usually not more than two at a time)**

- **Limitations include:**
  - sample size; subscale testing only
  - combined radiative/convective heating (no facility exists)
  - non-Earth gas mixture (no domestic facility exists)
  - difficult to simulate time-varying (trajectory based) conditions
  - freestream characterization (what are we testing in anyway?)

Arc Jets
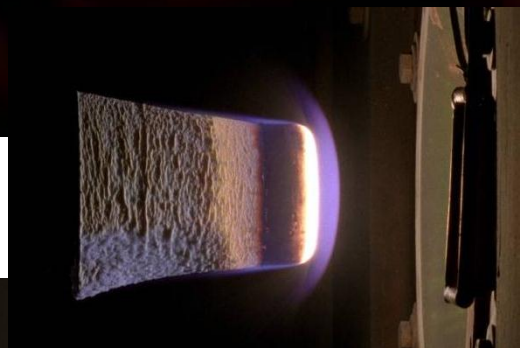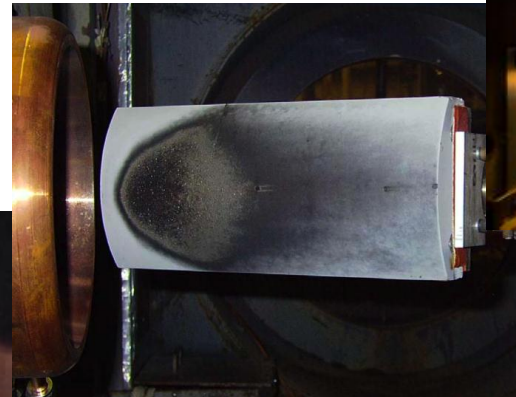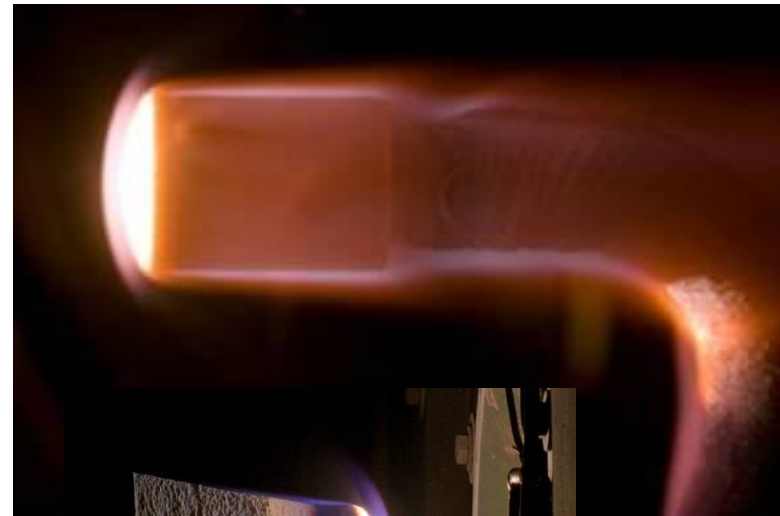
Sandia Solar Tower

Up to ~200 W/cm^2
Concentrated solar radiation

Advantages:
Large models possible
Good for system level testing

Disadvantages:
No flow (other than wind)
Non flight like application of heat flux (only matching one of q,h,p,τ)
Only works on sunny, cloudless days (but it is in desert!)

Courtesy Bill Congdon, ARA
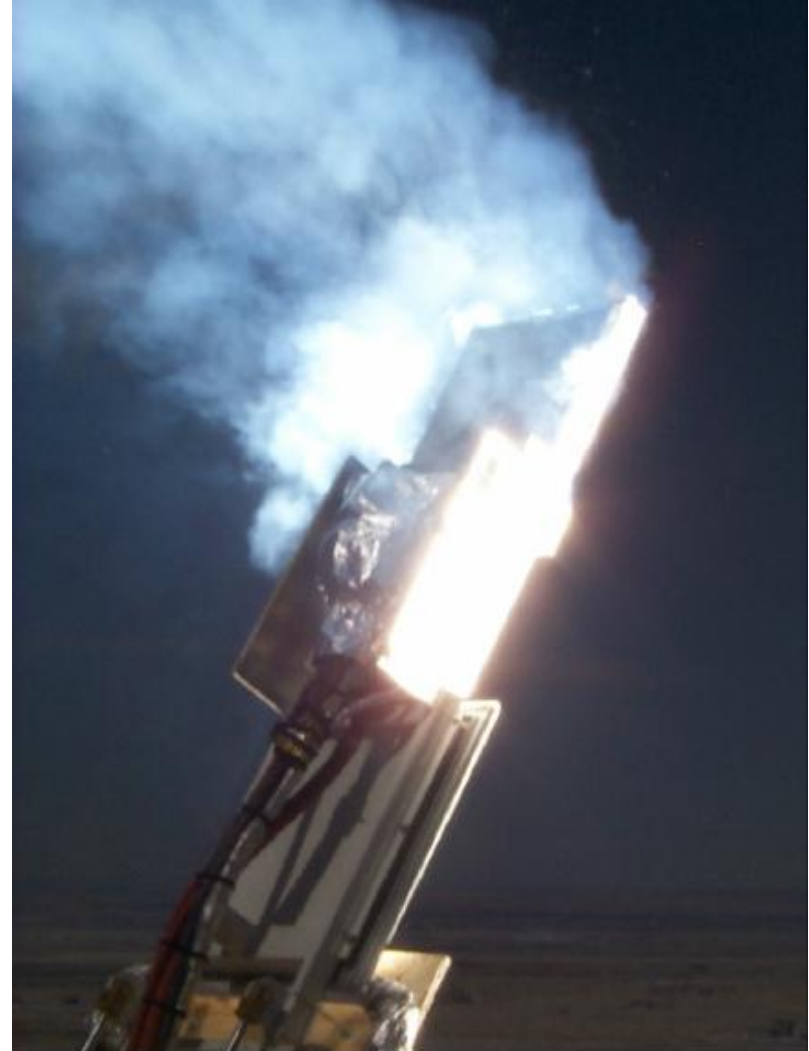
Sandia Solar Tower

Midday Test of SRAM-20 Panel 490 at 151 W/cm^2 for 230 Sec – 2-15-07

National Geographic Photo– Oct. 2007 Issue – Pg.118.

Courtesy Bill Congdon, ARA

Sandia Solar Tower

Within Seconds of Exposure

Near End of 210-Sec Exposure

Steve Moon Test Photos

1 meter aeroshell test (ISP program)

Courtesy Bill Congdon, ARA

LHMEL Laser Facility

Up to 100 kW on user-defined spot size for up to 100 seconds
CO_2 radiation

Advantages:
Large models possible
High throughput
Very low uncertainty in applied heat flux

Disadvantages:
No flow (other than wind)
Non flight like application of heat flux (only matching one of q, h, p, τ)

Small Laser at LHMEL
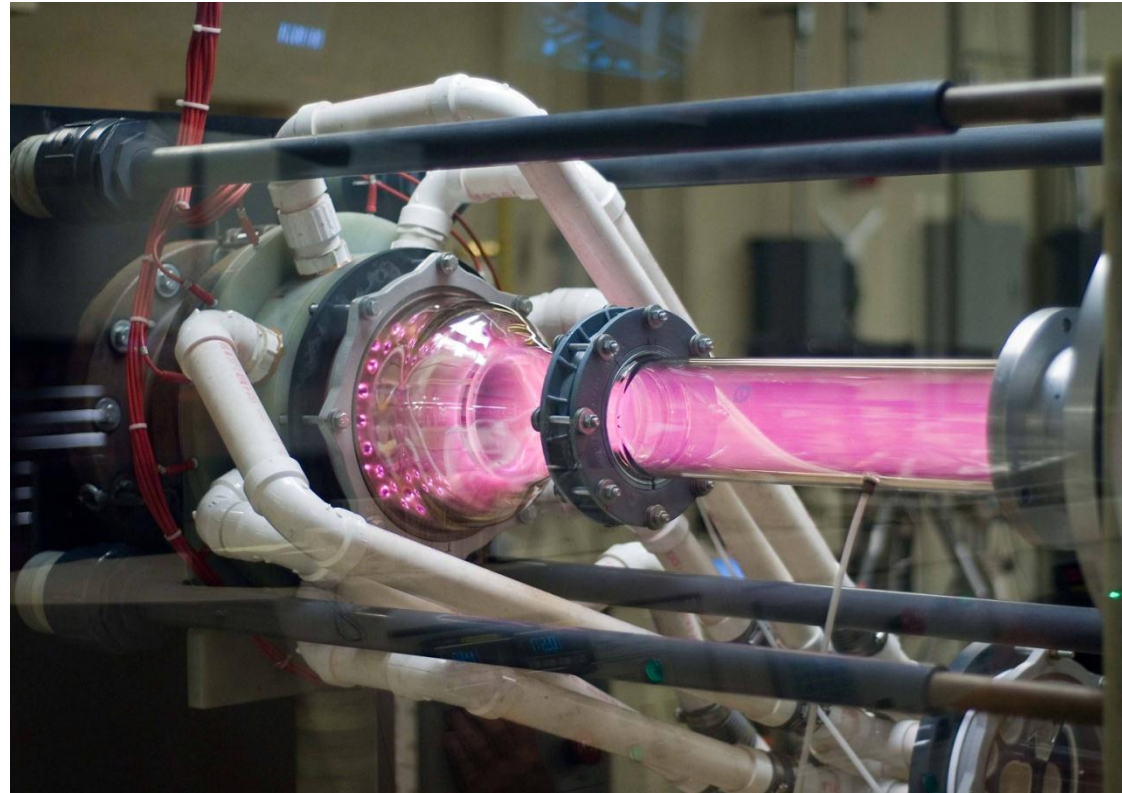
Current Research

- Current modeling research is geared towards making improvements
  - Multi-dimensional geometry
  - Orthotropic material properties
  - Loose coupling to CFD codes
  - Loose coupling to grid and trajectory codes
  - Coupled ablator thermochemistry
  - Coupled thermal stress
  - Multi-dimensional pyrolysis gas flow
  - Non-equilibrium surface thermochemistry
  - Probabilistic heat shield sizing

Current Research

Deployable/Inflatable Entry Systems

Trailing ballute concept
(Courtesy Ball Aerospace)

IRVE-3
Vehicle
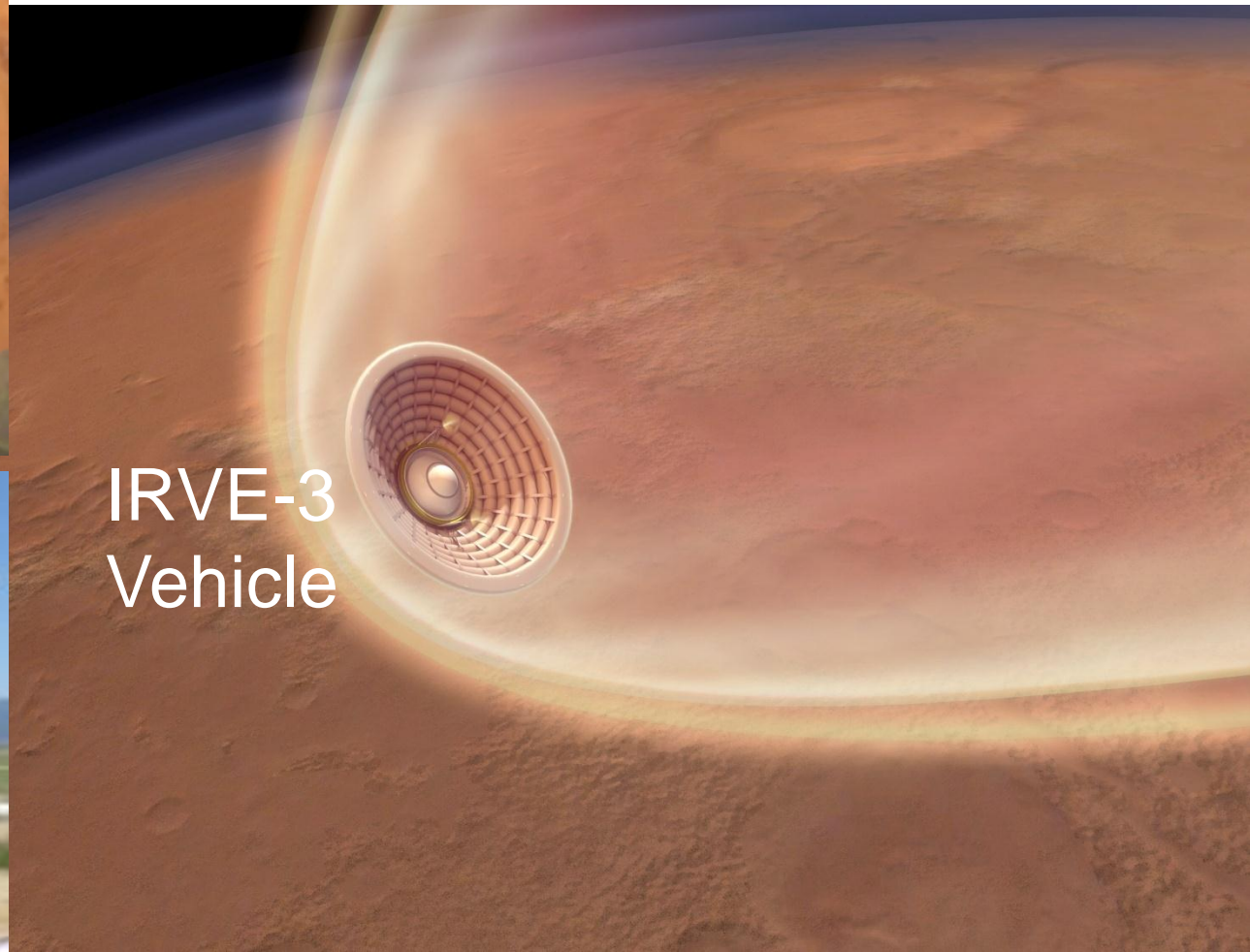
Flexible Thermal Protection Systems

- Flexible TPS materials act as mission enabler for large mechanically deployable or inflatable entry system aeroshells

- Large aeroshell diameter reduces ballistic coefficient and therefore peak aerodynamic heating
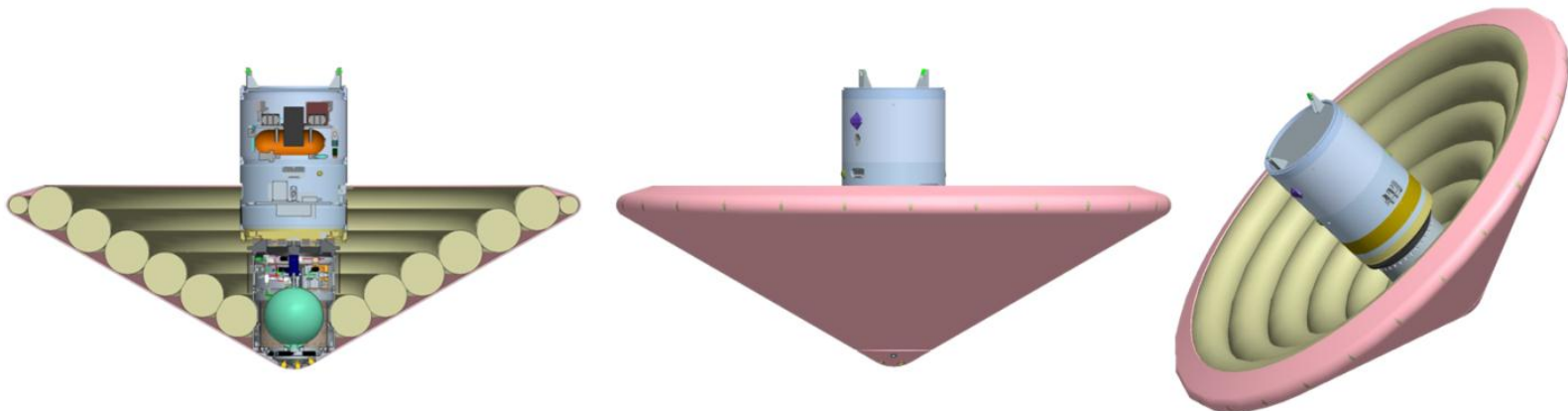
Thermal Protection Systems

- Flexible TPS consist of multiple layers of different materials
  - Outer reinforcing fabric
  - Inner insulation
  - Impermeable gas barrier

Convective heating

Radiative heat transfer to the surroundings

Surface material

Insulation

Gas barrier

In-depth
- Solid conduction
- Gas conduction
- Internal radiative transport

Pressure and temperature dependant

- Material decomposition
- Pyrolysis gas flow
- Pyrolysis gas convective heat transfer
(not included in the model yet)

Summary
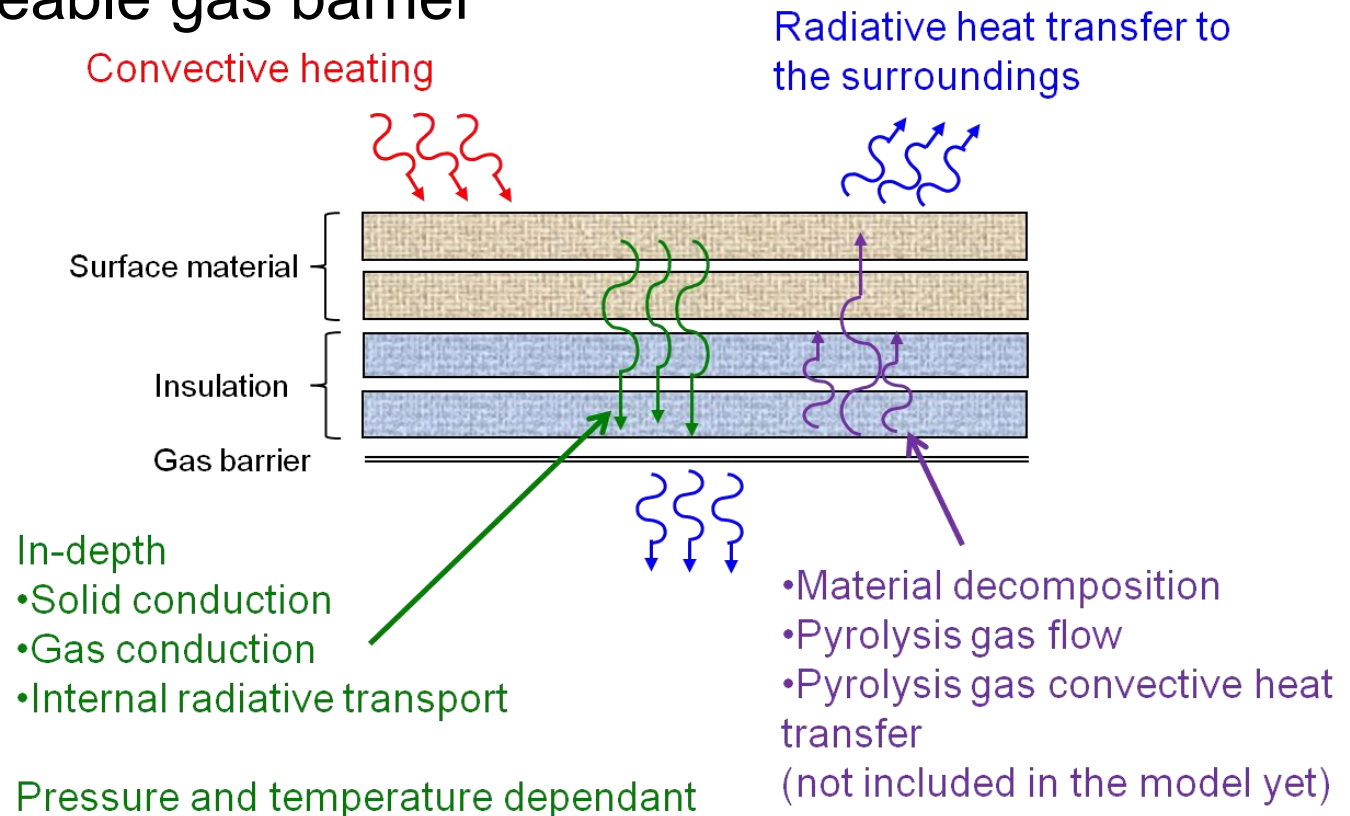
- **The current generation of ablative TPS models must be significantly improved to support the next generation of complex NASA entry missions**

- **Advanced modeling and new systems will be a key component of reducing mass while increasing system reliability**

- **Improvements required**
  - Finite-rate gas-surface interaction capability
  - Loose coupling to CFD codes
  - Loose coupling to grid and trajectory codes
  - True multidimensional analysis, including gaps, seams and other interfaces
  - Coupled ablator thermochemistry
  - Built in models for melt flow (glassy ablators), mechanical erosion, etc.
  - Robust models for multi-layer ablative systems

Nomenclature

Nomenclature

A	area, m^2
B_i	pre-exponential factor for the ith resin component
B'_c	non-dimensional charring rate
B'_g	non-dimensional pyrolysis gas rate at the surface
B'	total non-dimensional blowing rate
C_H	Stanton number for heat transfer
C_M	Stanton number for mass transfer
C_p	solid material specific heat, J/kg-K
C_{p_g}	pyrolysis gas specific heat, J/kg-K
E_{a_i}	activation energy for the ith resin component, J/kg-mole
$\dot{E}_{st}$	rate of energy storage in the control volume, W
H_r	recovery enthalpy, J/kg
H_w	wall enthalpy, J/kg
$H_{air}^{T_w}$	enthalpy of air evaluated at the wall temperature, J/kg
H_g	pyrolysis gas enthalpy, J/kg
h_i^0	enthalpy of formation of species i, J/kg
h_{ref}	reference enthalpy at 298K, J/kg
h_g	enthalpy of pyrolysis gas, J/kg
h_c	enthalpy of char, J/kg
h_w	enthalpy of the boundary layer edge gas evaluated at the wall temperature, J/kg

Nomenclature

i	node index, or resin component index (A,B,C)
k	thermal conductivity, W/m-K
$\dot{m}_g$	mass flow rate of pyrolysis gas, kg/s
$\dot{m}_g''$	mass flux of pyrolysis gas, kg/m^2-s
$\dot{m}_c''$	mass flux of char, kg/m^2-s
m_{cv}	mass stored in the control volume, kg
q	source term in the general heat equation
q^*	condensed phase energy removal, W/m^2
$\dot{q}_{rad}$	stagnation point radiative heat flux, W/m^2
$\dot{q}_{conv}$	stagnation point convective heat flux, W/m^2
$\dot{q}_{cond}$	conductive heat flux, W/m^2
$\dot{q}_{cw}$	cold wall heat flux, W/m^2
$\dot{q}_{hw}$	hot wall heat flux, W/m^2
Q^*	thermochemical heat of ablation, J/kg
	also hot wall heat of ablation, J/kg
R	universal gas constant, J/kg-mole-°K
$\dot{s}$	recession rate, m/s
ss	steady state

Nomenclature

T	temperature, °C or K
T_w	wall temperature, °C or K
T_0, T_i	initial temperature, °C or K
T_s	surface temperature, °C or K
T_{surr}	surrounding, or ambient temperature, °C or K
t	time, sec
u_e	boundary layer edge gas velocity, m/s
x	distance measured from the original surface of the ablating material, m
x_S	distance measured from the moving surface of the ablating material, m
Z_{ie}^*	diffusion driving potential at the boundary layer edge
Z_{iw}^*	diffusion driving potential at the wall
α	solar absorptivity, or thermal diffusivity m^2/s
ε	emissivity
η	transpiration coefficient

Nomenclature

ΔH_v enthalpy of vaporization, J/kg

ΔH enthalpy difference, J/kg

ΔH_d heat of decomposition, J/kg

ΔT temperature difference, °C

Γ resin volume fraction

ρ_r residual density, kg/m^3

$\rho, or\ \rho_s$ solid material density, kg/m^3

ρ_e boundary layer edge gas density, kg/m^3

ρ_{resin} density of resin component, kg/m^3

ρ_{fiber} density of fiber reinforcement, kg/m^3

$(\rho v)_w$ total mass flux entering the boundary layer, kg/m^2-s

σ Stephan-Boltzman constant, W/m^2-K^4

ψ_i density exponent factor

ϕ transpiration correction factor

References

1. Katsikas, C.J., Castle, G.K. and Higgins, J.S., "Ablation Handbook – Entry Materials Data and Design," AFML-TR-66-262, September 1966.

2. Holzknecht, B., "An Analytical Model of the Transient Ablation of Polytetrafluoroethylene Layers," *Int. J. Heat Mass Transfer*, Vol. 20, pp./ 661-668, 1977.

3. Clark, B.L., "A Parametric Study of the Transient Ablation of Teflon," *J. Heat Transfer,* pp. 347-354, November 1972.

4. Friedman, H., "The Mechanisms of Polytetrafluoroethylene Pyrolysis, General Electric Report TIS R59SD385, June 1959.

5. Heister, N.K. and C.F. Clark, "Feasibility of Standard Evaluation Procedure for Ablating Materials, NASA CR-379, February 1966.

6. Steg, L. and H.Lew, "Hypersonic Ablation," General Electric Report TIS R62SD55. May 1962.

7. Hurwicz, H., "Aerothermochemistry Studies in Ablation," 5th AGARD Combustion and Propulsion Colloquium, April 1962.

8. Bethe H.A. and M.C. Adams, "A Theory for the Ablation of Glassy Materials," *J. Aerospace Sci.*, Vol. 26, pp. 321-328, 1959.

9. Scala, S.M., "The Ablation of Graphite in Dissociated Air, Part I: Theory," General Electric Report R62SD72, September 1962.

10. Beecher, N. and R.E. Rosensweig, "Ablation Mechanisms in Plastics with Inorganic Reinforcement," *ARS J.*, Vol. 31, pp. 532-539, 1961.

1. "JANAF Thermochemical Tables," Third Edition, *J. of Physical and Chemical Reference Data,* Vol. 14, 1985.

2. Anon., "User's Manual, Aerotherm Chemical Equilibrium Computer Program (ACE81)," Acurex Corporation, Aerotherm Division, Mountain View, California, August 1981.

3. Bethe, H.A. and M.C. Adams, "A Theory for the Ablation of Glassy Materials," *J. Aerospace Sci.,* Vol. 26, pp. 321-328, 1959.

4. Adams, M.C., Powers, W.E. and S. Georgiev, "An Experimental and Theoretical Study of Quartz Ablation at the Stagnation Point," J. Aerospace Sci., Vol., 27, pp. 535-543, 1960.

5. Scala, S.M., The Ablation of Graphite in Dissociated Air, Part I: Theory," General Electric Report R62SD72, Sept., 1962.

6. Diaconis, N.S. Gorsuch, P.D. and R.A. Sheridan, "The Ablation of Graphite in Dissociated Air, Part II" Experimental Investigation," General Electric Report R62SD86, Sept. 1962.

7. Beecher, N. and R.E. Rosensweig, "Ablation Mechanism in Plastics with Inorganic Reinforcement," *AIAA J.,* Vol. 31, pp 532-539, 1961.

8. Lundell, J.H. and R.R. Dickey, "The Ablation of Graphitic Materials in the Sublimation Regime," AIAA Paper No., 72-298, April 1972.

9. Milos, F.S. and Y.-K. Chen, "Comprehensive Model for Multicomponent Ablation Thermochemistry," AIAA Paper No. 97-0141, Jan. 1997.

10. Schneider, P.J., Dolton, T.A. and Reed, G.W., "Mechanical Erosion of Charring Ablators in Ground-Test and Re-Entry Environments, AIAA Journal , Vol. 6, No. 1.

11. Mathieu, Richard D., "Mechanical Spallation of Charring Ablators in Hyperthermal Environments", AIAA Journal, Vol. 2, No. 9, September 1964.

References - Surface Recession

12. Stokes, Eric H., "Gas Permeability of RSRM Carbon Phenolic Composites as a Function of Across Ply Tensile Stress, Strain, and Temperature, 1992 JANNAF Rocket Nozzle Technology Subcommittee Meeting, Sunnyvale California.

13. Jortner, Julius, "Microstructures of Rapidly Heated Carbon-Phenolics", SPIP Program, Document No. HI-054F/1.2.9, March 1993.

14. Koenig, John, "Solid Propulsion Integrity Program Exploratory Testing", SPIP Program, Document No. H)-053F/1.2.9, March 1993.

15. Ross, R.B., Strobel, F.A., Fretter, E.F., "Plasma Arc Testing and Thermal Characterization of NARC FM5055 Carbon-Phenolic", SPIP Program, Document No. HI-046F/1.2.9, April 1992.

16. Hercules Aerospace Company, "Solid Propulsion Integrity Program Final Report", SPIP Program, Document No. HI-080F/1.2.9, December 1994.

11. Strobel, F.A., King, B.K., "ASRM Nozzle Thermal Analysis", Aerotherm Final Report 7186-93-15, November 1993, Aerotherm Corporation, Huntsville, Alabama. Crose, J.G., Marx, D.A., Holman, R.L., "Solid Propulsion Program Mechanical Property Dependencies", SPIP Program, Document No. HI-079F/1.2.9, December 1994.

12. Kuhlman, Tim L., "Thermo-Chemical-Structural Analysis of Carbon-Phenolic Composites with Pore Pressure and Pyrolysis Effects", SPIP Program, Document No. HI-017F/1.2.5, August 1992.

13. Stokes, Eric H., "Kinetics of Pyrolysis Mass Loss From MX4926 Standard Density NARC Based Carbon-Phenolic Composite" Volumes I, II, and III, SPIP Program, Document No. HI-063F/1.2.9, September 1994.

14. Poteat, R.M., Lundblad, W.E., Koenig, J.R., "Mechanical Property Evaluations Solid Propulsion Integrity Program Exploratory Testing" Volumes I and II, SPIP Program, Document No., HI-069F/1.2.9, November 1994.

References - Response Models

1. Anon., "User's Manual, Aerotherm Charring Material Thermal response and Ablation Program (CMA87), Acurex UM-87-11/ATD, Acurex Corporation, Aerotherm Division, Mountain View, California, August 1987.

2. Anon., "User's Manual, Aerotherm Chemical Equilibrium Computer Program (ACE81), Acurex Report UM-81-11/ATD, Acurex Corporation, Aerotherm Division, Mountain View, California, August 1981.

3. Ladacki, M., Hamilton, J.V., and S.N. Cohz, "Heat of Pyrolysis of Resin in Silica Phenolic Ablator," AIAA J., Vol. 4, No. 10, pp. 1798-1802, October 1966.

4. Beck, R.A.S., Laub, B., Johnson, P.A. and M. L. Gordon, "IUS Nozzle Materials Thermal Characterization," Acurex Final Report FR-84-21/ATD, August 1984.

5. Suchsland, K.E., Laub, B. and A. L. Murray, "Mathematical Modeling of Ablation Problems," presented at the Winter Annual Meeting of the ASME, San Francisco, California, December 1978.

6. Beck, R.A.S. and Laub, B. "Characterization and Modeling of Low Density TPS Materials for Recovery Vehicles," with R.A.S. Beck, SAE Paper 941368, presented at the 24th International Conference on Environmental Systems and 5th European Symposium on Space Environmental Control Systems, Friedrichshafen, Germany, June 20-23, 1994.

7.   Beck, R.A.S., Laub, B., Delano, C.B., Minell, C.L., Magyary, J.G. and E.F. Fretter, "The Performance of P-45 Cork for Titan IV TPS Applications," Acurex Final Report FR-91-10/ATD, May 31, 1991.

8.   Bartlett, E.P., Abbett, M.J., Nicolet, W.E. and C.B. Moyer, "Improved Heat-Shield Design Procedures for Manned Entry Systems: Part II, Application to Apollo," Aerotherm Report 70-15, Part II, Aerotherm Corporation, Mountain View, California, June 1970.

9.   Curry, D.M. and E.W. Stephens, "Apollo Ablator Thermal Performance at Superorbital Entry Velocities," NASA TN D-5969, September 1970.

10.   Laub, B., "The Apollo Heatshield - Why Performance Exceeded Expectations," 1st Atmospheric Reentry Vehicles and Systems Symposium, Arcachon, France, March 1999.

11.   Roberts, W., Laub, B., Suchsland, K., Shimizu, A. and J. Chambers, "Ramburner Internal Insulation Investigation, Task I - Modeling and Computer Program," AFAPL-TR-75-109, Vol. 1, Air Force Aero Propulsion Laboratory, Wright-Patterson Air Force Base, Ohio, December 1975.

References – Numerical Modeling

1. Moyer, C. B., and Rindal, R. A., "An Analysis of the Coupled Chemically Reacting Boundary Layer and Charring Ablator – Part II. Finite Difference Solution for the In-Depth Response of Charring Materials Considering Surface Chemical and Energy Balances", NASA CR-1061, 1968.

2. Katsikas, C. J., Castle, G. K., and Higgins, J. S., "Ablation Handbook – Entry Materials Data and Design", AFML-TR-66-262, September 1966.

3. Kratsch, K. M., Hearne, L. F., and McChesney, H. R., "Thermal Performance of Heat Shield Composites During Planetary Entry", Lockheed Missiles and Space, LMSC-803099, Sunnyvale, CA, October 1963.

4. Munson, T. R., and Spindler, R. J., "Transient Thermal Behavior of Decomposing Materials. Part I, General Theory and Application to Convective Heating", AVCO RAD-TR-61-10, AVCO Corp., Wilmington, MA, May 1961.

5. Curry, D. M., "An Analysis of a Charring Ablation Thermal Protection System", NASA TN D-3150, November 1, 1965.

6. Goldstein, H. E., "Kinetics of Nylon and Phenolic Pyrolysis", Lockheed Missiles and Space Company, Sunnyvale, CA. LMSC-667876, October 1965.

7. Lees, L., "Convective Heat Transfer With Mass Addition and Chemical Reactions", Third AGARD Colloquim on Combustion and Propulsion, Pergamon Press, New York, 1959.